THE UNIVERSITY
OF MICHIGAN

SEP 12 1962

ENGINEERING
LIBRARY

АВТОМАТИКА
И
ТЕЛЕМЕХАНИКА

Vol. 22, No. 3, March, 1961

Translation Published October, 1961

SOVIET INSTRUMENTATION AND
CONTROL TRANSLATION SERIES

Automation and Remote Control

(The Soviet Journal *Avtomatika i Telemekhanika* in English Translation)

■ This translation of a Soviet journal on automatic control is published as a service to American science and industry. It is sponsored by the Instrument Society of America under a grant in aid from the National Science Foundation, continuing a program initiated by the Massachusetts Institute of Technology.

SOVIET INSTRUMENTATION AND CONTROL TRANSLATION SERIES

Instrument Society of America

Philip A. Sprague
President
Dr. Ralph H. Tripp
Past President
Nathan Cohn
President-elect-Secretary
Henry J. Noebels
Dept. Vice President
Dr. Benjamin W. Thomas
Dept. Vice President-elect
E. A. Adler
Dept. Vice President
Francis S. Hoag
Dept. Vice President
John J. McDonald
Dept. Vice President
John R. Mahoney
Dept. Vice President-elect
John C. Koch
Treasurer
Alonzo B. Parsons
Dist. I Vice President
H. Kirk Fallin
Dist. II Vice President
Harold J. Bowman
Dist. III Vice President
Fred R. Gilmer
Dist. IV Vice President
Charles H. Callier
Dist. V Vice President
Otto J. Lessa
Dist. VI Vice President
J. Howard Park, III
Dist. VII Vice President
C. Roy Horton
Dist. VIII Vice President
Max Curtis
Dist. IX Vice President
Kenneth S. Vriesen
Dist. X Vice President
Allan E. Lee
Dist. XI Vice President

International Headquarters

William H. Kushnick
Executive Director
Charles W. Covey
Editor, ISA Journal
Herbert S. Kindler
Director, Tech. & Educ. Services

ISA Publications Committee

Charles O. Badgett, *Chairman*
Jere E. Brophy, George A. Larsen, Joshua Stern
Dr. Enoch J. Durbin, Thomas G. MacAnespie, Frank S. Swaney
Prof. Richard W. Jones, John E. Read, Richard A. Terry

Translations Advisory Board of the Publications Committee

Jere E. Brophy, *Chairman*
T. J. Higgins, S. G. Eskin, G. Werbizky

■ This translation of the Soviet Journal *Avtomatika i Telemekhanika* is published and distributed at nominal subscription rates under a grant in aid to the Instrument Society of America from the National Science Foundation. This translated journal, and others in the Series (see back cover), will enable American scientists and engineers to be informed of work in the fields of instrumentation, measurement techniques, and automatic control reported in the Soviet Union.

The original Russian articles are translated by competent technical personnel. The translations are on a cover-to-cover basis and the Instrument Society of America and its translators propose to translate faithfully all of the scientific material in *Avtomatika i Telemekhanika*, permitting readers to appraise for themselves the scope, status, and importance of the Soviet work. All views expressed in the translated material are intended to be those of the original authors and not those of the translators nor the Instrument Society of America.

Publication of *Avtomatika i Telemekhanika* in English translation started under the present auspices in April, 1958, with Russian Vol. 18, No. 1 of January, 1957. The program has been continued with the translation and printing of the 1958-1961 issues.

Transliteration of the names of Russian authors follows the system known as the British Standard. This system has recently achieved wide adoption in the United Kingdom, and is currently being adopted by a large number of scientific journals in the United States.

Readers are invited to submit to the Instrument Society of America comments on the quality of the translations and the content of the articles. Pertinent correspondence will be published in the Society's monthly publication, the ISA JOURNAL. Space will also be made available in the ISA JOURNAL for such replies as may be received from Russian authors to comments or questions by the readers.

1961 Volume 22 Subscription Prices:

Per year (12 issues), starting with Vol. 22, No. 1

General:	*United States and Canada*	$35.00
	Elsewhere	38.00
Libraries of nonprofit academic institutions:		
	United States and Canada	$17.50
	Elsewhere	20.50
Single issues to everyone, each		$ 6.00

1957 Volume 18, 1958 Volume 19, 1959 Volume 20, and 1960 Volume 21 issues also available. Prices upon request.

See back cover for combined subscription to entire Series.

Subscriptions and requests for information on back issues should be addressed to the:

Instrument Society of America
530 William Penn Place, Pittsburgh 19, Penna.

Translated and printed by Consultants Bureau Enterprises, Inc.

Copyright © 1961 by the Instrument Society of America

Automation and Remote Control

A translation of Avtomatika i Telemekhanika, a publication of the Academy of Sciences of the USSR

EDITORIAL BOARD OF AVTOMATIKA I TELEMEKHANIKA

D. I. Ageikin
M. A. Aizerman
A. B. Chelyustkin *(Assoc. Editor)*
E. G. Dudnikov
N. Ya. Festa
V. A. Ilin
A. G. Iosuf'yan
V. V. Karibskii
A. V. Khramoi
B. Ya. Kogan
V. S. Kulebakin
S. A. Lebedev
A. Ya. Lerner
A. M. Letov *(Assoc. Editor)*
V. S. Malov
B. N. Petrov
Yu. P. Portnov-Sokolov
B. S. Sotskov
A. A. Tal' *(Corresp. Secretary)*
V. A. Trapeznikov *(Editor in Chief)*
Ya. Z. Tsypkin
G. M. Ulanov
A. A. Voronov
S. V. Yablonskii

Vol. 22, No. 3 | Russian Original Dated March, 1961 | October, 1961

CONTENTS

	PAGE	RUSS. PAGE
Representing Nonstationary Linear Differential Polynomial Operators in the Form of Sums of Stationary Operators. A. N. Sklyarevich	255	297
On the Synthesis of Linear Automatic Control Systems. D. I. Gladkov	263	306
A Servosystem with Logical Control. E. K. Shigin	271	314
On the Theory of Single-Type Intercoupled Automatic Control Systems with Symmetric Cross-Coupling Networks. V. T. Morozovskii	277	322
The Transfer Function of an Automatic Control System with a Modulator and a Half-Wave Demodulator. E. L. L'vov	291	338
A Generalized Graphical Method for Designing Contact Circuits. V. N. Roginskii	301	350
A Digital Computer for Programming Second-Degree Curves. Yang Hsi-jêng	309	359
The Use of Semiconductor Diodes in Making of Symmetrical Nonlinear Resistances. Tai Tzŭ-hsin	317	369
Sensitive Magnetic Modulator with Two-Phase Input. F. I. Kerbnikov and M. A. Rozenblat	323	376
Contactless Switches with Steel E310 Magnetic Cores. K. G. Mityushkin	330	383
On the Design of Push-Pull Magnetic Amplifiers. V. L. Benin	338	393
Nomogram for Determining Phase by Means of an Asymptotic Logarithmic Amplitude-Frequency Characteristic. B. M. Menskii	344	400
On the Method of Generating Random Processes with a Given Matrix of Spectral Densities. I. Matyash, L. Prouza, and Ya. Shilkhanek	346	403
The Positioning of Sensing Devices in a Converter. A. I. Ivushkin	349	406
The Calculation of a Two-Terminal Network with One Semiconductor Thermistor Operating under Linear Conditions. N. P. Udalov	352	409
BIBLIOGRAPHY		
List of Foreign Literature on Magnetic Elements Used in Automation, Remote Control and Computer Technique for the Year 1959 (Conclusion). G. V. Subbotina and I. S. Trefilova	356	413

ERRATA

Automation and Remote Control, Vol. 22, No. 1, translation published August, 1961

On p. 46, 2nd paragraph, 2nd line, instead of "any values of A_j and B_j", it should read "any values of A_k and B_k."

On p. 87, 4th paragraph (1st paragraph extending full width of page), next to last line, instead of "conditions (26)," it should read "conditions (28)."

REPRESENTING NONSTATIONARY LINEAR DIFFERENTIAL POLYNOMIAL OPERATORS IN THE FORM OF SUMS OF STATIONARY OPERATORS

A. N. Sklyarevich

(Riga)

Translated from Avtomatika i Telemekhanika, Vol. 22, No. 3,
pp. 297-305, March, 1961
Original article submitted October 1, 1960

It is being shown that an arbitrary nonstationary linear differential polynomial operator can be represented in the form of a sum of stationary operators with associated kernels. An algorithm is given which enables one to find all the components of the representation. In the Appendix a formula for transforming of linear operators is derived of which use is made in the theoretical investigations and in the determination of the structure of automatic control systems.

In many cases the study of the structure of an automatic control system, the determination of the weighting function as well as establishing the exactness criteria of the operation of the system can be simplified considerably if its behavior, describable by an equation

$$\Phi(p, t)\, x = f(t), \tag{1}$$

with $\Phi(p, t)$ being the known nonstationary operator, $x(t)$ the sought response to the excitation $f(t)$, is transformed into

$$\sum_{k=1}^{s} \Phi_k(p)\,[\varphi_k(t)\, x] = f(t). \tag{2}$$

In the latter equation $\Phi_k(p)$ are the known stationary operators, and $\varphi_k(t)$ are known functions of time.

The case of $s = 1$ is a particular one of the formula (2). Now the study of the nonstationary system can be reduced to that of a stationary one. It is certainly of interest to show that such a reduction is actually possible, and to provide an algorithm which brings the equation (1) to assume the form (2). When $s > 1$ the weighting function and the exactness criteria may, in a number of cases, be obtained in a fairly straightforward manner, if use is made of the Laplace transforms.

The operator $\Phi(p, t)$ will be regarded as differentiable if it can be expanded into a Taylor series with respect to the differentiation operator $p \equiv d/dt$. The operator $\Phi(p, t)$ will be regarded as nonstationary if it depends explicitly on the independent variable of differentiation, and will be regarded as stationary when there is no such dependence. We shall presume that a nonstationary operator $\Phi(p, t)$ is reducible to the stationary $\Phi_1(p)$ with kernel $\varphi(t)$ if for any sufficiently differentiable function $x(t)$ there is valid the equality

$$\Phi(p, t)\, x = \Phi_1(p)\,[\varphi(t)\, x]. \tag{3}$$

The reducibility of the operator $\Phi(p, t)$ to a stationary operator $\Phi(p)$ with kernel $\varphi(t)$ will be denoted by

$$\Phi(p, t) = \Phi(p)\,[\varphi(t)],$$

i.e., cutting out, for brevity, the arbitrary function $x(t)$, as well as the closing bracket.

We shall show that an arbitrary nonstationary linear differential polynomial operator $\Phi(p, t)$ which can be expanded into a finite Taylor series with respect to the operator p and the independent variable t can be represented in the form of a sum of stationary operators with associated kernels:

$$\Phi(p, t) = \sum_k \Phi_k(p)\,[\varphi_k(t)]. \tag{4}$$

We shall establish as a preliminary result the conditions under which an operator $\Phi(p, t)$ reduces to a stationary operator $\Phi_1(p)$ with kernel $\varphi(t)$. These conditions can be found by using the formula

$$\Phi_1(p)[\varphi(t) = \varphi(t + q)\Phi_1(p) = \Phi(p, t), \tag{5}$$

in which $q = \partial/\partial p$, and whose derivation is given in the Appendix. A particular form of the formula (5) without derivation and without shortened notation was given in A. V. Solodov's work [1].

We expand the operator $\varphi(t+q)$ as a Taylor series with respect to the operator q:

$$\varphi(t + q) = \sum_{r=0}^{\infty} \frac{\varphi^{(r)}(t)}{r!} q^r, \tag{6}$$

and substitute this result in (5) and use the identity

$$q^r \Phi_1(p) = \Phi_1^{(r)}(p). \tag{7}$$

As a result, we obtain

$$\Phi(p, t) = \varphi(t + q)\Phi_1(p) = \sum_{r=0}^{\infty} \frac{\varphi^{(r)}(t)\,\Phi_1^{(r)}(p)}{r!}. \tag{8}$$

An arbitrary nonstationary linear differential operator $\Phi(p, t)$ reduces therefore to a stationary operator provided there exist functions $\varphi(t)$ and $\Phi_1(p)$ which satisfy the equation (8).

We now determine the functions $\varphi(t)$ and $\Phi_1(p)$ assuming that such a reduction is possible and also that $\Phi(p, t)$ is a polynomial of degree m with respect to the variable t and of degree n with respect to the operator p:

$$\Phi(p, t) = \sum_{i=0}^{m} \sum_{j=0}^{n} c_{ij} t^i p^j. \tag{9}$$

In this case it seems reasonable to take

$$\varphi(t) = \sum_{k=0}^{m} a_k t^k, \qquad \Phi_1(p) = \sum_{l=0}^{n} b_l p^l. \tag{10}$$

We represent the functions $\varphi(t)$ and $\Phi_1(p)$ in the following form:

$$\varphi(t) = \sum_{k=0}^{m} \frac{k!}{k!} a_k t^k, \qquad \Phi_1(p) = \sum_{l=0}^{n} \frac{l!}{l!} b_l p^l$$

and we designate

$$R_{kl} = \min[m - k,\ n - l]. \tag{11}$$

Then with $r \le R_{00}$ we have

$$\varphi^{(r)}(t) = \sum_{k=r}^{m} \frac{k!}{(k-r)!} a_k t^{k-r}, \qquad \Phi_1^{(r)}(p) = \sum_{l=r}^{n} \frac{l!}{(l-r)!} b_l p^{l-r};$$

but when $r > R_{00}$, one of the derivatives of order r vanishes identically. Consequently

$$\Phi(p, t) = \sum_{r=0}^{R_{00}} \sum_{k=r}^{m} \sum_{l=r}^{n} \frac{k!l!}{r!\,(k-r)!\,(l-r)!} a_k b_l t^{k-r} p^{l-r}. \tag{12}$$

We introduce new indices $i = k - r$, $j = l - r$ and invert the order of summation in the formula (12):

$$\Phi(p, t) = \sum_{i=0}^{m} \sum_{j=0}^{n} \sum_{r=0}^{R_{ij}} \frac{(i+r)!\,(j+r)!}{r!\,i!\,j!} a_{i+r} b_{j+r} t^i p^j. \tag{13}$$

Comparing (13) with the equality (9) we find

$$c_{ij} = \sum_{r=0}^{R_{ij}} \frac{(i+r)!\,(j+r)!}{r!\,i!\,j!}\, a_{i+r} b_{j+r}. \tag{14}$$

When the coefficients c_{ij} are known, the relations (14) represent equations with unknown products $a_i b_j$. We introduce the notation

$$a_i b_j = d_{ij} \tag{15}$$

and it can be shown by the method of mathematical induction that the solutions of the equations (14) can be expressed by the formulas

$$d_{ij} = \sum_{r=0}^{R_{ij}} \frac{(-1)^r\,(i+r)!\,(j+r)!}{r!\,i!\,j!}\, c_{i+r,\ j+r}. \tag{16}$$

With the known matrix $\|c_{ij}\|$ of the coefficients, the equations (16) determine the matrix of the quantities $\|d_{ij}\|$. Conversely, when the matrix $\|d_{ij}\|$ is known, the formulas

$$c_{ij} = \sum_{r=0}^{R_{ij}} \frac{(i+r)!\,(j+r)!}{r!\,i!\,j!}\, d_{i+r,\ j+r} \tag{17}$$

provide the corresponding coefficient matrix $\|c_{ij}\|$. The matrices $\|c_{ij}\|$ and $\|d_{ij}\|$ have an equal number of rows and an equal number of columns. It proves helpful to number their rows from bottom upwards and the columns from left to right. The elements will be correspondingly equal to one another (in particular $c_{mn} = d_{mn} \neq 0$) in the top rows and in the marginal right columns of the matrices $\|c_{ij}\|$ and $\|d_{ij}\|$.

Thus we can establish the $(m+1)(n+1)$ relations

$$a_i b_j = d_{ij}, \tag{18}$$

connecting the $m+1$ coefficients of the kernel $\varphi(t)$ and the $n+1$ coefficients of the operator $\Phi_1(p)$. When the operator $\Phi(p, t)$ is reducible to the operator $\Phi_1(p)$ with kernel $\varphi(t)$, all the above relations are true. Taking the particular values $i=\alpha$, $i=\beta$, $j=\gamma$, $j=\delta$, we obtain

$$a_\alpha b_\gamma = d_{\alpha\gamma}, \qquad a_\alpha b_\delta = d_{\alpha\delta}, \qquad a_\beta b_\gamma = d_{\beta\gamma}, \qquad a_\beta b_\delta = d_{\beta\delta},$$

and hence

$$\begin{vmatrix} d_{\alpha\gamma} & d_{\alpha\delta} \\ d_{\beta\gamma} & d_{\beta\delta} \end{vmatrix} = 0. \tag{19}$$

As the indices α, β, γ, δ can assume any integral values within the bounds $0 \leq \alpha \leq m$, $0 \leq \beta \leq m$, $0 \leq \gamma \leq n$, $0 \leq \delta \leq n$, the relation (19) is valid for all the second order minors of the matrix $\|d_{ij}\|$. This signifies that the matrix $\|d_{ij}\|$ is of rank one [2].

Therefore, when the operator $\Phi(p, t)$ is reducible to the operator $\Phi_1(p)$ with kernel $\varphi(t)$, the matrix $\|d_{ij}\|$, corresponding to the coefficients of the operator $\Phi(p, t)$, is of rank one. The converse statement is also true: if the matrix $\|d_{ij}\|$ corresponding to an operator $\Phi(p, t)$ is of rank one then the operator $\Phi(p, t)$ is reducible to an operator $\Phi_1(p)$ with kernel $\varphi(t)$. The proof of the converse statement follows from the simultaneous validity of the equations (18).

We determine the coefficients a_i and b_j in the case when the operator is reducible. The representation

$$\Phi(p, t) = \Phi_1(p)\,[\varphi(t)$$

is obviously not a unique one, as all the coefficients a_i can be increased k times provided that at the same time we reduce the b_j coefficients by an equal number of times. One of the coefficients a_i or b_j can, therefore, assume an arbitrary value. It seems in order to take $b_n = 1$ in view of the usual way of listing transfer functions; then

$$d_{in} = a_i b_n = a_i. \tag{20}$$

We shall now concentrate on the value $i = m$. As $d_{mj} = a_m b_j$,

$$b_j = \frac{d_{mj}}{d_{mn}}. \tag{21}$$

But $c_{in} = d_{in}$, $c_{mj} = d_{mj}$; therefore

$$a_i = c_{in}, \qquad b_j = \frac{c_{mj}}{c_{mn}}. \tag{22}$$

The formulas (20)-(22) determine the coefficients of the operator $\Phi_1(p)$ and of the kernel $\varphi(t)$ when the operator $\Phi(p, t)$ is reducible to the operator $\Phi_1(p)$ with kernel $\varphi(t)$. All these coefficients only depend on the quantities in the top row and in the furthest right column of the matrices $\|c_{ij}\|$ and $\|d_{ij}\|$.

It follows from the above that in the general case a nonstationary operator $\Phi(p, t)$ is not reducible to a stationary one $\Phi_1(p)$. If an arbitrary nonstationary polynomial operator is given, $\Phi(p, t)$, then by using only the top row and the last right column of the coefficient matrix $\|c_{ij}\|$ of the operator $\Phi(p, t)$ one is able to determine the corresponding operator $\Phi_1(p)$, the kernel $\varphi_1(t)$ and the matrices $\|c_{ij1}\|$, $\|d_{ij1}\|$ of the operator $\Phi_1(p)[\varphi_1(t)$. In this case, however, the identity $\Phi(p, t) = \Phi_1(p)[\varphi_1(t)$ is not valid. We shall now find the operator $\Phi_1(p, t) = \Phi(p, t) - \Phi_1(p)[\varphi_1(t)$.

All the elements vanish in the top row and the last right column of the coefficient matrix of the operator $\Phi_1(p, t)$. This means that the operator $\Phi_1(p, t)$ represents a polynomial of the $m-1$ degree with respect to the variable t, and of the $n-1$ degree with respect to the operator p. Applying this procedure $R_{00}-1$ times we arrive at a nonstationary operator $\varphi_m(t)$ if $m \leq n$, or if $m > n$ at a stationary one $\Phi_n(p)$. In the coefficient matrices of the operators $\varphi_m(t)$ and $\Phi_n(p)$ the nonvanishing elements can only be found in the bottom row and the first left column. But, as the nonstationary operator $\varphi_m(t)$ reduces to the stationary operator p^0 with kernel $\varphi_m(t)$, therefore by a successive adding up of the relations

$$\Phi_k(p, t) = \Phi_{k-1}(p, t) - \Phi_k(p)[\varphi_k(t), \tag{23}$$

which express the outcome of each transformation stage, we obtain the formula

$$\Phi(p, t) = \sum_{k=1}^{R_{00}} \Phi_k(p)[\varphi_k(t). \tag{24}$$

The above is a formula which shows that it is possible to reduce an arbitrary nonstationary polynomial operator to a sum of stationary operators with associated kernels.

In view of the linearity of the formulas (16) and (17) with respect to the quantities d_{ij} and c_{ij}, one can give the following simple procedure to determine the operators $\Phi_k(p)$ and the kernels $\varphi_k(t)$. The matrix $\|d_{ij}\|$ is found from the coefficient matrix $\|c_{ij}\|$ of the operator $\Phi(p, t)$. The former matrix is represented in the form of a sum of matrices of rank one in such a way that by adding the first k matrices we obtain a matrix with k upper rows and k columns furthest on the right, which are the same as in the matrix $\|d_{ij}\|$. From the k-th matrix we detach the top row and the last right column both of which consist of nonvanishing elements. Taking into account that this matrix represents the matrix $\|d_{ijk}\|$ corresponding to the operator $\Phi_k(p)[\varphi_k(t)$, the coefficients b_{jk} of the operator $\Phi_k(p)$ and the coefficients a_{ik} of the kernel $\varphi_k(t)$ are found with the aid of the formulas which differ from (20) and (21) only by their index numbering.

Examples

1. The behavior of a dynamical system is described by the equation

$$(t^3 + 2t + 1)\ddot{x} + (2t^2 + 8t + 6)\dot{x} + (t^2 + 6t + 7)x = f(t), \tag{25}$$

where $f(t)$ is a known function. In this case

$$\Phi(p, t) = (1 + 2t + t^3)p^2 + (6 + 8t + 2t^2)p + (7 + 6t + t^2) \tag{26}$$

and consequently $m = n = 2$.

The coefficient matrix $\|c_{ij}\|$ of the operator $\Phi(p, t)$ is now

$$\|c_{ij}\| = \begin{Vmatrix} 1 & 2 & 1 \\ 6 & 8 & 2 \\ 7 & 6 & 1 \end{Vmatrix}.$$

Using the formulas (16) we find the matrix $\|d_{ij}\|$:

$$\|d_{ij}\| = \begin{Vmatrix} 1 & 2 & 1 \\ 2 & 4 & 2 \\ 1 & 2 & 1 \end{Vmatrix}.$$

The matrix $\|d_{ij}\|$ is of rank one. Therefore the operator $\Phi(p, t)$ reduces to a stationary operator $\Phi_1(p)$ with the kernel $\varphi(t)$, and in agreement with equalities (22) we have

$$\Phi_1(p) = 1 + 2p + p^2,$$
$$\varphi(t) = 1 + 2t + t^2.$$

The equation (25) is thus equivalent to the equation

$$(p^2 + 2p + 1)[(1 + 2t + t^2)x] = f(t). \tag{27}$$

2. Given a nonstationary operator

$$\Phi(p, t) = (2t^3 - 3t^2)p^2 + (6t^3 + 3t^2 - 10t - 1)p + (4t^3 + 12t^2 - 2t - 10).$$

It is required to reduce it to a sum of stationary operators with associated kernels. Writing down the coefficient matrix $\|c_{ij}\|$ of the operator $\Phi(p, t)$:

$$\|c_{ij}\| = \begin{Vmatrix} 4 & 6 & 2 \\ 12 & 3 & -3 \\ -2 & -10 & 0 \\ -10 & -1 & 0 \end{Vmatrix},$$

we find the matrix $\|d_{ij}\|$ with the aid of the formulas (16):

$$\|d_{ij}\| = \begin{Vmatrix} 4 & 6 & 2 \\ -6 & -9 & -3 \\ 4 & 2 & 0 \\ -6 & -1 & 0 \end{Vmatrix}.$$

The matrix $\|d_{ij}\|$ is of rank three which shows that the operator $\Phi(p, t)$ cannot be reduced to a single stationary operator $\Phi_1(p)$ with the kernel $\varphi(t)$. The matrix $\|d_{ij}\|$ shall be presented in the form of a sum of matrices of rank one such that the rule on obtaining the elements of the original $\|d_{ij}\|$ matrix is satisfied:

$$\begin{Vmatrix} 4 & 6 & 2 \\ -6 & -9 & -3 \\ 4 & 2 & 0 \\ -6 & -1 & 0 \end{Vmatrix} = \begin{Vmatrix} 4 & 6 & 2 \\ -6 & -9 & -3 \\ 0 & 0 & 0 \\ 0 & 0 & 0 \end{Vmatrix} + \begin{Vmatrix} 0 & 0 & 0 \\ 0 & 0 & 0 \\ 4 & 2 & 0 \\ -2 & -1 & 0 \end{Vmatrix} + \begin{Vmatrix} 0 & 0 & 0 \\ 0 & 0 & 0 \\ 0 & 0 & 0 \\ -4 & 0 & 0 \end{Vmatrix}.$$

To each of the component matrices there corresponds a definite stationary operator $\Phi_k(p)$ and also a definite kernel $\varphi_k(t)$. Taking into account the formulas (20) and (21), we find

$$\Phi_1(p) = 2 + 3p + p^2, \qquad \varphi_1(t) = 2t^3 - 3t^2,$$
$$\Phi_2(p) = 2 + p, \qquad \varphi_2(t) = 2t - 1,$$
$$\Phi_3(p) = 1, \qquad \varphi_3(t) = -4.$$

Consequently, for any function x(t) we have

$$\Phi(p,\ t)\,x = (p^2 + 3p + 2)\,[(2t^3 - 3t^2)\,x] + (p + 2)\,[(2t - 1)\,x] - 4x.$$

It would be of interest to mention that in the investigated cases the rank of matrix $\|d_{ij}\|$ is equal to the number of the components in the representation of the given nonstationary polynomial operator by a sum of stationary operators with associated kernels.

APPENDIX

Transformation Formula for Linear Operators

We shall derive a formula which will enable one to simplify the performing of transformations of the type

$$y = \Phi(p,\ t)\,[\varphi(t)\,x], \tag{28}$$

where $\varphi(t)$ and x(t) are functions of the independent variable t, the former assumed known, the latter unknown and sought.

We shall assume that there exists a Laurent expansion for the function $\varphi(t)$ in powers of the variable t, and also for the operator $\Phi(p, t)$ in powers of the operator p:

$$\varphi(t) = \sum_{i=-\infty}^{\infty} a_i\,t^i, \tag{29}$$

$$\Phi(p,\ t) = \sum_{j=-\infty}^{\infty} b_j(t)\,p^j. \tag{30}$$

Also

$$\Phi(p,\ t)\,[\varphi(t)x] = \sum_{i=-\infty}^{\infty} a_i\Phi(p,\ t)\,(t^i x). \tag{31}$$

We now find the value of the component $\Phi(p, t)(t^i x)$ for different values of i. When i = 1 and j is an integer, we have

$$p^j(tx) = tp^j x + jp^{j-1}x. \tag{32}$$

We multiply the equality (32) by the function $b_j(t)$ and then we sum with respect to index j. From the formula (30) the relation

$$\sum_{j=-\infty}^{\infty} jb_j(t)\,p^{j-1} = \frac{\partial\Phi(p,\ t)}{\partial p} \tag{33}$$

follows and the result of the summation can thus be written as

$$\Phi(p,\ t)\,(tx) = \left[t\Phi(p,\ t) + \frac{\partial\Phi(p,\ t)}{\partial p}\right]x. \tag{34}$$

The formula (34) is a generalization of a formula known in the operational calculus [3]:

$$\Phi(p)\,(tx) = [t\Phi(p) + \Phi'(p)]\,x.$$

By introducing the differentiation operator $q \equiv \partial/\partial p$ we are able to write the formula (34) as

$$\Phi(p,\ t)\,(tx) = [(t + q)\,\Phi(p,\ t)]\,x. \tag{35}$$

By twice applying the formula (35), we find

$$\Phi(p,t)\,(t^2x) = [(t + q)\,\Phi(p,\ t)]\,(tx) = \{(t + q)\,[(t + q)\,\Phi(p,\ t)]\}\,x,$$

or more briefly,

$$\Phi(p,\ t)\,(t^2x) = [(t + q)^2\,\Phi(p,\ t)]\,x.$$

Analogously, we establish

$$\Phi(p, t)(t^i x) = [(t+q)^i \Phi(p, t)]\, x, \tag{36}$$

where i denotes a positive integer.

The equality (36) is also valid when i = 0, simply from the way it is written down. This equality can be transformed by raising formally the sum t+q to the i-th power with the subsequent use of the formula

$$q^s \Phi(p, t) = \frac{\partial^s \Phi(p, t)}{\partial p^s}. \tag{37}$$

When i = -1 and j = 1 we have

$$p\left(\frac{x}{t}\right) = \frac{1}{t}\left(p - \frac{1}{t}\right)x = \left[\frac{1}{t}\left(1 - \frac{q}{t}\right)p\right]x,$$

but when $s \geq 2$

$$q^s p = 0,$$

and therefore

$$p\left(\frac{x}{t}\right) = \left[\frac{1}{t}\left(1 - \frac{q}{t} + \frac{q^2}{t^2} - \frac{q^3}{t^3} + \ldots\right)p\right]x = \left[\frac{1}{t}\,\frac{1}{1+\frac{q}{t}}\,p\right]x,$$

or

$$p\left(\frac{x}{t}\right) = \left[\frac{1}{t+q}\,p\right]x. \tag{38}$$

A generalization of the formula (38) is

$$p^j\left(\frac{x}{t}\right) = \left[\frac{1}{t+q}\,p^j\right]x, \tag{39}$$

which is proved for j > 0 by mathematical induction.

We assume that the formula (39) is valid when j = n. Then

$$p^{n+1}\left(\frac{x}{t}\right) = p\left\{\left[\frac{1}{t+q}\,p^n\right]x\right\}.$$

But

$$\left[\frac{1}{t+q}\,p^n\right]x = \frac{1}{t}\left[\sum_{m=0}^{n}(-1)^m\left(\frac{q}{t}\right)^m p^n\right]x =$$
$$= \frac{1}{t}\,p^n x - \frac{n}{t^2}\,p^{n-1}x + \frac{n(n-1)}{t^3}\,p^{n-2}x + \ldots$$

and therefore

$$p\left\{\left[\frac{1}{t+q}\,p^n\right]x\right\} = \frac{1}{t}\,p^{n+1}x - \frac{1+n}{t^2}\,p^n x + \frac{2n+n(n-1)}{t^3}\,p^{n-1}x + \ldots$$

After some reduction and by introducing the operator q we obtain

$$p\left\{\left[\frac{1}{t+q}\,p^n\right]x\right\} = \frac{1}{t}\left[\left(1 - \frac{q}{t} + \frac{q^2}{t^2} - \frac{q^3}{t^3} + \ldots\right)p^{n+1}\right]x,$$

or

$$p^{n+1}\left(\frac{x}{t}\right) = \left[\frac{1}{t+q}\,p^{n+1}\right]x.$$

Thus the formula (39) is valid when $j = n+1$, and consequently it is valid for any $j > 0$. A direct check will show the correctness of the formula when $j = 0$. We shall now study the values of $j < 0$. By applying successively the integration by parts formula

$$\frac{1}{p}[\varphi(t)\,x(t)] = \varphi(t)\,\frac{1}{p}[x(t)] - \frac{1}{p}\left\{p\varphi(t)\,\frac{1}{p}\,x(t)\right\}, \tag{40}$$

we obtain, when $j = -1$,

$$\frac{1}{p}\left(\frac{x}{t}\right) = \frac{1}{t}\,\frac{x}{p} + \frac{1}{p}\left(\frac{1}{t^2}\,\frac{x}{p}\right) = \frac{1}{t}\,\frac{x}{p} + \frac{1}{t^2}\,\frac{x}{p^2} + \frac{1}{p}\left(\frac{2}{t^3}\,\frac{x}{p^2}\right) =$$
$$= \frac{1}{t}\,\frac{x}{p} + \frac{1}{t^2}\,\frac{x}{p^2} + \frac{2}{t^3}\,\frac{x}{p^3} + \ldots + \frac{1}{p}\left(\frac{n!}{t^{n+1}}\,\frac{x}{p^n}\right). \tag{41}$$

If the function x/t can be expanded into a Taylor series, the last term on the right-hand side of the formula (41) becomes arbitrarily small with $n \to \infty$. Therefore, when proceeding to the limit, we can suppose that

$$\frac{1}{p}\left(\frac{x}{t}\right) = \frac{1}{t}\left[\left(1 - \frac{q}{t} + \frac{q^2}{t^2} - \frac{q^3}{t^3} + \ldots\right)\frac{1}{p}\right]x$$

or

$$\frac{1}{p}\left(\frac{x}{t}\right) = \left[\frac{1}{t+q}\,\frac{1}{p}\right]x. \tag{42}$$

A generalization of the formula (42) is

$$\frac{1}{p^j}\left(\frac{x}{t}\right) = \left[\frac{1}{t+q}\,\frac{1}{p^j}\right]x, \tag{43}$$

which can be proved by mathematical induction. The representation of the operator $\left[\frac{1}{t+q}\,\frac{1}{p^n}\right]$ in the form of a series with respect to the operator p, the subsequent application of the formula (40) to each term of this series, the introduction of the operator q and the contracting of the series to the equivalent operator $\left[\frac{1}{t+q}\,\frac{1}{p^{n+1}}\right]$ are the main stages of the proof.

The formula (43) can be regarded as a particular case of the formula (39) if the latter is widened to negative integral values of the index j.

We multiply the relation (39) by the function $b_j(t)$ and then we sum with respect to the index j. Shifting the place of the function $b_j(t)$ and of the operator $1/(t+q)$ and taking into account the formula (30) we find

$$\Phi(p, t)\left(\frac{x}{t}\right) = \left[\frac{1}{t+q}\,\Phi(p, t)\right]x. \tag{44}$$

The formula (44) leads to the formula

$$\Phi(p, t)\,(t^i x) = [(t+q)^i\,\Phi(p, t)]\,x, \tag{45}$$

valid for all negative i. The right-hand side of the formula (45) is convergent if the function $t^i x$ has a Taylor expansion.

The formula (36) may be looked upon as a particular case of the formula (45) if the latter is widened to include all integral values of the index i. Transforming the relation (31) with the aid of the formula (45), we obtain

$$\Phi(p, t)\,[\varphi(t)\,x] = \sum_{i=-\infty}^{\infty} a_i\,[(t+q)^i\,\Phi(p, t)]\,x.$$

In accordance with the formula (29), we have

$$\sum_{i=-\infty}^{\infty} a_i\,(t+q)^i = \varphi(t+q),$$

and therefore

$$\Phi(p,\ t)\,[\varphi(t)\,x] = [\varphi(t+q)\,\Phi(p,\ t)]\,x. \tag{46}$$

By using another notation, the formula (46) becomes

$$\Phi(p,\ t)\,[\varphi(t)\,x] = \left[\varphi\left(t+\frac{\partial}{\partial p}\right)\Phi(p,\ t)\right]x, \tag{47}$$

and this shows distinctly that the component $\varphi(t+q)$ represents an operator acting on the operator $\Phi(p, t)$. In order to dispense with the square brackets, it is necessary to expand formally the operator $\varphi(t+q)$ in a series of the powers of q, and then use the equality (37).

We should like to mention two results of the formula (46).

1. The shift theorem

$$\Phi(p,\ t)\,(e^{at}x) = [e^{a(t+q)}\Phi(p,\ t)]\,x = e^{at}\Phi(p+a,\ t)\,x. \tag{48}$$

2. The interchange of the operators $\varphi(t+q)$ and $\Phi(p, t)$:

$$\begin{aligned}[\Phi_1(p,\ t)\,\Phi_2(p,\ t)]\,[\varphi(t)\,x] &= \{\Phi_1(p,\ t)\,[\varphi(t+q)\,\Phi_2(p,\ t)]\}\,x = \\ &= \{\varphi(t+q)\,[\Phi_1(p,\ t)\,\Phi_2(p,\ t)]\}\,x.\end{aligned} \tag{49}$$

The formula (5) is a particular case of the formula (46).

1. A. V. Solodov, Elements of the Theory of Linear Systems with Variable Parameters [in Russian] (Izd. AIA im. Dzerzhinskii, 1958).
2. V. I. Smirnov, Course in Higher Mathematics [in Russian] (Gostekhizdat, 1951) vol. 3, pt. I.
3. V. A. Ditkin and P. A. Kuznetsov, Handbook of Operational Calculus [in Russian] (Gostekhizdat, 1951).

ON THE SYNTHESIS OF LINEAR AUTOMATIC CONTROL SYSTEMS

D. I. Gladkov

(Moscow)

Translated from Avtomatika i Telemekhanika, Vol. 22, No. 3,
pp. 306-313, March, 1961
Original article submitted April 20, 1960

A method for synthesizing linear dynamic systems with constant and variable parameters is considered. The structure and the parameters of the compensating networks are determined. A method for an accurate realization of the integrating factor is proposed.

The block diagram of an automatic control system is basically determined by the purpose of the system and the system's theoretical ability to solve the assigned problem. The assignment of any additional properties to the system is realized by introducing compensating networks. For this, the synthesis problem can be stated in the following manner.

Assume that the linear dynamic system shown in Fig. 1a is given.

It is necessary to determine the block diagram and the parameters of compensating networks which would bring the dynamic properties of the given system closer to those of a certain optimum system. The dynamic properties of the optimum system can be conveniently characterized by a weighting function. For linear systems that are described

by differential equations, this function can be represented in the following form:

$$g_0(t, \tau) = \sum_{j=1} f_j(t)\, \varphi_j(\tau). \tag{1}$$

The optimum weighting function can be determined on the basis of different principles [1].

Let us introduce the compensating networks in the manner shown in Fig. 1b. It should be noted that

$$g_1(t, \tau) = \int_{\tau}^{t} g_{11}(\eta, \tau)\, g_{12}(t, \eta)\, d\eta.$$

The differential equations describing the operation of systems with the weighting functions $g_{11}(t, \tau)$ and $g_{12}(t, \tau)$ will be given by

$$\sum_{\rho=0}^{m} a_\rho p^\rho x_{out} = x_{in}, \tag{2}$$

$$\sum_{\mu=0}^{k} b_\mu p^\mu x_{out} = x_{in}, \tag{3}$$

respectively, where $p = d/dt$, the exponents ρ and μ determine the order of the derivatives, and $\underline{k}$ and $\underline{m}$ determine the order of the differential equations. The coefficients a_ρ and b_μ are generally functions of time.

Let us determine the weighting function $g_k(t, \tau)$ of the compensating networks.

Let $g_k^*(t, \tau)$ be the weighting function of the forward network in the block diagram of the assigned automatic control system with the introduced compensating networks, and let $g_{k1}(t, \tau)$ be the weighting function of a series assembly of compensating networks and of a dynamic system with the weighting function $g_{12}(t, \tau)$.

For determining $g_k^*(t, \tau)$, it is necessary [2] to solve the Volterra integral equation of the second kind:

$$g_k^*(t, \tau) = g_0(t, \tau) + \int_{\tau}^{t} g_k^*(t, \eta) \int_{\tau}^{\eta} g_0(\xi, \tau)\, g_2(\eta, \xi)\, d\xi\, d\eta. \tag{4}$$

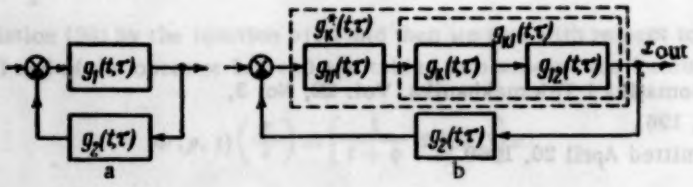

Fig. 1.

Equation (4) can be solved by using the method of successive approximations. The $g_0(t, \tau)$ and $g_2(\eta, \xi)$ functions are represented in the form of a sum. Each term of the sum is equal to the product of two factors, one of which is a function of the first, and the other is a function of the second argument of the weighting function. This fact enables us to state that the solution of Eq. (4) is given by

$$g_k^*(t, \tau) = \sum_{i=1}^{n} c_i(t)\, d_i(\tau). \tag{5}$$

The value of $\underline{n}$ is determined by the required accuracy with which Eq. (4) is to be solved.

If we know the $g_k^*(t,\tau)$ function, we can determine $g_{k1}(t,\tau)$. For this, the method of inverse factors [2] must be used:

$$g_{k1}(t,\tau)=\int_{\tau}^{t} g_{11}^{-}(\eta,\tau)\,g_k^*(t,\eta)\,d\eta. \tag{6}$$

By using the known $g_{k1}(t,\tau)$ and $g_{12}^{-}(t,\tau)$ functions, the weighting function of the compensating networks is determined in exactly the same manner:

$$g_k(t,\tau)=\int_{\tau}^{t} g_{k1}(\xi,\tau)\,g_{12}^{-}(t,\xi)\,d\xi. \tag{7}$$

In Eqs. (6) and (7), $g_{11}^{-}(t,\tau)$ and $g_{12}^{-}(t,\tau)$ denote the weighting functions of systems that are inverse with respect to the dynamic systems described by differential equations (2) and (3), respectively.

The functions $g_{11}^{-}(t,\tau)$ and $g_{12}^{-}(t,\tau)$ can be determined by putting $x_{out}=\delta(t-\tau)$ in equations (2) and (3). With this, we obtain

$$g_{11}^{-}(t,\tau)=\sum_{\rho=0}^{m} a_\rho(t)\,\delta^{(\rho)}(t-\tau), \tag{8}$$

$$g_{12}^{-}(t,\tau)=\sum_{\mu=0}^{k} b_\mu(t)\,\delta^{(\mu)}(t-\tau). \tag{9}$$

By substituting (5) and (8) in Eq. (6), we find

$$g_{k1}(t,\tau)=\int_{\tau}^{t}\sum_{\rho=0}^{m} a_\rho(\eta)\,\delta^{(\rho)}(\eta-\tau)\sum_{i=1}^{n} c_i(t)\,d_i(\eta)\,d\eta$$

or

$$g_{k1}(t,\tau)=\sum_{i=1}^{n} c_i(t)\,d_{0i}(\tau)+\sum_{\rho=1}^{m}\sum_{i=1}^{n}\int_{\tau}^{t}\delta^{(\rho)}(\eta-\tau)\,a_\rho(\eta)\,c_i(t)\,d_i(\eta)\,d\eta. \tag{10}$$

Here, the notation $d_{0i}(\tau)=a_0(\tau)d_i(\tau)$ is used.

By further substituting (9) and (10) in Eq. (7), we obtain the expression for the weighting function of the compensating networks:

$$g_k(t,\tau)=\int_{\tau}^{t}\Big[\sum_{i=1}^{n} c_i(\xi)\,d_{0i}(\tau)+$$

$$+\sum_{\rho=1}^{m}\sum_{i=1}^{n}\int_{\tau}^{\xi}\delta^{(\rho)}(\eta-\tau)\,a_\rho(\eta)\,c_i(\xi)\,d_i(\eta)\,d\eta\Big]\sum_{\mu=0}^{k} b_\mu(t)\,\delta^{(\mu)}(t-\xi)\,d\xi$$

or

$$g_k(t,\tau)=\sum_{i=1}^{n} c_{0i}(t)\,d_{0i}(\tau)+\sum_{\rho=1}^{m}\sum_{i=1}^{n}\int_{\tau}^{t}\delta^{(\rho)}(\eta-\tau)\,a_\rho(\eta)\,c_{0i}(t)\,d_i(\eta)\,d\eta+$$

$$+\sum_{i=1}^{n}\sum_{\mu=1}^{k}\int_{\tau}^{t} c_i(\xi)\,d_{0i}(\tau)\,b_\mu(t)\,\delta^{(\mu)}(t-\xi)\,d\xi+ \tag{11}$$

$$+\sum_{\rho=1}^{m}\sum_{i=1}^{n}\sum_{\mu=1}^{k}\int_{\tau}^{t}\int_{\tau}^{\xi}\delta^{(\rho)}(\eta-\tau)\,a_\rho(\eta)\,c_i(\xi)\,d_i(\eta)\,b_\mu(t)\,\delta^{(\mu)}(t-\xi)\,d\eta\,d\xi.$$

Here, the notation $c_{0i}(t) = b_0(t)c_i(t)$ was introduced.

An analysis of expression (11) indicates that the compensating network represents a parallel combination of dynamic systems with weighting functions of the following types:

$$g_{01}(t, \tau) = c_{0i}(t)\, d_{0i}(\tau),$$

$$g_{02}(t, \tau) = \int_{\tau}^{t} \delta^{(\rho)}(\eta - \tau)\, a_\rho(\eta)\, c_{0i}(t)\, d_i(\eta)\, d\eta,$$

$$g_{03}(t, \tau) = \int_{\tau}^{t} c_i(\xi)\, d_{0i}(\tau)\, b_\mu(t)\, \delta^{(\mu)}(t - \xi)\, d\xi,$$

$$g_{04}(t, \tau) = \int_{\tau}^{t}\int_{\tau}^{\xi} \delta^{(\rho)}(\eta - \tau)\, a_\rho(\eta)\, c_i(\xi)\, d_i(\eta)\, b_\mu(t)\, \delta^{(\mu)}(t - \xi)\, d\eta\, d\xi.$$

We shall now see how systems with such weighting functions can be realized.

The block diagram of a dynamic system with the weighting function $g_{01}(t,\tau)$ will be composed in the form shown in Fig. 2a [3].

The integrating element is preceded by the amplifying element with the variable gain $d_{0i}(t)$, which is equal to that portion of the weighting function which depends only on the second argument; the integrating element is followed by the amplifying element with the variable gain $c_{0i}(t)$, which is equal to that part of the weighting function $g_{01}(t,\tau)$ which depends only on the first argument.

An elementary check:

$$x_1 = d_{0i}(t)\, \delta(t - \tau), \qquad x_2 = \int_{0}^{t} d_{0i}(\eta)\, \delta(\eta - \tau)\, d\eta = d_{0i}(\tau),$$

$$d_{0i}(\tau)\, c_{0i}(t) = g_{01}(t, \tau)$$

confirms the above reasoning.

Let us compose the block diagram and determine the parameters of a dynamic system with the weighting function $g_{04}(t,\tau)$.

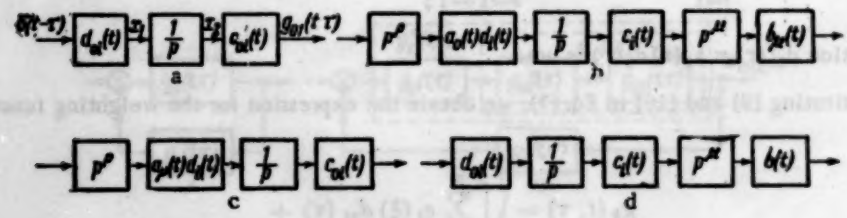

Fig. 2.

On the basis of the expression for the weighting function pertaining to the series coupling of a system or its elements, the following can be stated. A dynamic system with the weighting function $g_{04}(t,\tau)$ represents a series assembly of systems with the weighting functions

$$g_{041}(t, \tau) = \int_{\tau}^{t}\int_{\tau}^{\xi} \delta^{(\rho)}(\eta - \tau)\, a_\rho(\eta)\, c_i(\xi)\, d_i(\eta)\, \delta^{(\mu)}(t - \xi)\, d\eta\, d\xi$$

and

$$g_{042}(t, \tau) = b_\mu(t)\, \delta(t - \tau).$$

A system with the weighting function $g_{041}(t,\tau)$ is represented by a series assembly of systems with the weighting functions

$$g_{0411}(t,\ \tau) = \int_{\tau}^{t} \delta^{(\rho)}(\eta - \tau)\, a_\rho(\eta)\, c_i(t)\, d_i(\eta)\, d\eta \text{ and } g_{0412}(t,\ \tau) = \delta^{(\mu)}(t - \tau).$$

A system with the weighting function $g_{0411}(t,\tau)$ represents, in turn, a series assembly of dynamic systems with the weighting functions

$$g_{04111}(t,\ \tau) = \delta^{(\rho)}(t - \tau) \text{ and } g_{04112}(t,\ \tau) = c_i(t)\, a_\rho(\tau)\, d_i\tau.$$

Figure 2b shows the block diagram of a dynamic system with the weighting function $g_{04}(t,\tau)$.

The block diagrams of systems with the weighting functions $g_{02}(t,\tau)$ and $g_{03}(t,\tau)$ can be obtained in a similar manner (Fig. 2, c and d).

Thus, a compensating network which would bring the dynamic properties of the given system closer to the optimum properties will represent a parallel assembly of networks consisting of differentiating, integrating, and amplifying elements with variable gain values.

A different method of composing the block diagram of compensating networks can be used.

In analyzing Eqs. (6) and (7), the following can readily be noticed. A system with the weighting function $g_{k1}(t,\tau)$ represents a series assembly of systems with the weighting functions $g_{11}^{-}(t,\tau)$ and $g_k^{*}(t,\tau)$. On the other hand, a compensating network with $g_k(t,\tau)$ represents a series assembly of systems with the weighting functions $g_{k1}(t,\tau)$ and $g_{12}^{-}(t,\tau)$. Consequently, the compensating network consists of a series assembly of systems or elements with the weighting functions $g_{11}^{-}(t,\tau)$, $g_k^{*}(t,\tau)$, and $g_{12}^{-}(t,\tau)$. Hence, by the way, the following rule: The weighting function of the middle of the three elements connected in series (see the forward path in Fig. 1b) is determined by substituting the weighting function $g_k^{*}(t,\tau)$ of the entire assembly for the $g_k(t,\tau)$ function which is to be found, and by replacing the weighting functions of the end elements by the corresponding functions of the inverse elements.

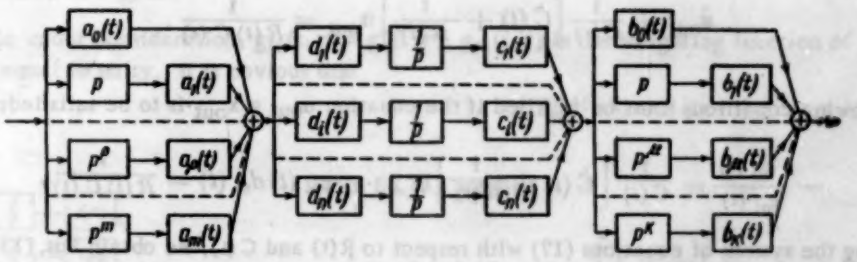

Fig. 3.

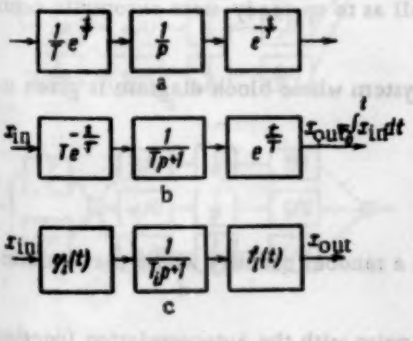

Fig. 4.

By taking into account Eqs. (5), (8), and (9), we obtain the block diagram of the compensating network (Fig. 3).

In constructing actual compensating networks, the realization of the integrating element entails considerable difficulties. A method of accurate replacement of the integrating element by an inertial element with variable parameters [3] is proposed below.

The weighting function of an inertial element with the time constant T is given by

$$g(t,\tau) = \frac{1}{T} e^{-\frac{t}{T}} e^{\frac{\tau}{T}}.$$

The block diagram of such an element can be represented in the form shown in Fig. 4a. If we connect amplifying elements whose variable gains are respectively equal to $Te^{-t/T}$ and $e^{t/T}$ to the input and output of such an element, we shall obtain an integrating element (Fig. 4b).

The block diagram of a system with the weighting function $g_{0i}(t, \tau)$ can be now represented in the form shown in Fig. 4c, where the following notation has been introduced:

$$\varphi_i(t) = T_i d_{0i}(t)\, e^{-\frac{t}{T_i}}, \quad f_i(t) = c_{0i}(t)\, e^{\frac{t}{T_i}}. \tag{12}$$

In practice, such a system can be realized in the form of an RC-filter (Fig. 5) with a variable resistor and a variable capacitor.

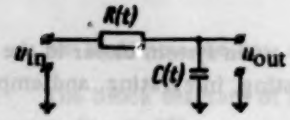

Fig. 5.

The resistance R(t) is determined according to the equation

$$R(t) = \frac{1}{d_{0i}(t)}\, e^{\int_0^t c_{0i}(\eta)\, d_{0i}(\eta)\, d\eta}. \tag{13}$$

The capacitor variable capacitance is given by the equation

$$C(t) = \frac{1}{c_{0i}(t)}\, e^{-\int_0^t c_{0i}(\eta) d_{0i}(\eta)\, d\eta} \tag{14}$$

Equations (13) and (14) are derived on the basis of the following principles. By using the diagrams in Figs. 2a and 5, we can readily obtain the differential equations describing the operation of the corresponding dynamic systems:

$$\dot{x}_{out} - \frac{\dot{c}_{0i}(t)}{c_{0i}(t)} x_{out} = c_{0i}(t)\, d_{0i}(t)\, \dot{x}_{in}, \tag{15}$$

$$\dot{u}_{out} + \frac{1}{C(t)}\left[\dot{C}(t) + \frac{1}{R(t)}\right] u_{out} = \frac{1}{R(t)\, C(t)}. \tag{16}$$

The following conditions must be fulfilled if the equation $u_{out} = x_{out}$ is to be satisfied:

$$-\frac{\dot{c}_{0i}(t)}{c_{0i}(t)} = \frac{1}{C(t)}\left[\dot{C}(t) + \frac{1}{R(t)}\right], \qquad c_{0i}(t)\, d_{0i}(t) = \frac{1}{R(t)\, C(t)}. \tag{17}$$

By solving the system of equations (17) with respect to R(t) and C(t), we obtain Eqs. (13) and (14).

The $c_{0i}(t)$ and $d_{0i}(t)$ functions are components of the weighting function $g_{0i}(t, \tau)$. For the element in question, $c_{0i}(t) = d_{0i}(t) = 1$. By using Eqs. (13) and (14), we find: $R(t) = e^t$, $C(t) = e^{-t}$.

The considered synthesis method is applicable to steady-state as well as to unsteady-state automatic control systems.

Example. The following signal acts on the output of the dynamic system whose block diagram is given in Fig. 1a:

$$Z(t) = S(t) + X(t),$$

where S(t) is the signal useful portion, and X(t) is the noise.

The useful signal is a linear function of time, S(t) = Ut, where U is a random quantity whose mathematical expectation is equal to zero and whose dispersion is D_u.

We shall assume that the interference is given in the form of white noise with the autocorrelation function

$$K_x(t, \tau) = k_0 \delta(t - \tau).$$

The forward path of the system's block diagram contains an inertial element, the inverse weighting function of which is given by

$$g_1^{-}(t, \tau) = \frac{T}{k}\,\delta(t-\tau) + \frac{1}{k}\,\delta(t-\tau). \tag{18}$$

Feedback is provided by an integrating element with the weighting function

$$g_2(t, \tau) = 1(t-\tau). \tag{19}$$

It is necessary to determine the block diagram and the parameters of compensating networks which would secure the separation of the useful signal derivative from noise with the minimum root-mean-square error.

The weighting function of a dynamic system which would be optimum in the above sense can be determined by using the well-known methods [1]. In this case,

$$g_0(t, \tau) = \frac{D_u \tau}{1 + \frac{D_u}{3k_0}\,t^3}. \tag{20}$$

It is obvious that

$$g_0(t, \tau) = f_0(t)\,\varphi_0(\tau), \tag{21}$$

where

$$f_0(t) = \frac{D_u}{1 + \frac{D_u}{3k_0}\,t^3}, \tag{22}$$

$$\varphi_0(\tau) = \tau. \tag{23}$$

We shall assume that the compensating networks with the weighting function $g_k(t, \tau)$ are connected to the system in the manner shown in Fig. 1b.

In the example under consideration, $g_{11}(t, \tau) = g_1(t, \tau)$; $g_{12}(t, \tau)$ is the weighting function of the amplifying element whose gain is equal to unity. It is obvious that

$$g_{12}^{-}(t, \tau) = \delta(t-\tau). \tag{24}$$

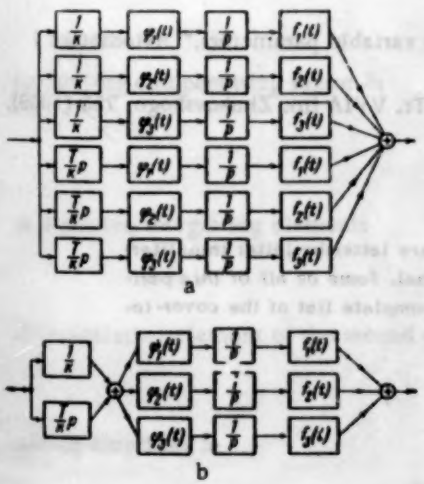

a

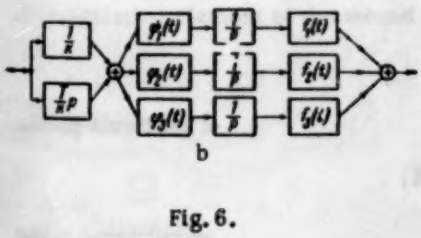

b

Fig. 6.

From Eq. (4), we find

$$g_k^{\bullet}(t, \tau) = f_0(t)\,\varphi_0(t) + \int_{\tau}^{t} g_k^{\bullet}(t, \eta) \int_{\tau}^{\eta} f_0(\xi)\,\varphi_0(\tau)\,1(h-\xi)\,d\xi\,d\eta. \tag{25}$$

We shall assume that the first approximation provides a sufficiently accurate solution of the integral equation (21). Then,

$$g_k^{\bullet}(t, \tau) = f_1(t)\,\varphi_1(\tau) + f_2(t)\,\varphi_2(\tau) + f_3(t)\,\varphi_3(\tau), \tag{26}$$

where

$$f_1(t) = f_0(t), \quad f_2(t) = f_0(t)\,b(t), \quad f_3(t) = -f_0(t)\,c(t),$$

$$\varphi_1(\tau) = [\varphi_0(\tau)\,a(\tau)\,c(\tau) - \varphi_0(\tau)\,b(\tau) + \varphi_0(\tau)],$$

$$\varphi_2(\tau) = \varphi_0(\tau), \quad \varphi_3(\tau) = \varphi_0(\tau)\,a(\tau),$$

$$b(t) = \int_0^{\tau} \varphi_0(\eta)\,a(\eta)\,d\eta,$$

$$c(t) = \int_0^{t} \varphi_0(\eta)\,d\eta, \quad a(t) = \int_0^{t} f(\xi)\,d\xi.$$

If we know (18) and (26), by using Eq. (6), we find

$$g_{k1}(t,\tau) = \frac{1}{k}[f_1(t)\varphi_1(\tau) + f_2(t)\varphi_2(\tau) + f_3(t)\varphi_3(\tau)] + \int_{\tau}^{t} \frac{T}{k}\delta(\eta-\tau) f_1(t)\varphi_1(\eta)\,d\eta +$$

$$+ \int_{\tau}^{t} \frac{T}{k}\delta(\eta-\tau) f_2(t)\varphi_2(\eta)\,d\eta + \int_{\tau}^{t} \frac{T}{k}\delta(\eta-\tau) f_3(t)\varphi_3(\eta)\,d\eta.$$

By using Eq. (7) and by taking into account Eq. (24), we find that $g_{k1}(t,\tau) = g_k(t,\tau)$.

In correspondence with Figs. 2a and 2b, we shall obtain the block diagram of the compensating networks (Fig. 6a).

The structural transformations are given in Fig. 6b.

The same diagram will be obtained if the compensating networks are realized directly as a series assembly of systems with the weighting functions $g_{11}^{-}(t,\tau)$, $g_k^{*}(t,\tau)$, $g_{12}^{-}(t,\tau)$.

The actual expressions for the $f_1(t)$, $\varphi_1(t)$, $f_2(t)$, $\varphi_2(t)$, $f_3(t)$, $\varphi_3(t)$ functions depend on the $f_0(t)$ and $\varphi_0(t)$ functions, as can be seen from the equations. In determining a(t), b(t), and c(t), the integration can be performed analytically, numerically, or graphically. No substantial difficulties will be encountered in this.

In the example under consideration, the a(t) and c(t) functions can be determined analytically in a relatively simple manner: They are given by the following expressions:

$$a(t) = \frac{\alpha D_u}{3}\left[\frac{1}{2}\ln\frac{(t+\alpha)^2}{t^2-\alpha t+\alpha^2} + \sqrt{3}\operatorname{arc\,tg}\frac{t\sqrt{3}}{2\alpha-t}\right],$$

$$c(t) = \frac{1}{2}t^2, \qquad \alpha = \sqrt[3]{\frac{3k_0}{D_u}}.$$

The b(t) function can be more easily determined by using the numerical or the graphical method.

LITERATURE CITED

1. V. S. Pugachev, Theory of Random Functions and Its Application to Problems in Automatic Control [in Russian] (Fizmatgiz, 1960), 2nd ed.
2. S. V. Mal'chikov, "Synthesis of linear automatic control systems with variable parameters," Avtomatika i Telemekhanika 20, 12 (1959).
3. D. I. Gladkov, "Synthesis of linear unsteady-state dynamic systems," Tr. VVIA im. Zhukovskogo, 753 (1959).

All abbreviations of periodicals in the above bibliography are letter-by-letter transliterations of the abbreviations as given in the original Russian journal. *Some or all of this periodical literature may well be available in English translation.* A complete list of the cover-to-cover English translations appears at the back of this issue.

A SERVOSYSTEM WITH LOGICAL CONTROL

E. K. Shigin

(Voronezh)

Translated from Avtomatika i Telemekhanika, Vol. 22, No. 3,
pp. 314-321, March, 1961
Original article submitted August 5, 1959

The present article describes an electromechanical servosystem where the parameters of the compensating elements change in steps, which is secured by means of a semiconductor logical unit. The logical laws of the parameter jump-like variations are assigned in such a manner that a system with second-order astatism with respect to the control input and with first order astatism with respect to the disturbance is not subject to overcontrol for jump-like control inputs. The experimental results are given.

There are definite limitations imposed on the performance figure of automatic control systems containing compensating elements with nonvariable parameters. For a given system to be controlled and a given final element, the performance figure cannot be improved beyond a certain limiting value [3]. The effect of the element characteristic nonlinearities and the limitation of the maximum allowable acceleration of the quantity to be controlled lower the limiting performance figures.

By securing jump-like or continuous variation of the compensating element parameters during the transient process, the above-mentioned limiting performance figures can be considerably exceeded. Certain possible laws according to which the parameters of the compensating elements (in the first place, differentiating elements) can vary have been described in the literature [2].

A typical block diagram of servosystems which are widely used in technology is shown in Fig. 1 [3 and 4]. A system constructed on the basis of this diagram exhibits second-order astatism with respect to the control input and first-order astatism with respect to the disturbance.

The system consists of elements and factors (Fig. 1) which are described by the following equations, respectively: sensing element 1:

$$x_1 = x_0 - x_7, \tag{1}$$

differentiating compensating element 2:

$$(T_1 p + 1)\, x_2 = K_1 T_1 p x_1, \tag{2}$$

integrating compensating factor 3:

$$x_3 = \frac{K_3}{T_3 p} x_1, \tag{3}$$

or a passive integrating element:

$$(T_3 p + 1)\, x_3 = K_3 x_1, \tag{4}$$

differentiating element of the second order 4:

$$(T_3' p + 1)\, x_4 = -K_3 T_3^2 p^2 x_7, \tag{5}$$

adding amplifier 5:

$$(T_4 p + 1)\, x_5 = K_4 (x_1 + x_2 + x_3 + x_4), \tag{6}$$

power amplifier 6:

$$(T_5 p + 1)\, x_6 = K_5 x_5, \tag{7}$$

system to be controlled 7:

$$(T_7T_6p^2 + T_6p)\,x_7 = x_6 + f(t), \tag{8}$$

where $f(t)$ is the disturbance, x_0 is the command input, x_1 is the error, x_2, x_3, x_4, x_5, and x_6 are the output quantities, T_1, T_2, T_3, T_4, T_5, T_6, and T_7 are the time constants, and K_1, K_2, K_3, K_4, and K_5 are the gains of the respective elements and factors in the system, x_7 is the controlled variable, and p is the differentiation symbol.

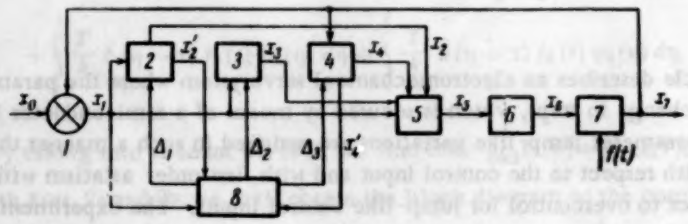

Fig. 1. Servosystem block diagram.

As was shown in [5], jump-like variation of the parameters of differentiating element 2 and integrating element 3 must be secured in such a system in order to reduce the transient process time.

If integration with the opposite sign is introduced together with forced damping, the transient process will take place without excessive overcontrol [6].

By securing the variability of the sign of the element 4 output quantity and the jump-like variation of K_3, we can reduce the transient process time and the maximum deviation of the controlled variable during the stabilization period [7].

The logical laws of the jump-like switching of the parameters of elements and factors 2, 3, and 4 can be written in the following manner:

$$K_1 = \begin{cases} K_{10} & \text{for} \quad x_1x_2' \leqslant 0 \text{ and } x_2'x_4' \leqslant 0, \quad (9) \\ K_{\Delta 1}K_{10} & \text{for} \quad x_1x_2' < 0 \text{ and } x_2'x_4' > 0, \quad (10) \\ K_{\Delta 1}K_{10} & \text{for} \quad x_1x_2' > 0, \quad (11) \end{cases}$$

$$K_2 = \begin{cases} K_{20} & \text{for} \quad x_1x_2' \leqslant 0 \text{ and } x_2'x_4' \leqslant 0, \quad (12) \\ K_{\Delta 2}K_{20} & \text{for} \quad x_1x_2' > 0, \quad (13) \\ -K_{\Delta 2}'K_{20} & \text{for} \quad x_1x_2' < 0 \text{ and } x_2'x_4' > 0 \quad (14) \end{cases}$$

while the equation of factor 3 will be written thus:

$$x_3 = x_{30} + \frac{K_3}{T_3p}\,x_1 \quad \text{or} \quad x_3 = x_{30} + \frac{K_3}{T_3p + 1}\,x_1,$$

where x_{30} is the factor 3 output value at the moment of parameter switching,

$$K_3 = \begin{cases} K_{30} & \text{for} \quad x_1x_2' > 0 \text{ and } x_2'x_4' > 0, \quad (15) \\ -K_{\Delta 3}K_{30} & \text{for} \quad x_1x_2' > 0 \text{ and } x_2'x_4' < 0, \quad (16) \\ K_{30} & \text{for} \quad x_1x_2' \leqslant 0. \quad (17) \end{cases}$$

Here, K_{10}, K_{20}, and K_{30} are the basic gain values of the corresponding elements and factors, $K_{\Delta 1}$, $K_{\Delta 2}$, $K_{\Delta 2}'$, and $K_{\Delta 3}$ are the gains of the corresponding parameters, and

$$x_2' = \frac{K_1'T_1px_1}{T_1p + 1}, \quad x_4' = \frac{K_3'T_3^2p^2x_7}{T_3'p + 1} \quad (K_1' = \text{const}, \quad K_3' = \text{const}).$$

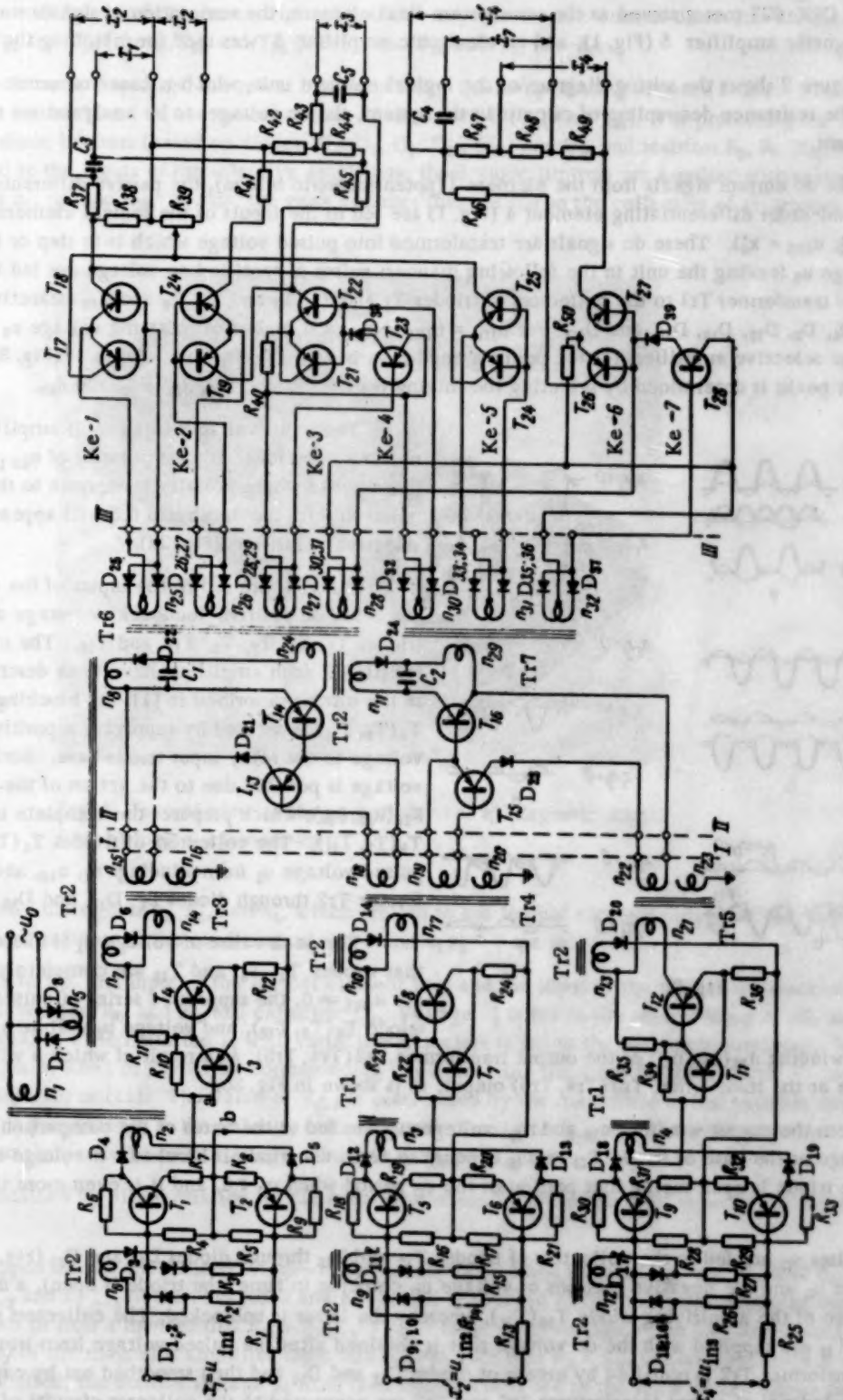

Fig. 2. Wiring diagram of the unit with logical elements.

Logical operations following the laws given by (9)-(17) were realized in an experimental servosystem by means of a unit with logical elements, to the input of which the quantities x_1, x_2^*, and x_4^* were fed. By performing the logical operations of comparing the signs of these quantities, the unit exerts actions Δ_1, Δ_2, and Δ_3 on elements 2, 3, and 4 (Fig. 1) by varying the parameters of the latter.

A DRK-627 motor served as the servosystem final element, the summation of signals was performed by means of a magnetic amplifier 5 (Fig. 1), and an electronic amplifier 6 was used for matching the load.

Figure 2 shows the wiring diagram of the logical element unit, which is based on semiconductors. In order to secure the resistance decoupling of circuits in the system, the dc voltages to be analyzed are transformed into pulses in this unit.

The dc current signals from the element 1 (potentiometric bridge), the passive differentiating element 2, and the second-order differentiating element 4 (Fig. 1) are fed to the inputs of the logical element unit ($u_{in1} = x_1$, $u_{in2} = x_2^*$, $u_{in3} = x_4^*$). These dc signals are transformed into pulsed voltage which is in step or in phase opposition to the dc voltage u_0 feeding the unit in the following manner: pulses of rectified ac voltage are fed from the windings n_2, n_3, and n_4 of transformer Tr1 to the collectors of triodes T_1 and T_2, T_5 and T_6, T_9 and T_{10} (selective amplifiers) through diodes D_4, D_5, D_{12}, D_{13}, D_{18}, and D_{19}. For $u_{in1} = u_{in2} = u_{in3} = 0$, pulses of pulsating voltage u_1 will appear at the output of the selective amplifiers (at the points a and b), as is shown in the time diagrams (Fig. 3a). The magnitude of the pulse peaks is determined by selecting the mixing resistors R_6, R_9, R_{18}, R_{21}, R_{30}, and R_{33}.

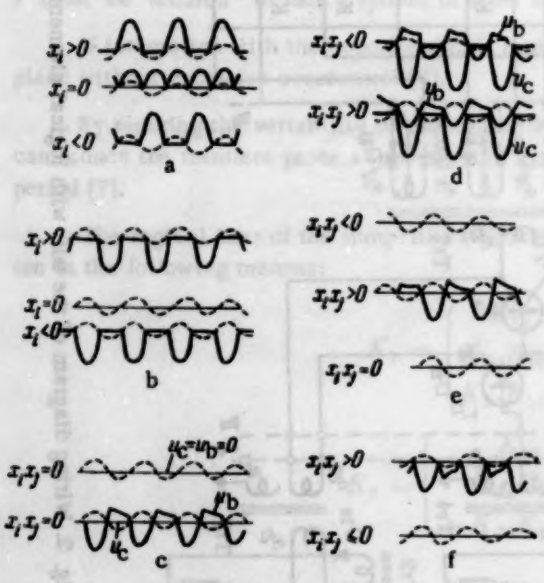

Fig. 3.

The input voltages ($u_{in\,i} \neq 0$) amplify those pulses whose polarity coincides with the polarity of $u_{in\,i}$, and they suppress those pulses whose polarity is opposite to that of $u_{in\,i}$. In this, pulses u_1 with the duty ratio 0.5 will appear at the output of the selective amplifiers (Fig. 3a).

Pulses u_1 are fed to the inputs of the relay amplifiers, which are based on positive-feedback two-stage amplifier circuits with triodes T_3, T_4, T_7, T_8, T_{11}, and T_{12}. The circuits and the characteristics of such amplifiers have been described in [1]. In contrast to the circuit described in [1], the blocking of the output triode T_4 (T_8, T_{12}) is secured by supplying a positive instead of a negative voltage to the relay input triode base. Such action of the positive voltage is possible due to the action of the biasing resistance R_{10} (R_{22}, R_{34}), which prepares the complete unblocking of triode T_3 (T_7, T_{11}). The collectors of triodes T_4 (T_8, T_{12}) are supplied with pulsed voltage u_2 from windings n_7, n_{10}, and n_{13} of the pulse transformer Tr2 through diodes D_8, D_{12}, and D_{20} (Fig. 3b).

The peak value of voltage u_1 is chosen in such a manner that triodes T_4, T_8, and T_{12} are completely blocked for $u_{in\,i} = 0$. For $u_{in\,i} \neq 0$, the suppressed series of pulses u_1 will not block the triode T_4 (T_8, T_{12}), and voltage u_2 will be applied in steps to the primary winding n_{14} (n_{17}, n_{21}) of the output transformer Tr3 (Tr4, Tr5), as a result of which a voltage of complex form will arise at the transformer Tr3 (Tr4, Tr5) output, as is shown in Fig. 3c.

From the output windings n_{18} and n_{19}, voltages u_b are fed to the bases of the comparison triodes T_{13} and T_{15}. If the voltage at the base of triode T_{13} or T_{15} is equal to zero, the triode is blocked. If voltage $u_b \neq 0$ is fed to the base, the triode is open during that portion of the u_b period when $u_b < 0$, and it is even more thoroughly blocked for $u_b > 0$.

Pulses u_c are fed to the collectors of triodes T_{13} and T_{15} through diodes D_{21} and D_{23} (Fig. 3d). In the case where the pulses u_c and the negative portions of voltage u_b coincide in time (the triode is open), a negative voltage is fed to the base of the amplifying triode T_{14} (T_{16}), whereby the latter is unblocked. The collectors of the amplifying triodes T_{14} and T_{16} are supplied with the dc voltage that is obtained after the pulsed voltage from windings n_8 and n_{11} of the pulse transformer Tr2 is rectified by means of diodes D_{22} and D_{24} and then smoothed out by capacitors C_1 and C_2. The primary windings of output transformers Tr6 and Tr7 are connected to the collector circuits of triodes T_{14} and T_{16}. When triodes T_{14} and T_{16} are unblocked, current pulses, which induce a voltage of complex form, u_3, at the outputs of

transformers Tr6 and Tr7, pass through the windings n_{24} and n_{29} (Fig. 3e); after rectification, voltage u_3 is fed to the electronic keys for parameter switching (u_4 in Fig. 3f).

The triode keys are based on an amplifier circuit with a common emitter. When negative voltage u_4 is fed to the bases of triodes T_{17} and T_1 (Fig. 2, Ke-1), both triodes are unblocked, and the resistance for the large signal between the triode collectors drops to 5-10 ohms. The other triode keys for the two current directions consist of triodes T_{19} and T_{20} (Ke-2), T_{21} and T_{22} (Ke-3), T_{24} and T_{25} (Ke-5), and T_{26} and T_{27} (Ke-6).

In most automatic control systems, the power consumption of the compensating network is low. This made it possible to construct a circuit based on low-power triodes P1-G and P2-B (T_{14} and T_{16}). For protecting the input triodes from overloads, diode limiters (based on diodes D_1, D_2, D_9, D_{10}, D_{15}, and D_{16} and resistors R_2, R_3, R_{14}, R_{15}, R_{26}, and R_{27}) are connected to the inputs of the selective amplifiers; these diode limiters are supplied with pulsed blocking voltage from windings n_6, n_9, and n_{12}. In this, the peak voltages that are fed to the collectors of all triodes do not exceed 12 v.

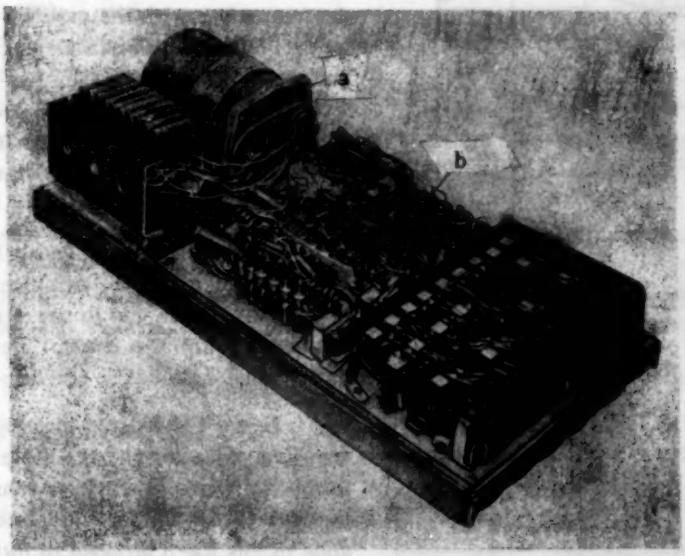

Fig. 4. General view of the control device. a) Magnetic amplifier; b) logical element unit.

In our servosystem, the signals x_1, x_2', and x_4', which are fed to the logical element unit, have polarities for which voltage u_4 appears in jumps if the conditions $x_2'x_4' > 0$ and $x_1x_2' > 0$ are satisfied.

Voltage x_1 is fed to the first input of the logical element unit and the input of the passive differentiating network, which consists of resistors R_{37} and R_{38} and capacitor C_3. Voltage x_2' is fed to the second input of the unit ($u_{in2} = x_2'$), and the signal of differentiation x_4 with variable parameters is fed to the magnetic amplifier. When voltage u_4 is fed to the input of Ke-1 or Ke-2, the corresponding key opens, and the amplification factor K_1 increases in correspondence with Eqs. (10) or (11). The value of $K_{\Delta 1}$ is determined by the magnitude of the variable resistance R_{39}. The voltage that is proportional to the velocity of the controlled variable $\dot{x}_7$, which is obtained from a tachometer generator, is fed to the passive differentiating network (R_{47}, R_{48} and C_4).

The x_4' value, obtained by differentiation for constant parameters, is fed to the third input of the logical element unit ($u_{in3} = x_4'$).

Voltage x_4 is tapped off the unbalanced bridge-which is formed by fixed resistors R_{46}, R_{47}, R_{48}, and R_{49} and the variable resistors R_{Ke-2} and R_{Ke-3} of the keys Ke-2 and Ke-3-and is then fed to the magnetic amplifier input. The arm resistance is chosen in such a manner that $R_{46} + R_{Ke-6} > R_{49}$ if there is no voltage at the key Ke-6 input. The magnitude and polarity of the magnetic amplifier input voltage are such that $K_3 = K_{30}$ in correspondence with (17). If condition (15) is satisfied, the control voltage u_4 from transformer Tr6 is fed to the input of key Ke-6; however, since key Ke-7 is blocked by the control voltage from transformer Tr7 for one current direction, the input of key Ke-6 is shunted, and the latter remains open ($K_3 = K_{30}$).

If the sign relationship (16) is realized, key Ke-7 is deenergized, the shunting of Ke-6 is discontinued, voltage u_4 from Tr6 closes key Ke-6, and the ratio of the bridge arm resistances will be such that $R_{46} + R_{Ke-6} < R_{49}$. As a result of this, the sign and the magnitude of the differentiating network output signal will change in accordance with (16).

The error signal x_1 is fed to the input of the passive integrating network, which connects resistor R_{43}, capacitor C_5, and the unbalanced bridge, which consists of resistors R_{41}, R_{42}, R_{44}, and R_{45}. If condition (13) is satisfied, voltage u_4 causes forced error integration as it arrives at the input of key Ke-2, since $R_{41} + R_{Ke-2} < R_{45} + R_{Ke-3}$ when key Ke-2 closes. At the same time, u_4 arrives at the input of key Ke-4, which shunts the input of key Ke-3, and relationship (13) is realized independently of the sign of $x_2 x_4'$.

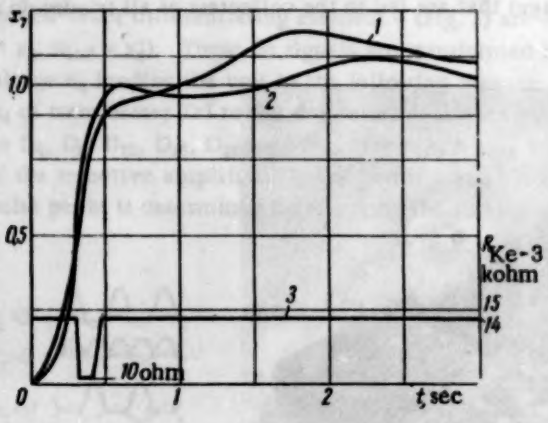

Fig. 5.

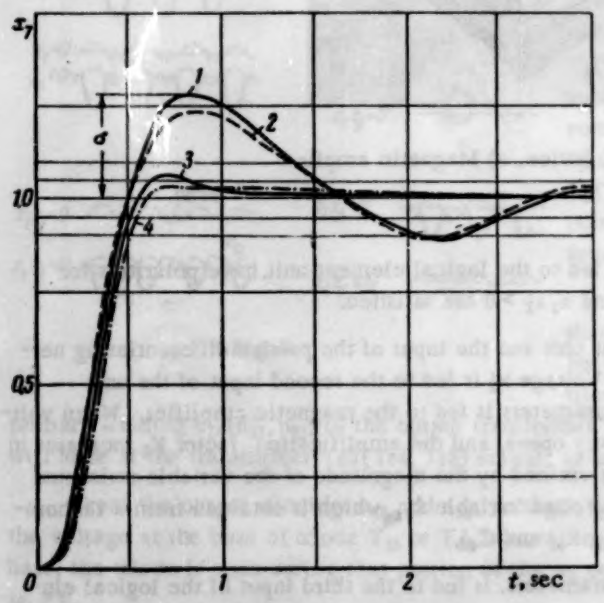

Fig. 6. Transient process curves. 1) Theoretical and 2) experimental curves for a system with constant parameters; 3) theoretical and 4) experimental curves for a system whose parameters change stepwise.

For $x_1 x_2' < 0$, key Ke-2 opens, and the integration is performed with the changed gain $K_2 = K_{20}$ and time constant T_2 (since the change in the time constant T_2 is insignificant in comparison with the gain K_2 variation, the change in T_2 can be neglected in calculating the transient process). If relationship (14) holds, key Ke-4 is open, voltage u_4 from Tr6 closes key Ke-3, and the inequality for the bridge arms is reversed: $R_{41} + R_{Ke-2} > R_{45} + R_{Ke-3}$. In this case, integration of the error with the opposite sign takes place according to (14).

Figure 4 shows the general view of the control device—the summing magnetic amplifier and the logical element unit. This system was in operation under conditions where it tracked jump-like control inputs, which amounted to 6° on the final axle of the potentiometric bridge.

Figure 5 shows the oscillograms of the servosystem transient processes and the diagram representing variations in the resistance of the keys connected to the circuit shown in Fig. 2 (Ke-3 and Ke-4). For condition (14), the resistance of key Ke-3 dropped stepwise almost to zero. In Fig. 5, curve 1 represents the transient process in a system with constant parameters ($K_1 = 7$, $T_1 = 0.15$ sec, $K_2 = 3$, $T_2 = 0.6$ sec, $K_3 = 0$, $K_5 = 1$; $T_4 = T_5 = 0$, $K_6 = 1$, $T_7 = 1.9$ sec, $T_6 = 0.1$ sec); curve 2 represents the transient process in a system where the parameters change stepwise ($K_{10} = 3$, $K_{\Delta 1} = 2$, $T_1 = 0.15$ sec, $K_{20} = 1$, $K_{\Delta 2} = 3$, $K_{\Delta 2}' = 9$; the other parameters are the same); curve 3 indicates the variation in the resistance of keys Ke-3 when the sign of the integrating element input quantity is reversed.

From an analysis of the oscillograms, it is obvious that the introduction of logical control according to the laws given by (9)-(14) makes it possible to obtain a system without considerable overcontrol. Although the introduction of a passive integrating element does not make this system an astatic system of the second order with respect to the control input, the rather short integration time in the transient process allows us to determine the basic dynamic properties of such systems. Due to the variability of the system parameters, it was possible to reduce the transient process time sixfold.

Figure 6 shows the oscillograms of the transient processes in a system with a second-order differentiating element (4 in Fig. 1) and the theoretical curves for the transient processes, which were plotted by using the Bashkirov graphoanalytical method. The parameter values for this system are the same as those obtained before. The param-

eters of the second-order differentiating element for curve 2 are: $K_\beta = 6$, $T_\beta^2 = 0.01\,sec^2$, $T_\beta^1 = 0.007\,sec$; for curve 4, the parameters varied in the following manner: $K_{\beta 0} = 1$, $K_{\Delta\beta} = 6$. In this, the transient process time was reduced by a factor of 4.5, and overcontrol was reduced sixfold.

CONCLUSIONS

1. We have presented one of the methods for the contactless variation of the compensating element parameters in a servosystem by using a semiconductor logical unit with the aim of improving the transient process quality.

2. The logical laws governing the variation of the system parameters make it possible to reduce four- to sixfold the transient process time and overcontrol.

LITERATURE CITED

1. F. L. Varpakhovskii and R. A. Lipman, "Contactless relay with semiconductor triodes," Avtomatika i Telemekhanika, 19, 11 (1958).
2. Science Abstracts. Problems in the Theory of Nonlinear Automatic Control and Regulation Systems [in Russian] (AN SSSR Press, 1957), ed. by Ya. Z. Tsypkin.
3. Automatic Control Fundamentals [in Russian] (Mashgiz, 1954), ed. by V. V. Solodovnikov.
4. T. N. Sokolov, Automatic Control Electromechanical Systems [in Russian] (Gosénergoizdat, 1952).
5. E. K. Shigin, "Improvement of transient processes by means of compensating elements with variable parameters," Avtomatika i Telemekhanika, 19, 4 (1958).
6. E. K. Shigin, "Synthesis of automatic control systems where the integrating compensating elements have alternating-sign inputs," Nauchnye Doklady Vysshei Shkoly, Machine and Instrument Construction, 1 (1958).
7. E. K. Shigin, "Regulation of automatic control systems by means of units with logical and operational elements," Nauchnye Doklady Vysshei Shkoly, Machine and Instrument Construction, 1 (1959).

ON THE THEORY OF SINGLE-TYPE INTERCOUPLED AUTOMATIC CONTROL SYSTEMS WITH SYMMETRIC CROSS-COUPLING NETWORKS

V. T. Morozovskii

(Moscow)

Translated from Avtomatika i Telemekhanika, Vol. 22, No. 3,
pp. 322-337, March, 1961
Original article submitted April 15, 1960

The principles of the synthesis of equivalent single-loop systems for single-type multichannel automatic control systems with symmetric cross-coupling networks are considered. The concept of synchronizing and averaging cross-coupling networks is introduced and a method for determining reduced disturbances is given.

Introduction

Intercoupled automatic control systems with symmetric cross-coupling networks are used fairly often in practice. Such systems consist of several identical automatic control channels which are intercoupled by means of equal cross-coupling networks. As an example, we can cite a system consisting of n identical electric power generators which are equipped with identical regulators and which operate on a common line; a two-channel servosystem for controlling the position of an axis in space; a system for controlling several duplicate-milling machines; computers, etc.

The feasibility of developing a special theory for systems of this type, which would considerably simplify the stability analysis, was indicated in a paper by A. A. Krasovskii [1]. This paper presented the concept of symmetric and antisymmetric cross-coupling networks in such systems and provided a method for investigating two-channel single-type systems with antisymmetric coupling networks by means of complex transfer functions. The present paper is concerned with the further development of methods for investigating such automatic control systems and with the extension of these methods to a special class of single-type multichannel systems which are characterized by the presence of the so-called synchronizing and averaging cross-coupling networks.

The block diagram of a single-type multichannel automatic control system is shown in Fig. 1. In single-type automatic control systems, the input and output variables of identical elements are identical physical quantities. For the purpose of simplifying the analysis of such systems, it is convenient to introduce the concept of two types of motion for the input and output variables of identical elements. The motion of the first type is the averaged motion, which corresponds to the average value of the input and output variables of identical elements. We shall assume that the number of channels in a single-type automatic control system is equal to n. We shall denote by i the number of the identical elements under consideration (in Fig. 1, the number of elements in a single channel is equal to m). The average value of the variable for the ith identical elements is equal to

$$x_{i+} = \frac{1}{n}\sum_{k=1}^{n} x_{ik}, \tag{1}$$

where x_{i+} is the average value of the variable of the ith element group, and x_{ik} is the variable value of the ith element in the kth channel. The average values of variables for all other elements are determined in a similar manner. Motions of the second type are relative motions which correspond to the difference between the input and output variables of identical elements. These differences can be conveniently taken with respect to any single channel, for instance, the first channel. Thus, for the kth channel (Fig. 1), we can write

$$x_{ik-} = x_{i1} - x_{ik}. \tag{2}$$

It is obvious that for n channels there must be (n-1) such independent relative motions. Actually, a physical system whose parameters are strictly identical cannot be realized. Therefore, the question arises whether the idealization which forms the basis of the consideration of single-type intercoupled systems is admissible: Is there a possibility that the small-value parameters which interfere with the identity of channels will cause substantial changes in the transient processes in the system?

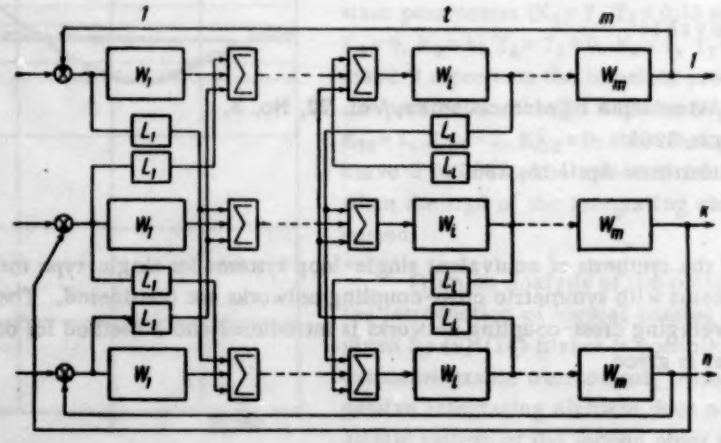

Fig. 1.

The small-value parameters which disturb the identity of channels in the system should be divided into two types.

Small-value parameters of the first type (for instance, parasitic time constants) raise the order of the single-channel differential equation from N to N+ν, i.e., they change the system's structure. In this case, the general dif-

ferential equation of the system will have additional roots, which are located at a considerable distance from the Nn basic roots, and the Nn basic roots are subject to small changes if the parameters of this type are small. When these small-value parameters tend to zero, the basic Nn roots are shifted toward values which correspond to the identity of channels, and the additional roots tend to infinity. M. V. Meerov devoted a number of papers [2 and 3] to the investigation of the effect of small-value parameters of this type. M. V. Meerov found that the linear systems belonging to the large class which also comprises the multichannel systems considered in the present article are approximate in the sense defined by A. A. Andronov.

Small-value parameters of the second type are such that they do not raise the order of the differential equation of a single channel, i. e., they do not affect the system's structure. Such small-value parameters comprise, for instance, small differences between gains or time constants in identical channels. The presence of small-value parameters of this type changes the arrangement of the roots of the general differential equation; however, not all of the N(n-1) roots are multiple roots. It is known that the roots of a linear differential equation are continuous functions of its parameters [4]. Therefore, if the initial single-type automatic control system has a sufficiently large stability margin, small-value parameters of the second type cannot substantially change the character of the system's motion. Thus, the multichannel single-type linear systems considered in the present article are approximate in A.A. Andronov's sense, and a small departure from the identity of channels will cause a small deviation of the transient processes in comparison with the processes corresponding to the perfect identity of channels.

Transfer Functions of the Equivalent Elements

In order to investigate the averaged and the relative motions, it is necessary to compose equivalent block diagrams for these motions. These block diagrams represent simple single-loop control systems, and they contain some equivalent elements whose transfer functions can be readily determined. The form of equivalent element transfer functions is determined by the character of the symmetric cross-coupling networks that are present in the system.

Symmetric cross-coupling networks connecting identical elements are networks which transmit the signals from the outputs of identical elements to the inputs of the subsequent or preceding elements in other channels in the same proportion and with the same sign. Figure 1 shows examples of symmetric cross-coupling networks. There are forward and feedback symmetric cross-coupling networks. A forward symmetric cross-coupling network is a network through which the signal from the output of an element in one channel is transmitted to the outputs (or inputs) of the subsequent identical elements in other channels. In Fig. 1, the first group of identical elements is provided with forward symmetric cross-coupling networks with the transfer functions L_1 (for the sake of clarity, Fig. 1 shows only three channels). Symmetric cross-coupling feedback networks are those through which the signal from the output of an element in one channel is transmitted to the inputs of the preceding identical elements in other channels. In Fig. 1, the ith group of identical elements is provided with symmetric cross-coupling feedback networks with the transfer functions L_i. Let us first consider the case where the identical elements are provided with forward cross-coupling networks with the transfer functions L. From the definition of the forward cross-coupling network for the ith group of identical elements, we can write the following n equations:

$$x_{ik\,\mathrm{out}} = W_i x_{ik\,\mathrm{in}} + L\sum_{\substack{j=1\\ j\neq k}}^{n} x_{ij\,\mathrm{in}} \qquad (k = 1, 2, \ldots, n), \tag{3}$$

where $x_{ik\,\mathrm{out}}$ is the output variable of the ith element in the kth channel, $x_{ik\,\mathrm{in}}$ is the input variable of the ith element in the kth channel, W_i is the transfer function of the ith element, and L is the transfer function of the forward cross-coupling network. By summing these n equations, we obtain

$$\sum_{k=1}^{n} x_{ik\,\mathrm{out}} = W_i \sum_{k=1}^{n} x_{ik\,\mathrm{in}} + L\left(n\sum_{j=1}^{n} x_{ij\,\mathrm{in}} - \sum_{k=1}^{n} x_{ik\,\mathrm{in}}\right).$$

Considering that

$$\sum_{k=1}^{n} x_{ik\,\mathrm{out}} = n x_{i\,\mathrm{out}+}, \qquad \sum_{k=1}^{n} x_{ik\,\mathrm{in}} = n x_{i\,\mathrm{in}+},$$

we finally obtain

$$x_{i\,\mathrm{out}+} = [W_i + (n-1)L]\, x_{i\,\mathrm{in}+}.$$

Thus, in the presence of a forward symmetrical cross-coupling network for averaged motion, the transfer function of the equivalent element in a single-type multichannel system is given by

$$W_{i+} = \frac{x_{i\,\text{out}+}}{x_{i\,\text{in}+}} = W_i + (n-1)L. \tag{4}$$

For determining the relative transfer function of the equivalent element, we shall subtract the output variable of the row j ($j \leq n$, $j \neq k$) from the output variable of row k in the system of equations (3):

$$x_{ik\,\text{out}} - x_{ij\,\text{out}} = W_i(x_{ik\,\text{in}} - x_{ij\,\text{in}}) + L(x_{ij\,\text{in}} - x_{ik\,\text{in}}).$$

Hence,

$$x_i = \frac{x_{ik\,\text{out}} - x_{ij\,\text{out}}}{x_{ik\,\text{in}} - x_{ij\,\text{in}}} = W_i - L. \tag{5}$$

From the definition of the cross-coupling feedback network for the ith group of identical elements, we have

$$x_{ik\,\text{out}} = W_i\left(x_{ik\,\text{in}} + L\sum_{\substack{j=1\\ j\neq k}}^{n} x_{ij\,\text{out}}\right) \qquad (k = 1, 2, \ldots, n). \tag{6}$$

By adding the left-hand and right-hand sides of the equations for all elements, we obtain

$$\sum_{k=1}^{n} x_{ik\,\text{out}} = W_i\left[\sum_{k=1}^{n} x_{ik\,\text{in}} + L\left(n\sum_{j=1}^{n} x_{ij\,\text{out}} - \sum_{k=1}^{n} x_{ik\,\text{out}}\right)\right]$$

or, by taking into account (1),

$$x_{i\,\text{out}+} = \frac{W_i}{1-(n-1)W_iL}\, x_{i\,\text{in}+}.$$

Thus, the transfer function of the equivalent element for averaged motion in the presence of cross-coupling feedback networks is given by

$$W_{i+} = \frac{W_i}{1-(n-1)W_iL}. \tag{7}$$

In order to find the transfer function of the equivalent element for relative motion, we shall subtract the jth row from the kth row in the system of equations (6):

$$x_{ik\,\text{out}} - x_{ij\,\text{out}} = W_i[x_{ik\,\text{in}} - x_{ij\,\text{in}} + L(x_{ij\,\text{out}} - x_{ik\,\text{out}})].$$

Hence, the transfer function for relative motion is given by

$$W_{i-} = \frac{W_i}{1+W_iL}. \tag{8}$$

Superimposed Cross-Coupling Networks

The above expressions for the equivalent transfer functions for relative and averaged motion pertain to the case where identical elements are provided only with forward or only with feedback symmetric cross-coupling networks. In practice, cases are encountered where identical elements are provided with superimposed forward and feedback cross-coupling networks.

Let us consider the typical cases of such superpositions of cross-coupling networks. Figure 2 shows the block diagram of a portion of a single-type multichannel system where the ith identical elements are provided with forward as well as feedback symmetric cross-coupling networks. In the block diagram of Fig. 2, the summation of signals from the feedback cross-coupling networks is performed up to the point from which the signals to be transmitted to the inputs of the symmetric forward networks are tapped off, and the summation of signals from the forward cross-

coupling networks is performed beyond the point from which the signals for the inputs of the symmetric feedback networks are tapped off. For determining the transfer functions of the equivalent element for relative and averaged motion, we shall write the equations relating the inputs and outputs of identical elements. For the ith identical elements, we can write

$$x_{ik\,\mathrm{out}} = W_i\lambda_{ik} + L_1\sum_{\substack{j=1\\ j\neq k}}^{n}\lambda_{ij} \quad \text{or} \quad x_{ik\,\mathrm{out}} = W_i\lambda_{ik} + L_1\sum_{j=1}^{n}\lambda_{ij} - L_1\lambda_{ik} \tag{9}$$

$$(k = 1, 2, \ldots, n),$$

where λ_{ik} is the input variable of the ith identical element in the kth channel, and L_1 is the transfer function of the forward cross-coupling network.

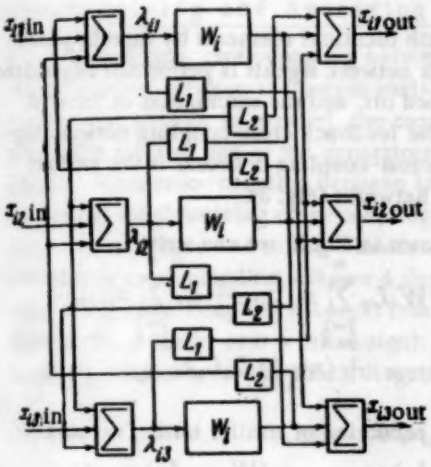

Fig. 2.

For λ_{ik}, we can write

$$\lambda_{ik} = x_{ik\,\mathrm{in}} + W_iL_2\sum_{\substack{j=1\\ j\neq k}}^{n}\lambda_{ij}$$

or

$$\lambda_{ik} = x_{ik\,\mathrm{in}} + W_iL_2\sum_{j=1}^{n}\lambda_{ij} - W_iL_2\lambda_{ik},$$

where L_2 is the transfer function of the feedback cross-coupling network. Hence,

$$\lambda_{ik} = \frac{x_{ik\,\mathrm{in}} + W_iL_2\sum_{j=1}^{n}\lambda_{ij}}{1 + W_iL_2}. \tag{10}$$

After adding the last expressions with respect to k (k = 1, 2, . . . , n), we obtain

$$(1 + W_iL_2 - nW_iL_2)\sum_{j=1}^{n}\lambda_{ij} = \sum_{k=1}^{n}x_{ik\,\mathrm{in}}$$

or

$$\sum_{j=1}^{n}\lambda_{ij} = \frac{\sum_{k=1}^{n}x_{ik\,\mathrm{in}}}{1 - (n-1)W_iL_2}. \tag{11}$$

In order to determine the equivalent transfer function for relative motion, we shall subtract the row j from row k in the system of equations (9):

$$x_{ik\,\mathrm{out}} - x_{ij\,\mathrm{out}} = (W_i - L_1)(\lambda_{ik} - \lambda_{ij}).$$

By substituting the pertinent expressions (10) for λ_{ik} and λ_{ij}, we obtain

$$x_{ik\,\mathrm{out}} - x_{ij\,\mathrm{out}} = (W_i - L_1)\frac{x_{ik\,\mathrm{in}} - x_{ij\,\mathrm{in}}}{1 + W_iL_2},$$

whence

$$W_- = \frac{x_{ik\,\mathrm{out}} - x_{ij\,\mathrm{out}}}{x_{ik\,\mathrm{in}} - x_{ij\,\mathrm{in}}} = \frac{W_i - L_1}{1 + W_iL_2}. \tag{12}$$

For determining the equivalent transfer functions for averaged motion, we shall add all n equations (9):

$$\sum_{k=1}^{n}x_{ik\,\mathrm{out}} = (W_i - L_1)\sum_{k=1}^{n}\lambda_{ik} + nL_1\sum_{k=1}^{n}\lambda_{ik}.$$

By substituting the found expression (11) for $\sum_{k=1}^{n} \lambda_{ik}$, we obtain

$$\sum_{k=1}^{n} x_{ik\,\text{out}} = \frac{W_i - L_1 + nL_1}{1-(n-1)W_iL_2} \sum_{k=1}^{n} x_{ik\,\text{in}},$$

whence

$$W_{i+} = \frac{\sum_{k=1}^{n} x_{ik\,\text{out}}}{\sum_{k=1}^{n} x_{ik\,\text{in}}} = \frac{W_i + (n-1)L_1}{1-(n-1)W_iL_2}. \tag{13}$$

A similar result is obtained for the second variant of coverage of the ith identical elements by superimposed cross-coupling networks, when the summation of the cross-coupling feedback network signals is performed beyond the point from which the signals of the forward cross-coupling networks are tapped off, and the summation of forward cross-coupling network signals is performed ahead of the point from which the feedback cross-coupling network signals are tapped off. Another variant of superimposed forward and feedback cross-coupling networks is the variant where the forward cross-coupling networks are enclosed inside the feedback networks (Fig. 3).

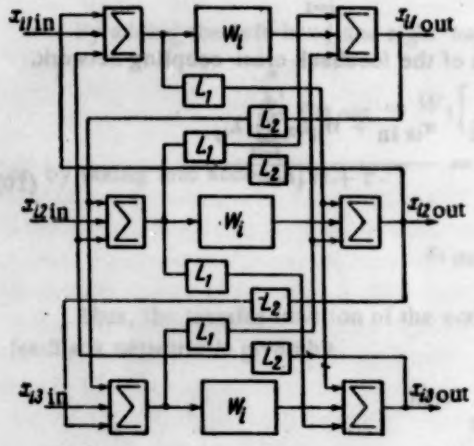

Fig. 3.

For the block diagram shown in Fig. 3, we can write

$$x_{ik\,\text{out}} = W_i x_{ik\,\text{in}} + W_iL_2 \sum_{\substack{j=1 \\ j\neq k}}^{n} x_{ij\,\text{out}} + L_1 \sum_{\substack{j=1 \\ j\neq k}}^{n} x_{ij\,\text{in}} +$$
$$+ (n-2)L_1L_2 \sum_{\substack{j=1 \\ j\neq k}}^{n} x_{ij\,\text{out}} + (n-1)L_1L_2 x_{ik\,\text{out}}.$$

After transformations and reduction of similar terms, we obtain

$$(1 + W_iL_2 - L_1L_2)\, x_{ik\,\text{out}} = (W_i - L_1)\, x_{ik\,\text{in}} +$$
$$+ [W_iL_2 + (n-2)\, L_1L_2] \sum_{j=1}^{n} x_{ij\,\text{out}} + L_1 \sum_{j=1}^{n} x_{ij\,\text{in}}. \tag{14}$$

By subtracting the jth row from kth row, we obtain

$$(1 + W_iL_2 - L_1L_2)(x_{ik\,\text{out}} - x_{ij\,\text{out}}) = (W_i - L_1)(x_{ik\,\text{in}} - x_{ij\,\text{in}}),$$

whence

$$W_{i-} = \frac{x_{ik\,\text{out}} - x_{ij\,\text{out}}}{x_{ik\,\text{in}} - x_{ij\,\text{in}}} = \frac{W_i - L_1}{1 + W_iL_2 - L_1L_2}. \tag{15}$$

By adding all n equations (14) and by reducing the similar terms, we have

$$[1 - (n-1)W_iL_2 - L_1L_2 - (n-2)nL_1L_2] \sum_{k=1}^{n} x_{ik\,\text{out}} =$$
$$= (W_i - L_1 + nL_1) \sum_{k=1}^{n} x_{ik\,\text{in}}$$

or

$$W_{i+} = \frac{W_i + (n-1)L_1}{1-(n-1)W_iL_2 - (n-1)^2L_1L_2}. \tag{16}$$

By using a similar procedure, we can readily find the equivalent transfer functions for the last variant of superimposed cross-coupling networks, where the feedback cross-coupling networks are internal and the forward ones are external networks. In this case, the equivalent transfer function for relative motion is given by

$$W_{i-} = \frac{W_i - W_i L_1 L_2 - L_1}{1 + W_i L_2}, \tag{17}$$

while, for averaged motion, we have

$$W_{i+} = \frac{W_i + (n-1)L_1 - (n-1)^2 W_i L_1 L_2}{1 - (n-1) W_i L_2}. \tag{18}$$

Synchronizing and Averaging Cross-Coupling Networks

In practice, cross-coupling between identical channels in single-type control systems is often a consequence of the difference between the output variables of identical elements. Thus, for instance, in a system of synchronous generators that operate in parallel, the cross-coupling of generators through the common load appears only in the case where the rotor of one of the generators starts to run out (to lead or to lag) with respect to the rotors of the other machines. Such cross-coupling between identical elements of single-type multichannel automatic control systems will be termed synchronizing cross-coupling [5]. Let us find the expressions for the transfer functions of equivalent elements for averaged and relative motion for the case where the ith identical elements are encompassed by forward synchronizing cross-coupling. Figure 4 shows a section of a multichannel single-type control system with forward synchronizing cross-coupling networks (the synchronizing cross-coupling with the unit transfer function is conventionally denoted by a circle with a minus sign). By using the definition of synchronizing cross-coupling, we can write the following n equations for the block diagram shown in Fig. 4:

$$x_{ik\,\mathrm{out}} = W_i x_{ik\,\mathrm{in}} + L \sum_{\substack{j=1 \\ j \neq k}}^{n} (x_{ik\,\mathrm{in}} - x_{ij\,\mathrm{in}}) \qquad (k = 1, 2, \ldots, n), \tag{19}$$

where W_i is the ith element transfer function, and L is the synchronizing cross-coupling transfer function. This system of equations can be rewritten in the following manner:

$$x_{ik\,\mathrm{out}} = [W_i + (n-1)L]\, x_{ik\,\mathrm{in}} - L \sum_{\substack{j=1 \\ j \neq k}}^{n} x_{ij\,\mathrm{in}}.$$

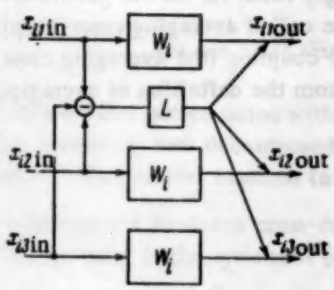

Fig. 4.

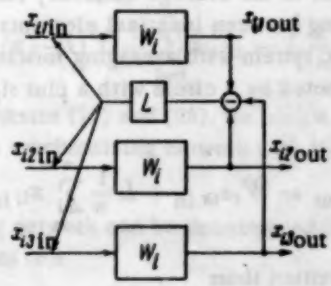

Fig. 5.

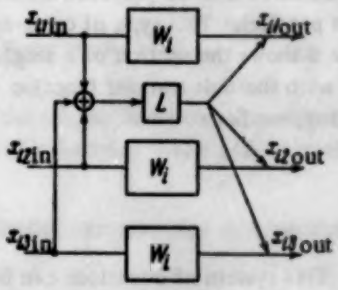

Fig. 6.

This system of equations describes the ith elements of a single-type system with ordinary forward symmetric cross-coupling networks, but with a different transfer function of the ith element [instead of W_i, the element transfer function is $W_i + (n-1)L$]. By using the above equations (4) and (5), we shall find the transfer functions for the equivalent elements: for averaged motion,

$$W_{i+} = [W_i + (n-1)L] + (n-1)(-L) = W_i; \tag{20}$$

for relative motion,

$$W_{i-} = [W_i + (n-1)L] - (-L) = W_i + nL. \tag{21}$$

On the basis of this, we can deduce that synchronizing cross-coupling does not change the character of averaged motion, since the equivalent transfer function for averaged motion is equal to the transfer function of an element in a separate channel. We shall find the equivalent transfer functions for the averaged and relative motion elements for the case where the ith elements are encompassed by synchronizing feedback cross-coupling. Figure 5 shows a section of a single-type multichannel system with synchronizing feedback cross-coupling. For such a block diagram, we can write

$$x_{ik\,\mathrm{out}} = W_i\left[x_{ik\,\mathrm{in}} + L\sum_{\substack{j=1\\ j\neq k}}^{n}(x_{ik\,\mathrm{out}} - x_{ij\,\mathrm{out}})\right]. \tag{22}$$

These equations can be rewritten in a somewhat different form:

$$x_{ik\mathrm{out}} = \frac{W_i}{1-(n-1)W_iL}\left[x_{ik\,\mathrm{in}} - L\sum_{\substack{j=1\\ j\neq k}}^{n} x_{ij\,\mathrm{out}}\right].$$

The obtained system of equations describes the ith elements of a single-type control system with ordinary feedback cross-coupling networks, but with a different transfer function for the ith element. By using the above equations (7) and (8), we shall find the transfer function of the equivalent elements: for averaged motion,

$$W_{i+} = \left[\frac{W_i}{1-(n-1)W_iL}\right]\left[1-(n-1)\frac{W_i}{1-(n-1)W_iL}(-L)\right]^{-1} = W_i; \tag{23}$$

for relative motion,

$$W_{i-} = \left[\frac{W_i}{1-(n-1)W_iL}\right]\left[1+\frac{W_i}{1-(n-1)W_iL}(-L)\right]^{-1} = \frac{W_i}{1-nW_iL}. \tag{24}$$

The same result has been obtained: Synchronizing cross-coupling does not affect averaged motion.

In practice, we can also encounter cross-coupling which is the result of action of the sum of all output and input variables of identical elements. As an example, we can again cite synchronous generators operating in parallel, when their frequency (or voltage) regulators are connected to common bus-bars. In this, the frequency (or voltage) compensation will be provided with respect to the average frequency (or voltage) value for all the generators operating in parallel. This type of cross-coupling between identical elements will be called averaging cross-coupling. Figure 6 shows the section of a single-type system with averaging forward cross-coupling (the averaging cross-coupling with the unit transfer function is denoted by a circle with a plus sign). From the definition of averaging cross-coupling, we have

$$x_{ik\,\mathrm{out}} = W_i x_{ik\,\mathrm{in}} + L\frac{1}{n}\sum_{j=1}^{n} x_{ij\,\mathrm{in}}. \tag{25}$$

This system of equations can be rewritten thus:

$$x_{ik\,\mathrm{out}} = \left(W_i + \frac{L}{n}\right)x_{ik\,\mathrm{in}} + \frac{L}{n}\sum_{\substack{j=1\\ j\neq k}}^{n} x_{ij\,\mathrm{in}}.$$

This system of equations describes the ith elements of a single-type control system with an ordinary forward cross-coupling network, but with a different transfer function of the ith element [$W_i + (1/n)L$ instead of W_i]. According to (5) and (4), the equivalent transfer functions of an element with forward averaging cross-coupling are given by:

for relative motion,

$$W_{i-} = W_i + \frac{L}{n} - \frac{L}{n} = W_i; \tag{26}$$

for averaged motion,

$$W_{i+} = W_i + \frac{L}{n} + (n-1)\frac{L}{n} = W_i + L. \tag{27}$$

It is obvious that averaging cross-coupling does not affect relative motion. By using a similar procedure, we can readily find the equivalent transfer functions for the case where the identical elements are encompassed by averaging feedback cross-coupling. For this, the equivalent transfer function for relative motion will be

$$W_{i-} = W_i, \tag{28}$$

while, for averaged motion, we shall have

$$W_{i+} = \frac{W_i}{1 - W_i L}. \tag{29}$$

A similar result is also obtained in this case: Averaging cross-coupling does not affect relative motion.

It can happen that, along with simple symmetric cross-coupling, synchronizing and averaging cross-coupling is also present in a single-type intercoupled automatic control system. Considering the simplicity of investigating intercoupled single-type systems where only synchronizing and averaging cross-coupling is present, it is convenient first to reduce all simple cross-coupling networks to synchronizing and averaging networks. Let us first consider how a simple forward symmetric cross-coupling network should be decomposed into a synchronizing and an averaging network. For the ith group of identical elements with forward symmetric cross-coupling, the n equations (3) hold. Let us transform the last term in this system of equations:

$$L\sum_{\substack{j=1\\ j\neq k}}^{n} x_{ij\,\mathrm{in}} = \frac{n-1}{n} L\sum_{j=1}^{n} x_{ij\,\mathrm{in}} + \frac{1}{n} L\sum_{j=1}^{n} x_{ij\,\mathrm{in}} - \frac{1}{n} L n x_{ik\,\mathrm{in}} =$$

$$= \frac{n-1}{n} L\sum_{j=1}^{n} x_{ij\,\mathrm{in}} - \frac{L}{n}\sum_{j=1}^{n} (x_{ik\,\mathrm{in}} - x_{ij\,\mathrm{in}}).$$

The system of equations (3) can now be rewritten thus:

$$x_{ik\,\mathrm{out}} = W_i x_{ik\,\mathrm{in}} + (n-1)\, L\frac{1}{n}\sum_{j=1}^{n} x_{ij\,\mathrm{in}} - L\frac{1}{n}\sum_{j=1}^{n} (x_{ik\,\mathrm{in}} - x_{ij\,\mathrm{in}}). \tag{30}$$

If we compare the last equation with the systems (19) and (25), we notice that the simple forward symmetric cross-coupling network is now decomposed into a synchronizing network with the transfer function $-L/n$ and an averaging network with the transfer function $(n-1)L$.

A symmetric feedback cross-coupling network can be decomposed in a similar manner. For this, we shall transform the last term in the system of equations (6):

$$L\sum_{\substack{j=1\\ j\neq k}}^{n} x_{ij\,\mathrm{out}} = (n-1)\, L\frac{1}{n}\sum_{j=1}^{n} x_{ij\,\mathrm{out}} - L\, x_{ik\,\mathrm{out}} + \frac{1}{n}\sum_{j=1}^{n} L x_{ik\,\mathrm{out}} =$$

$$= (n-1)\, L\frac{1}{n}\sum_{j=1}^{n} x_{ij\,\mathrm{out}} - L\frac{1}{n}\sum_{j=1}^{n} (x_{ik\,\mathrm{out}} - x_{ij\,\mathrm{out}}).$$

The system of equations (6) can now be written thus:

$$x_{ik\,\mathrm{out}} = W_i\left[x_{ik\,\mathrm{in}} + (n-1)\, L\frac{1}{n}\sum_{j=1}^{n} x_{ij\,\mathrm{out}} - L\frac{1}{n}\sum_{j=1}^{n} (x_{ik\,\mathrm{out}} - x_{ij\,\mathrm{out}})\right]. \tag{31}$$

Thus, the feedback cross-coupling network is now decomposed into a feedback synchronizing network with the transfer function $-L/n$ and feedback averaging network with the transfer function $(n-1)L$.

Equivalent Disturbances

In determining the transfer functions for averaged and relative motion, nothing has been said about disturbances that may be present at the inputs of identical elements. By using the superposition principle, we can formulate a rule for determining reduced disturbances for equivalent elements for averaged and relative motion.

We shall first assume that the disturbance q_{ik} acts at the input of the kth element in the ith group of identical elements. This disturbance can be represented in the form of the sum

$$q_{ik} = \frac{1}{n} q_{ik} + \frac{n-1}{n} q_{ik}.$$

We shall now assume that identical and opposed disturbances $\frac{1}{n} q_{ik}$ act at the inputs of the identical elements with the exception of the kth element. Then, we can consider that two disturbance systems act at the identical element inputs. The first disturbance system consists of n equal disturbance functions $(1/n)q_{ik}$. This disturbance system must be taken into account only in investigating averaged motion; it does not affect to any extent the relative motions. Thus, the equivalent disturbance for averaged motion will be $(1/n)q_{ik}$. The second disturbance system consists of $n-1$ equal disturbances $-(1/n)q_{ik}$, which act at the inputs of all elements with the exception of the kth element, and of the disturbance $\frac{n-1}{n} q_{ik}$, which acts at the kth element input. The sum of all these disturbances is equal to zero, and, therefore, the latter disturbance system does not exert any influence on averaged motion. For all relative motions with the exception of the kth motion, the equivalent disturbance for the second disturbance system is equal to zero, and, for the kth relative motion, the equivalent disturbance is equal to

$$q_{i1k-} = \frac{1}{n} q_{ik} - \frac{n-1}{n} q_{ik} = -q_{ik}.$$

Following a similar procedure, it can be readily shown that, in the general case, when disturbances act at the inputs of all identical elements, the equivalent disturbance for averaged motion is equal to

$$q_{ik+} = \frac{1}{n} \sum_{j=1}^{n} q_{ij}, \tag{32}$$

while, for relative motions, we have

$$q_{i1j-} = q_{i1} - q_{ij}. \tag{33}$$

In investigating the quality of control processes for relative motion, the greatest of all the $\frac{1}{2} n(n-1)$ disturbances should be selected, since this would represent the most adverse case.

As an illustration of the practical application of the concept of synchronizing and averaging cross-coupling, we shall consider here an example of the composition of equivalent block diagrams for the averaged and relative motions of a single-type control system consisting of n identical synchronous generators which operate in parallel with a common load and which are equipped with speed regulators, excitation regulators, and devices for the uniform distribution of resistive and reactive power. The schematic diagram for the parallel operation of single-type synchronous generators is shown in Fig. 7 (for clarity, only two generators are shown). The synchronous generators G are driven by piston motors, turbines, or hydraulic drives, which are provided with speed regulators SR. The synchronous generators are equipped with excitation regulators ER. Facilities for the automatic equalization of the resistive and the reactive power, based on the virtual statism method, are provided in the system [6]. Frequency compensators FC, which act on the speed regulators of the generator drives, serve for the automatic resistive power distribution. Voltage compensators VC, which act on the generator excitation regulators, serve for the automatic reactive power distribution. The frequency and the voltage compensators are controlled by the resistive load distributing device ResLDD and the reactive load distributing device ReaLDD. The frequency and voltage compensators are also controlled with respect to the average frequency and voltage values in the common bus-bars.

The following assumptions were made in composing the system equations:

1. All of the n units that operate in parallel are identical.

2. The generators operate with a fixed resistive load in the line, which is located symmetrically with respect to all the generators.

3. The effect of the stator aperiodic current components and the corresponding rotor periodic current components is not taken into account.

4. It is assumed that the generators are not provided with antihunt windings.

5. The synchronous generators have equal reactances in the longitudinal and transverse directions (the resistance of the stator windings is neglected). The last three assumptions are not basic, and the equations can be written without these assumptions.

The equations for the kth unit in operator form for the zero initial conditions are given below. The equations are written in relative units, while the steady-state values of the variables are taken as the basic quantities.

The drive equation for the kth unit is

$$(sT_M + R - 1)\,\nu_k = \sigma_k - Au_{Gk} - L_1\,\frac{1}{n}\sum_{j=1}^{n} u_{Gj} - L_2 \sum_{\substack{j=1 \\ j\neq k}}^{n} (\nu_k - \nu_j) + q_k.$$

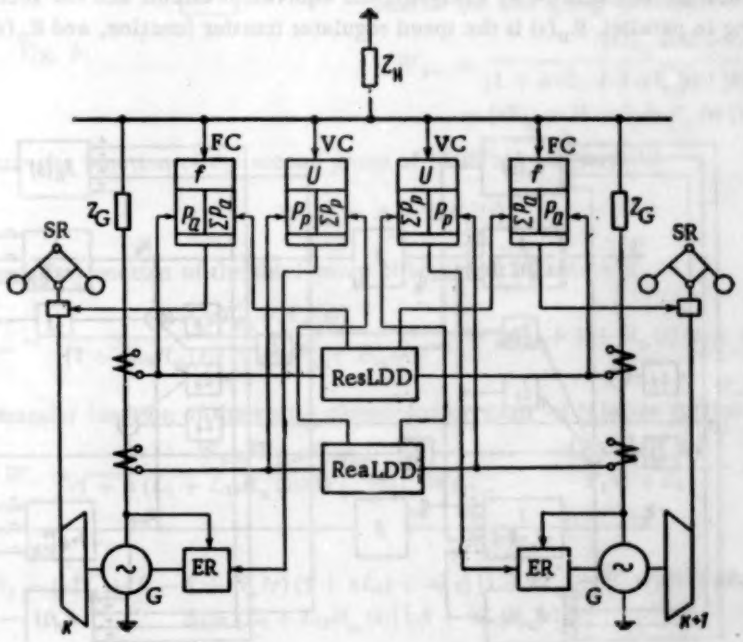

Fig. 7.

The equation of the speed regulator for the kth unit is

$$\sigma_k = -R_v(s)\,(\nu_k + \zeta_k).$$

The equation of the frequency compensator for the kth unit is

$$\zeta_k = L_3\,\frac{1}{h}\sum_{j=1}^{n}\nu_j + L_4\sum_{j=1}^{n}(u_{Gk} - u_{Gj}) + L_5\sum_{\substack{j=1 \\ j\neq k}}^{n}(\nu_k - \nu_j).$$

The equation of the electromagnetic processes in the kth unit generator is

$$(1 + sT'_{ex})\, u_{Gk} = e_{dek} + L_6 \frac{1}{n} \sum_{j=1}^{n} u_{Gj} - L_7 \sum_{\substack{j=1 \\ j \neq k}} (v_k - v_j).$$

The equation of the excitation regulator for the kth unit is

$$e_{dek} = -R_u(s)\,(u_{Gk} + \xi_k).$$

The equation of the voltage compensator for the kth unit is

$$\xi_k = L_8 \frac{1}{n} \sum_{j=1}^{n} u_{Gj} + L_9 \sum_{\substack{j=1 \\ j \neq k}}^{n} (u_{Gk} - u_{Gj}) + L_{10} \sum_{\substack{j=1 \\ j \neq k}}^{n} (v_k - v_j).$$

In all these equations, v_k is the relative rotating speed of the kth unit, σ_{1k} is the relative output variable of the kth unit speed regulator, ξ_k is the relative output variable of the kth unit frequency compensator, u_{Gk} is the relative voltage at the terminals of the kth synchronous generator, e_{dek} is the relative output variable of the kth unit excitation regulator, ξ_k is the relative output variable of the kth unit voltage compensator, q_k is the relative disturbance, A, L_1, L_2, L_3, L_4, L_5, L_6, L_7, L_8, L_9, and L_{10} are coefficients (generally operator coefficients) which depend on the system parameters and which are determined by analyzing the equivalent circuit and the vector diagrams of the synchronous machines operating in parallel, $R_v(s)$ is the speed regulator transfer function, and $R_u(s)$ is the excitation regulator transfer function.

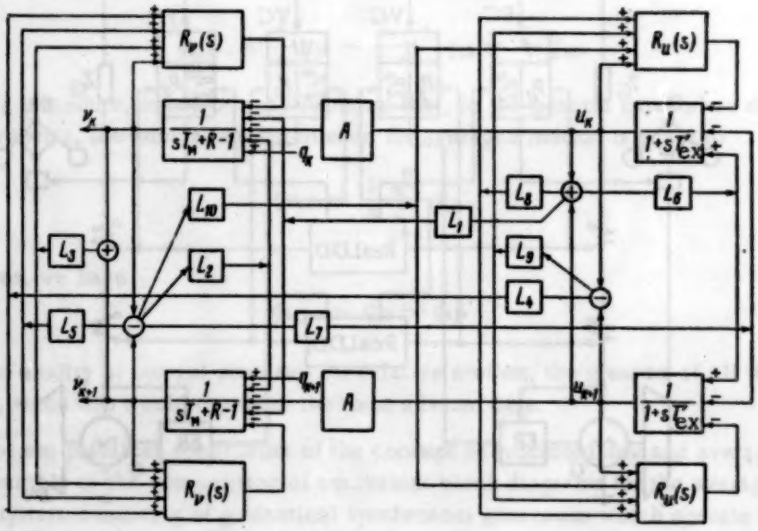

Fig. 8.

Figure 8 shows the block diagram of a system which is based on the above equations. For the sake of simplicity, only two units are shown in this block diagram. It follows from the above block diagram that a system consisting of n identical synchronous generators which operate in parallel represents a single-type multichannel automatic control system with symmetric synchronizing and averaging cross-coupling networks.

In investigating the stability of the system's relative motion, all averaging cross-couplings must be excluded from consideration. By using the detecting properties of the elements and the superposition principle, the block diagram for relative motion can be reduced to the form shown in Fig. 9. By combining the drive element with the speed regulator element and the generator element with the excitation regulator element, we obtain a block diagram representing a series assembly of three groups of identical elements.

The first group of identical elements with the transfer functions $[sT_M + R - 1 + R_v(s)]^{-1}$ is encompassed by negative synchronizing feedback couplings with the transfer functions $L_2 + L_5 R_v(s)$. The second group of identical elements with the transfer functions A is encompassed by negative forward synchronizing couplings with the transfer functions $L_4 R_v(s)$. The third group of identical elements with the transfer functions $[sT'_{ex} + 1 + R_u(s)]^{-1}$ is encompassed by negative synchronizing feedback couplings with the transfer functions $L_9 R_u(s)$. All of the three groups of identical elements are encompassed by negative synchronizing feedback couplings with the transfer functions $L_7 + L_{10} R_u(s)$.

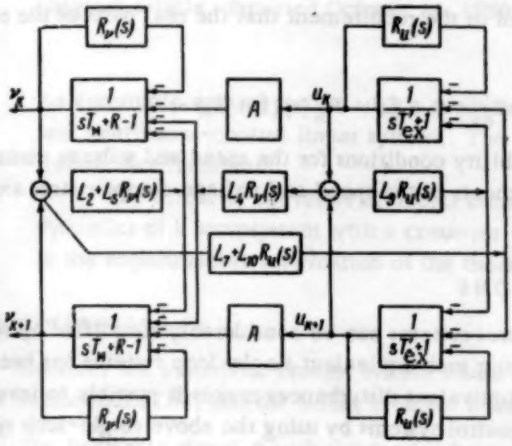

Fig. 9.

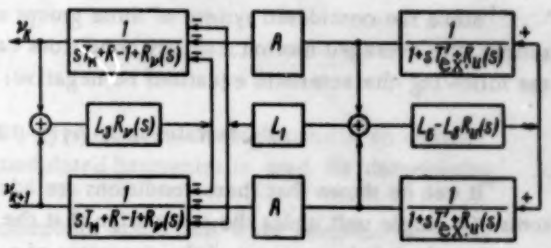

Fig. 10.

By using the above equations (21) and (24), we find the transfer functions of the individual groups of elements and of the system as a whole. The equivalent transfer function of the first group of identical elements is given by

$$W_{I-} = \frac{[sT_M + R - 1 + R_v(s)]^{-1}}{[1 + n(L_2 + L_5 R_v(s))]\,[sT_M + R - 1 + R_v(s)]^{-1}} = [sT_M + R - 1 + R_v(s)(1 + nL_5) + nL_2]^{-1}.$$

The equivalent transfer function of the second group of identical elements is

$$W_{II-} = A + L_4 R_v(s).$$

The equivalent transfer function of the third group of identical elements is

$$W_{III-} = \frac{[1 + sT'_{ex} + R_u(s)]^{-1}}{[1 + nL_9 R_u(s)]\,[1 + sT'_{ex} + R_u(s)]^{-1}} = [sT'_{ex} + 1 + R_u(s)(1 + nL_9)]^{-1}.$$

The equivalent transfer function of the entire closed-loop system for relative motion is given by

$$W_- = \frac{W_{I-} W_{II-} W_{III-}}{1 + n(L_7 + L_{10} R_u(s)) W_{I-} W_{II-} W_{III-}} = \frac{A + nL_4 R_v(s)}{S_1 + nS_2},$$

where

$$S_1 = [sT_M + R - 1 + R_v(s)(1 + nL_5) + nL_2]\,[1 + sT'_{ex} + R_u(s)(1 + nL_9)],$$
$$S_2 = [L_7 + L_{10} R_u(s)]\,[A + nL_4 R_v(s)].$$

Thus, the conditions for stable relative motion of a system consisting of n single-type synchronous generators which operate in parallel can be reduced to the requirement that the real parts of the roots of the following characteristic equation be negative:

$$[sT_M + R - 1 + R_v(s)(1 + nL_5) + nL_2]\,[1 + sT'_{ex} + R_u(s)(1 + nL_9)] + n[L_7 + L_{10} R_u(s)]\,[A + nL_4 R_v(s)] = 0.$$

The conditions for stable averaged motion can be determined in a similar manner. In this, the synchronizing cross-couplings must be excluded from consideration. The block diagram for averaged motion is shown in Fig. 10. The equivalent transfer functions for all of the three groups of identical elements can be found by using Eqs. (27) and (29). The equivalent transfer function for the first group of identical elements is

$$W_{I+} = [sT_M + R - 1 + R_v(s)(1 + L_5)]^{-1}.$$

The equivalent transfer function for the second group of identical elements is

$$W_{II+} = A - L_1.$$

The equivalent transfer function for the third group of identical elements is

$$W_{III+} = [sT'_{ex} + 1 - L_e + R_u(s)(1 + L_s)]^{-1}.$$

Since the considered system of three groups of identical elements for averaged motion represents an open-loop system, the averaged motion stability conditions can be reduced to the requirement that the real parts of the roots of the following characteristic equations be negative:

$$sT_M + R - 1 + R_v(s)(1 + L_s) = 0, \qquad sT'_{ex} + 1 + L_e - R_u(s)(1 + L_s) = 0.$$

It can be shown that these conditions are adequate as stability conditions for the speed and voltage control systems of a single unit under the assumption that the sensing elements of the speed and voltage compensators are connected to the bus-bars proper of the generator of a single unit.

CONCLUSIONS

The analysis of single-type multichannel automatic control systems can be considerably simplified by reducing them to equivalent single-loop systems. A method for composing such equivalent single-loop systems has been presented in this article. The described method for determining equivalent disturbances makes it possible to investigate not only the stability, but also the performance of automatic control systems by using the above single-loop systems. The concept of synchronizing and averaging cross-coupling networks has been introduced, and a rule for decomposing simple cross-coupling networks into synchronizing and averaging networks has been presented.

The investigation of single-type intercoupled automatic control systems with synchronizing and averaging cross-couplings has been greatly simplified due to the fact that relative motion is invariant with respect to signals that have passed through averaging cross-coupling networks and with respect to disturbances, which are equal for all channels, while averaged motion is invariant with respect to signals that have passed through synchronizing cross-coupling networks and with respect to disturbances, whose sum is equal to zero for all channels.

LITERATURE CITED

1. A. A. Krasovskii, "On two-channel automatic control systems with antisymmetric couplings," Avtomatika i Telemekhanika, 18, 2 (1957).
2. M. V. Meerov, "Consideration of small-value parameters in investigating the stability of self-regulation systems," Élektrichestvo, 6 (1947).
3. M. V. Meerov, Structural Synthesis of High-Accuracy Automatic Control Systems [in Russian] (Fizmatgiz, 1959).
4. K. P. Persidskii, "On the characteristic numbers of differential equations," Izvest. AN Kazakh. SSR, Mathematics and Mechanics Sect., 1 (1947).
5. V. T. Morozovskii, "Selective invariance in single-type intercoupled systems," Invariance Theory and Its Application to Automatic Devices [in Russian] (AN Ukr. SSR Press, 1959).
6. A. G. Moskalev, Automatic Frequency Regulation in Power Systems [in Russian] (Gosénergoizdat, 1952).

All abbreviations of periodicals in the above bibliography are letter-by-letter transliterations of the abbreviations as given in the original Russian journal. *Some or all of this periodical literature may well be available in English translation.* A complete list of the cover-to-cover English translations appears at the back of this issue.

THE TRANSFER FUNCTION OF AN AUTOMATIC CONTROL SYSTEM WITH A MODULATOR AND A HALF-WAVE DEMODULATOR

E. L. L'vov

(Moscow)

Translated from Avtomatika i Telemekhanika, Vol. 22, No. 3,
pp. 338-349, March, 1961
Original article submitted October 24, 1960

An automatic control system with a modulator and a half-wave demodulator is reduced to an equivalent continuous-control linear system. The method of modulated harmonics is used for determining the transfer functions.

The effect of converter elements consisting of a modulator and a half-wave demodulator on the dynamics of a servosystem with a crossover frequency of 25 cps is investigated. The results obtained in the experimental verification of the theoretical data are given.

1. Introduction

Consider the automatic control system whose block diagram is given in Fig. 1. The modulator M, the half-wave demodulator DM, and the linear element L form a closed group. Disturbance x_d acts on the system.

The harmonic signal ϑ with the carrier frequency ω_0, which is modulated by signal θ and is fed to the modulator input, is produced at the modulator output:

$$\vartheta(t) = K_M \theta(t) \sin \omega_0 t. \tag{1}$$

The demodulator rectifies the signal $\vartheta(t)$ with respect to the sign of the modulating signal $\theta(t)$. It is assumed that the coupling between the modulator and the demodulator is inertialess.

The demodulator output signal is expressed by the equation

$$\eta(t) = K_1 \theta(t) A(\omega_0 t), \tag{2}$$

where

$$\begin{aligned} A(\omega_0 t) &= \sin \omega_0 t \quad \text{for} \quad 2n\pi < \omega_0 t < (2n+1)\pi. \\ & \qquad (n = 0, 1, 2, 3) \\ A(\omega_0 t) &= 0 \quad \text{for} \quad (2n+1)\pi < \omega_0 t < (2n+2)\pi. \end{aligned} \tag{3}$$

The demodulator output signal $\eta(t)$ consists of a sequence of positive sinusoidal half-waves, which are modulated by the mismatching $\theta(t)$. The diagrams of $\theta(t)$, $A(\omega_0 t)$ and $\eta(t)$ are given in Fig. 2.

We shall assume that the transfer function

$$Y_L(s) = \frac{x(s)}{\eta(s)} \tag{4}$$

for the element L is known.

The system under consideration belongs to the class of unsteady-state linear systems with a periodically changing parameter. Such systems are often encountered in automatic control technology. As an example, we shall cite a servosystem where selsyns play the role of the summing unit and the modulator, a diode phase detector acts as the demodulator, and an amplifier and a motor represent the linear element.

The presence of a section with a modulator and a demodulator for which Eq. (2) holds in the automatic control loop entails certain difficulties in determining the transfer function of the closed-loop system. In analysis, it is customary to circumvent these difficulties by replacing the half-wave demodulator by an ideal one. In using this approach, the modulator input quantity is related to the demodulator output quantity by the equation

$$\eta(t) = K_p \theta(t), \tag{5}$$

where K_p are the amplification factors of the modulator–demodulator element.

The present article is concerned with the determination of the closed-loop transfer function where the relationship between the modulator input quantity and the demodulator output quantity as expressed by Eq. (2) is taken into account and also with the determination of the conditions under which the replacement of the half-wave demodulator by an ideal one is admissible.

We shall solve the stated problem by using the method of modulated harmonics [1], which we have used before for determining the transfer function of a step automatic control system.

2. Expansion of the Input and Output Quantities of Elements into Modulated Harmonic Series

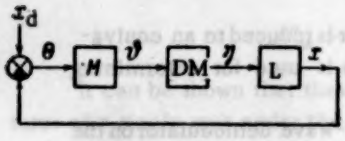

Fig. 1.

As was mentioned above, the demodulator output signal $\eta(t)$ represents a sequence of positive half-waves of the $A(\omega_0 t)$ sinusoid, which is modulated by mismatching $\theta(t)$. The function $A(\omega_0 t)$ can be expanded into a Fourier series and represented as a harmonic sum. The demodulator output signal $\eta(t)$ can then be considered as a harmonic series where the harmonic amplitudes vary in time.

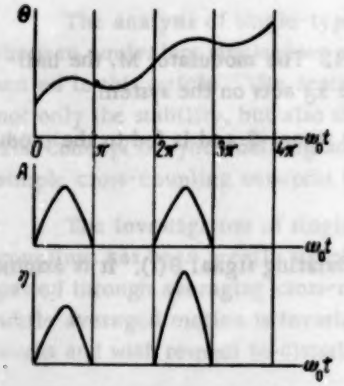

Fig. 2. Time diagrams of the mismatching θ, the transforming function A, and the demodulator output signal.

The $\eta(t)$ harmonics will pass through the linear element L and the summing unit. The output signals $x(t)$ of the linear element and $\theta(t)$ of the summing unit will also consist of harmonics whose amplitudes change in time:

$$\eta(t) = \sum_{k=-\infty}^{+\infty} \eta_k(t)\, e^{jk\omega_0 t},$$
$$x(t) = \sum_{k=-\infty}^{+\infty} x_k(t)\, e^{jk\omega_0 t}, \qquad (6)$$
$$\theta(t) = \sum_{k=-\infty}^{+\infty} \theta_k(t)\, e^{jk\omega_0 t}.$$

The $\eta_k(t)$, $x_k(t)$, and $\theta_k(t)$ functions define the variation in time of the kth harmonic amplitudes of the signals $\eta(t)$, $x(t)$, and $\theta(t)$.

We shall assume that the functions $\eta_k(t)$, $x_k(t)$, and $\theta_k(t)$ for all k from $-\infty$ to $+\infty$ satisfy the conditions under which Fourier transformation is possible. We shall denote by $\eta_k(\omega)$, $x_k(\omega)$, $\theta_k(\omega)$ and $x_d(\omega)$ the Fourier images of the functions $\eta_k(t)$, $x_k(t)$, $\theta_k(t)$, and $x_d(t)$.

The ratio of the image of the controlled variable kth harmonic amplitude to the disturbance image,

$$Y_c(\omega)_k = \frac{x_k(\omega)}{x_d(\omega)}, \qquad (7)$$

will be called the complex transfer function of the closed-loop system with respect to the kth harmonic.

The problem consists in determining the transfer functions $Y_c(\omega)_k$.

We shall write the equations relating the images of the amplitudes of harmonics η, x, and θ to the image of x_d.

The summing unit equations will relate $x_k(\omega)$ and $\theta_k(\omega)$ to $x_d(\omega)$, the modulator–demodulator equations will relate $\theta_k(\omega)$ to $\eta_k(\omega)$, and the linear element equations will relate $\eta_k(\omega)$ to $x_k(\omega)$.

a) Equations of the Summing Unit

Let us substitute in the summing unit equation

$$x(t) + \theta(t) = x_d(t) \qquad (8)$$

the values of x(t) and θ(t) from Eq. (6):

$$\sum_{k=-\infty}^{+\infty} [x_k(t) + \theta_k(t)]\, e^{jk\omega_0 t} = x_d(t). \tag{9}$$

Equation (9) will be identically satisfied for any t if the amplitudes of the harmonics are balanced:

$$x_0(t) + \theta_0(t) = x_d(t), \quad x_k(t) + \theta_k(t) = 0 \quad (k \neq 0). \tag{10}$$

The balance equations for the harmonic amplitude originals will correspond to the balance equations for the images:

$$x_0(\omega) + \theta_0(\omega) = x_d(\omega), \quad x_k(\omega) + \theta_k(\omega) = 0 \quad (k \neq 0). \tag{11}$$

b) Modulator–Demodulator Equations

Let us expand the function $A(\omega_0 t)$, which is expressed by Eq. (3), in a Fourier series that is given by

$$A(\omega_0 t) = \sum_{-\infty}^{+\infty} c_n e^{jn\omega_0 t}, \tag{12}$$

where

$$\begin{aligned} c_n &= -\frac{1}{\pi(n-1)(n+1)} \quad \text{for } n = 0, \pm 2, \pm 4, \ldots; \\ c_n &= 0 \quad \text{for } n = \pm 3, \pm 5, \pm 7, \ldots; \\ c_1 &= -c_{-1} = \frac{1}{4j}. \end{aligned} \tag{13}$$

By substituting θ(t) from (6) and $A(\omega_0 t)$ from (12) in Eq. (2), we obtain

$$\eta(t) = K_1 \Big[\sum_{k=-\infty}^{+\infty} \theta_k(t)\, e^{jk\omega_0 t}\Big]\Big[\sum_{n=-\infty}^{+\infty} c_n e^{jn\omega_0 t}\Big]. \tag{14}$$

After performing the multiplication operations and grouping the terms with equal exponents, we obtain, in correspondence with (6), the equations relating the amplitudes of harmonics η and θ:

$$\eta_k(t) = K_1 \sum_{n=-\infty}^{+\infty} c_n \theta_{n+k}(t) \quad (k = -\infty \text{ to } +\infty). \tag{15}$$

By applying Fourier transformation to (15), we obtain a system of equations which relate the images of the amplitudes of harmonics η and θ:

$$\eta_k(\omega) = K_1 \sum_{n=-\infty}^{+\infty} c_n \theta_{n+k}(\omega) \quad (k = -\infty \text{ to } +\infty). \tag{16}$$

c) Linear Element Equation

Let us denote by $\eta_{k,\omega_0}(t)$ and $x_{k,\omega_0}(t)$ the kth modulated harmonics at the linear element input and output:

$$\eta_{k,\omega_0}(t) = \eta_k(t)\, e^{jk\omega_0 t}, \quad x_{k,\omega_0}(t) = x_k(t)\, e^{jk\omega_0 t}. \tag{17}$$

The images of the modulated harmonics will be denoted by $\eta_{k,\omega_0}(\omega)$ and $x_{k,\omega_0}(\omega)$, respectively.

Let us apply Fourier transformation to Eqs. (17), denoting the variable in the region of images by Ω_k. By taking into account the the displacement theorem, we obtain

$$\eta_{k,\omega_0}(\Omega_k) = \eta_k(\Omega_k - k\omega_0), \quad x_{k,\omega_0}(\Omega_k) = x_k(\Omega_k - k\omega_0). \tag{18}$$

The images of the linear element input and output quantities are related by the linear element complex transfer function $Y_L(\Omega_k)$:

$$x_{k,\omega_0}(\Omega_k) = Y_L(\Omega_k)\,\eta_{k,\omega_0}(\Omega_k). \tag{19}$$

From (18) and (19), we obtain

$$x_k(\Omega_k - k\omega_0) = Y_L(\Omega_k)\,\eta_k(\Omega_k - k\omega_0). \tag{20}$$

We substitute for the independent variable of the image region by putting

$$\Omega_k - k\omega_0 = \omega. \tag{21}$$

Then,

$$x_k(\omega) = Y_L(\omega + k\omega_0)\,\eta_k(\omega) \quad (k = -\infty \text{ to} + \infty). \tag{22}$$

The system of equations (22) establishes a relationship between the images of the harmonic amplitudes at the linear element output and input.

3. Transfer Functions for the Amplitudes of the Controlled Variable Harmonics

Equations (11), (16), and (22) relate the images of the harmonic amplitudes of signals $\theta(t)$, $\eta(t)$, and $x(t)$ to the image of disturbance $x_d(t)$.

By eliminating the images of the amplitudes of harmonics $\eta_k(\omega)$ and $\theta_k(\omega)$, we obtain a system of equations which relates $x_k(\omega)$ to $x_d(\omega)$:

$$x_k(\omega) + K_1 Y_L(\omega + k\omega_0) \sum_{n=-\infty}^{+\infty} c_n x_{n+k}(\omega) = K_n c_{-k} Y_L(\omega + k\omega_0)\, x_d(\omega)$$
$$(k = -\infty \text{ to} + \infty). \tag{23}$$

The system of equations (23) can be solved for any x_k, and, in correspondence with (7), the closed-loop system transfer functions for the harmonic amplitudes are found.

In the general case, the system (23) consists of an infinite number of equations. In most automatic control systems that are encountered in practice, the linear element L has the properties of a low-frequency filter, and it causes an intensive attenuation of the input signal components, which have relatively high frequencies. In such cases, $x_k(\omega)$ and $Y_L(\omega + k\omega_0)$, which correspond to higher harmonics, can be omitted from the system of equations (23). We shall consider two particular cases.

a) Only the Zero-Harmonic Amplitude Is Retained in the System of Equations (23)

In a certain frequency range, let

$$Y_L(\omega + k\omega_0) = 0 \quad (k \neq 0). \tag{24}$$

The system of equations (23) then assumes the following form:

$$x_0(\omega) + K_1 c_0 Y_L(\omega)\, x_0(\omega) = K_1 c_0 Y_L(\omega)\, x_d(\omega), \tag{25}$$

$$x_k(\omega) = 0 \quad (k \neq 0). \tag{26}$$

Let us denote

$$K_1 c_0 Y_L(\omega) = \frac{K_1}{\pi} Y_L(\omega) = K_p Y_L(\omega) = Y(\omega), \tag{27}$$

where $Y(\omega)$ is the open-loop linear system transfer function, and K_p is gain of M and DM with respect to the direct component.

From Eqs. (7) and (25), by taking into account (27), we find the closed-loop system transfer function for the zero-harmonic amplitude:

$$Y_c(\omega)_0 = \frac{x_0(\omega)}{x_d(\omega)} = \frac{Y(\omega)}{1+Y(\omega)}. \tag{28}$$

Expression (28) corresponds to the transfer function of a linear closed-loop continuous-control system which consists of element L with the transfer function $Y_L(\omega)$ and an inertialess element with the transfer function K_p, which replaces the modulator and the demodulator. Equation (28) corresponds to the case of an ideal demodulator [$K_p=(K_1/\pi)$].

The stability of a closed-loop system with the transfer function (28) can be estimated with respect to the transfer locus $Y(\omega)$ of the open-loop system by using the Nyquist–Mikhailov criterion.

For the determination of stability, it is especially important to know positively the transfer locus portion which lies close to the critical point whose coordinates are -1, j0. For the crossover frequency $\omega=\omega_{co}$, the transfer function modulus is equal to unity. The transfer locus in the crossover vicinity will be determined in a sufficiently reliable manner if the following conditions are satisfied:

$$Y(\omega_{co}+k\omega_0) \approx 0 \quad (k \neq 0). \tag{29}$$

For a positive ω_{co} value and for $k=-1$, the most adverse condition will be

$$Y(\omega_{co}-\omega_0) \approx 0. \tag{30}$$

In calculating the closed-loop system transfer function for the zero-harmonic amplitude, the higher harmonics may be neglected if, for the $\omega_{co}-\omega_0$ frequency, the modulus of the open-loop system transfer function is small in comparison with unity.

b) Only the Amplitudes of the Zero and the First Harmonics Are Retained in the System of Equations (23)

In a certain frequency range, let

$$Y(\omega+k\omega_0)=0 \quad (|k|>1). \tag{31}$$

The system of equations (23) then assumes the following form:

$$\left[c_0+\frac{1}{K_1Y_L(\omega)}\right]x_0(\omega)+c_{-1}x_{-1}(\omega)+c_1x_1(\omega)=c_0x_d(\omega),$$
$$c_1x_0(\omega)+\left[c_0+\frac{1}{K_1Y_L(\omega-\omega_0)}\right]x_{-1}(\omega)+c_2x_1(\omega)=c_1x_d(\omega), \tag{32}$$
$$c_{-1}x_0(\omega)+c_{-2}x_{-1}(\omega)+\left[c_0+\frac{1}{K_1Y_L(\omega+\omega_0)}\right]x_1(\omega)=c_{-1}x_d(\omega),$$

$$x_k(\omega)=0 \quad (|k|>1). \tag{33}$$

We shall solve the system of equations (32) with respect to $x_0(\omega)$, $x_{-1}(\omega)$, and $x_1(\omega)$, and, by using relations (13) and (27) and taking into account (7), we shall find the closed-loop system transfer functions for the zero and the first harmonic amplitudes:

$$Y_c(\omega)_0=\frac{Y_e(\omega)}{1+Y_e(\omega)}, \tag{34}$$

$$Y_c(\omega)_{-1}=\frac{Y_{e-1}(\omega)}{1+Y_e(\omega)},\quad Y_e(\omega)_{+1}=\frac{Y_{e+1}(\omega)}{1+Y_e(\omega)} \tag{35}$$

Here,

$$Y_e(\omega)=Y(\omega)\left[1-\left(\frac{\pi}{4}\right)^2\frac{Y_c(\omega+\omega_0)+Y_c(\omega-\omega_0)-\frac{2}{3}Y_c(\omega+\omega_0)Y_c(\omega-\omega_0)}{1-\frac{1}{9}Y_c(\omega+\omega_0)Y_c(\omega-\omega_0)}\right], \tag{36}$$

$$Y_{e-1}(\omega) = \frac{\pi}{4j} Y_c(\omega - \omega_0) \frac{1 - \frac{1}{3} Y_c(\omega + \omega_0)}{1 - \frac{1}{9} Y_c(\omega + \omega_0) Y_c(\omega - \omega_0)},$$

$$Y_{e+1}(\omega) = \frac{-\pi}{4j} Y_c(\omega + \omega_0) \frac{1 - \frac{1}{3} Y_c(\omega - \omega_0)}{1 - \frac{1}{9} Y_c(\omega + \omega_0)}, \quad (37)$$

where $Y(\omega)$ is the open-loop linear system transfer function which is expressed by Eq. (27), and $Y_c(\omega+\omega_0)$ and $Y_c(\omega-\omega_0)$ are the closed-loop linear system transfer functions for the $\omega+\omega_0$ and $\omega-\omega_0$ frequencies, respectively,

$$Y_c(\omega + \omega_0) = \frac{Y(\omega + \omega_0)}{1 + Y(\omega + \omega_0)}, \quad Y_c(\omega - \omega_0) = \frac{Y(\omega - \omega_0)}{1 + Y(\omega - \omega_0)}. \quad (38)$$

The closed-loop system transfer function $Y_c(\omega)_0$ for the controlled variable zero harmonic, which is expressed by Eq. (34), corresponds to a block diagram where the element with the transfer function $Y_e(\omega)$ is provided with negative feedback (Fig. 3a). According to Eqs. (35), the closed-loop system transfer functions for the harmonics with $k=-1$ and $k=1$ correspond to the block diagrams shown in Figs. 3b and 3c. Thus, a closed loop consisting of a modulator, a half-wave demodulator, a linear element, and a summing unit is equivalent to a linear closed loop without the modulator and the demodulator. The transfer function $Y_e(\omega)$ of the equivalent open-loop linear system is expressed by Eq. (33), and the transfer functions of the equivalent elements whose output quantities correspond to the amplitudes of harmonics with $k=-1$ and $k=1$ are expressed by Eqs. (37).

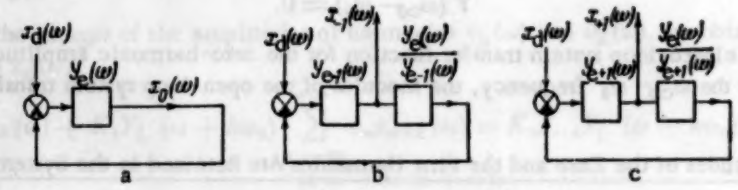

Fig. 3. Block diagrams for the zero (a) and the first (b and c) harmonics of the controlled variable.

It is obvious from Eq. (36) that $Y_e(\omega)$ differs from the open-loop linear system transfer function $Y(\omega)$, which corresponds to the case with an ideal demodulator.

Let us further assume that, for positive ω values in the frequency range $\omega \leq \omega_{co}$ (where ω_{co} is the crossover frequency for which $|Y(\omega_{co})| = 1$), the following inequality is satisfied:

$$|Y(\omega_{co} + \omega_0)| \ll 1. \quad (39)$$

Then, according to (38) and (39),

$$|Y_e(\omega_{co} + \omega_0)| \ll 1. \quad (40)$$

and the terms containing $Y_c(\omega+\omega_0)$ can be omitted in (36) and (37). In this case, the transfer functions of the equivalent linear elements will be expressed by the following equations:

$$Y'_e(\omega) = Y(\omega)\left[1 - \left(\frac{\pi}{4}\right)^2 Y_c(\omega - \omega_0)\right], \quad (41)$$

$$Y'_{e-1}(\omega) = \frac{\pi}{4j} Y_c(\omega - \omega_0), \quad Y'_{e+1}(\omega) = 0. \quad (42)$$

The stability of a closed-loop system with a modulator and a half-wave demodulator can be determined with respect to the transfer locus $Y_e(\omega)$ for the open-loop linear system by using the Nyquist–Mikhailov criterion.

It follows from (41) that the larger the modulus of the expression

$$\left(\frac{\pi}{4}\right)^2 Y_c(\omega_{co} - \omega_0),$$

the greater the effect of pulsations at the demodulator output on the transfer locus in the vicinity of ω_{co} and, consequently, on stability.

4. Investigation of Servosystems with a Half-Wave Demodulator

It was shown above that, under certain conditions, the transient processes can be considerably affected if the automatic control system contains a converter element consisting of a modulator and a half-wave demodulator which is not an ordinary linear continuous-action element.

The obtained results were checked experimentally by means of a servosystem which consisted of a selsyn measuring element, a half-wave demodulator, an electronic amplifier, and a dc motor.

The system performance was investigated for the 400-cps and 50-cps supply voltage frequencies of the selsyns. The system parameters were chosen in such a manner that the moduli of the transfer functions $Y_C(\omega_{co}+\omega_0)$ and $Y_C(\omega_{co}-\omega_0)$ had a value much smaller than unity for the frequency $f_0=400$ cps and a value of the order of unity for $f_0=50$ cps. The time constants and the gains of the system elements were equal for both frequencies f_0.

Servosystem Wiring Diagram (Fig. 4)

The servosystem measuring element is based on selsyns, which operate in conjunction with transformers. The output voltage of the selsyns is fed to the half-wave demodulator, which consists of transformers T1 and T2, a twin diode, L1, and load resistors R_2 and R_3. The resistor R_1 in the T1 primary winding circuit serves for regulating the demodulator gain. An ac reference voltage is fed to the T2 primary winding. The demodulator output voltage U_1 is added to the flexible feedback voltage U_5 (which is provided by resistors R_{15}) and then fed to the cathode follower L2. The cathode follower output voltage is fed to a three-stage push-pull electronic amplifier, whose preamplification stages are based on tubes L3 and L4 and whose end stage is based on tubes L5-L8. Filters C_2, R_7, and R_8, which serve for smoothing out the pulsations of the signal arriving at the amplifier input, are connected to the grid circuits of the L3 arms. Potentiometer R_{11} serves for balancing the amplifier.

The amplifier output voltage U_3 is fed to the final separate-excitation motor Mo. The motor armature is coupled through reducing gear Re with the rotor of the receiver selsyn RS and the armature of tachometer generator TG. Voltage U_T from the TG armature is fed to the differentiating feedback circuit C_1R_{15}, which is used for stabilization.

The servosystem block diagram is shown in Fig. 5. The servosystem elements have the following units: Element 1 includes the selsyns and the demodulator; element 2 consists of the electronic amplifier; element 3 combines the motor and the reducing gear (the output signal of element 3 is the reducing gear angular velocity ω); element 5 consists of the tachometer generator; element 6 consists of the differentiating circuit C_1R_{15}.

Element 4 acts as an integrator, and it converts the reducing gear shaft angular velocity into the rotation angle φ.

The transfer functions of the elements are given by

$$Y_1(\omega) = K_1$$

(for the direct component),

$$Y_2(\omega) = \frac{K_2(j\omega T_2+1)}{j\omega T_1+1}, \quad Y_3(\omega) = \frac{K_3}{j\omega T_m+1},$$
$$Y_4(\omega) = \frac{1}{j\omega}, \quad Y_5 = K_5, \quad Y_6(\omega) = \frac{j\omega T}{j\omega T+1}. \tag{43}$$

The experimentally found gain values are equal to: $K_1 = 0.36$ v/deg, $K_2 = 900$, $K_3 = 118$ deg/v-sec, $K_5 = 1.8 \cdot 10^{-3}$ v-sec/deg.

The feedback element time constant is $T = 2R_{15}C_1 = 17.5 \cdot 10^{-3}$ sec.

The amplifier filter time constant is $T_2 = R_8C_2 = 17.5 \cdot 10^{-3}$ sec; $T_1 = T_2\frac{R_8+R_7}{R_8} = 0.106$.

The motor time constant T_m was found with respect to the experimentally determined frequency response of the circuit portion consisting of the terminal amplifier stage, the motor, and the tachometer generator; it was $T_m = 0.106$ sec.

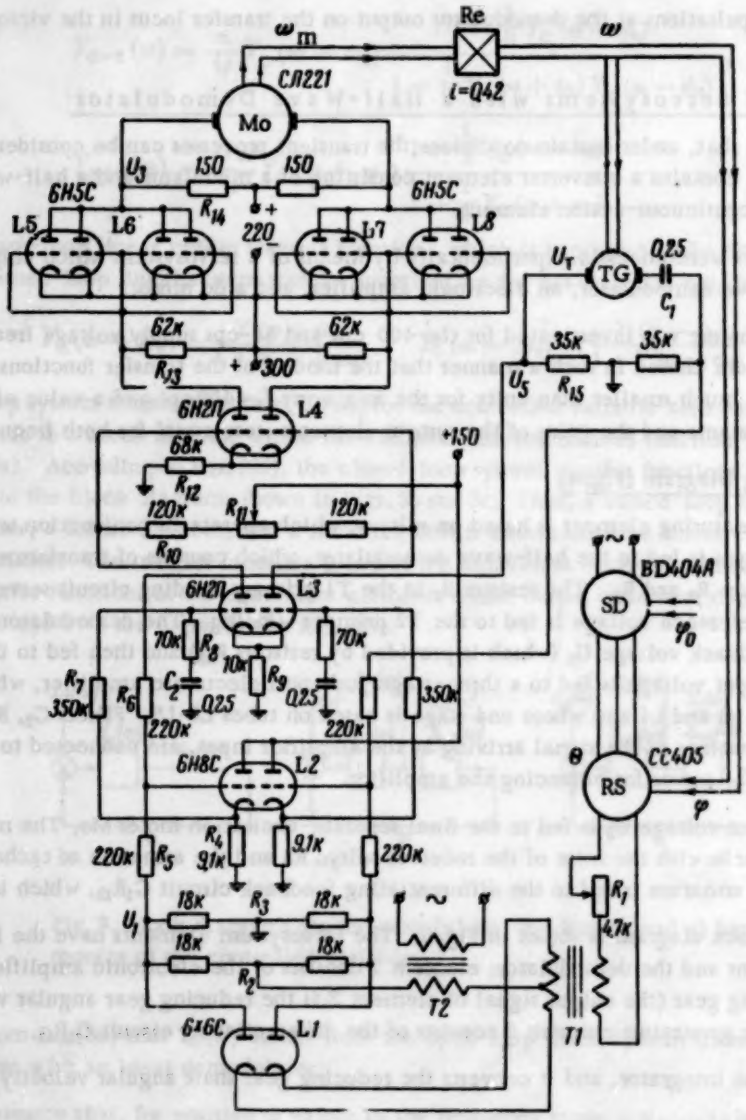

Fig. 4.

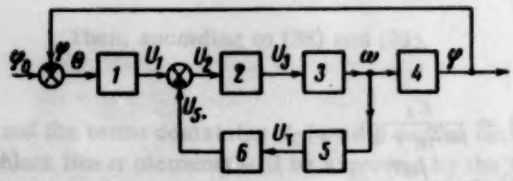

Fig. 5.

Transfer Functions and the Logarithmic Amplitude and Phase Responses of the Servosystem

Elements 2 and 3 (Fig. 5), which are provided with feedback through elements 5 and 6, can be represented in the block diagram by a single equivalent element with the transfer function

$$Y_7(\omega) = \frac{Y_2(\omega)\,Y_3(\omega)}{1 + Y_2(\omega)\,Y_3(\omega)\,Y_5(\omega)\,Y_6(\omega)}. \qquad (44)$$

By substituting expression (43) in (44) and considering that the filter time constants are $T_1 = T_m$ and $T_2 = T$, we obtain

$$Y_7(\omega) = \frac{K_2K_3(j\omega T + 1)}{(j\omega T_m + 1)^2 + K_2K_3K_5/\omega T}. \qquad (45)$$

It is obvious that the equivalent element is stable. Let us first consider the servosystem as a continuous-control system while neglecting the effect of pulsations of the converter element output signal.

The open-loop system transfer function will be equal to

$$Y(\omega) = Y_1(\omega) Y_7(\omega) Y_4(\omega) = K \frac{j\omega T + 1}{j\omega \left[(j\omega T_m + 1)^2 + jK_2K_3K_4\omega T\right]}. \quad (46)$$

Here, $K = K_1K_2K_3 = 38 \cdot 10^3\ \text{sec}^{-1}$ is the open-loop system gain.

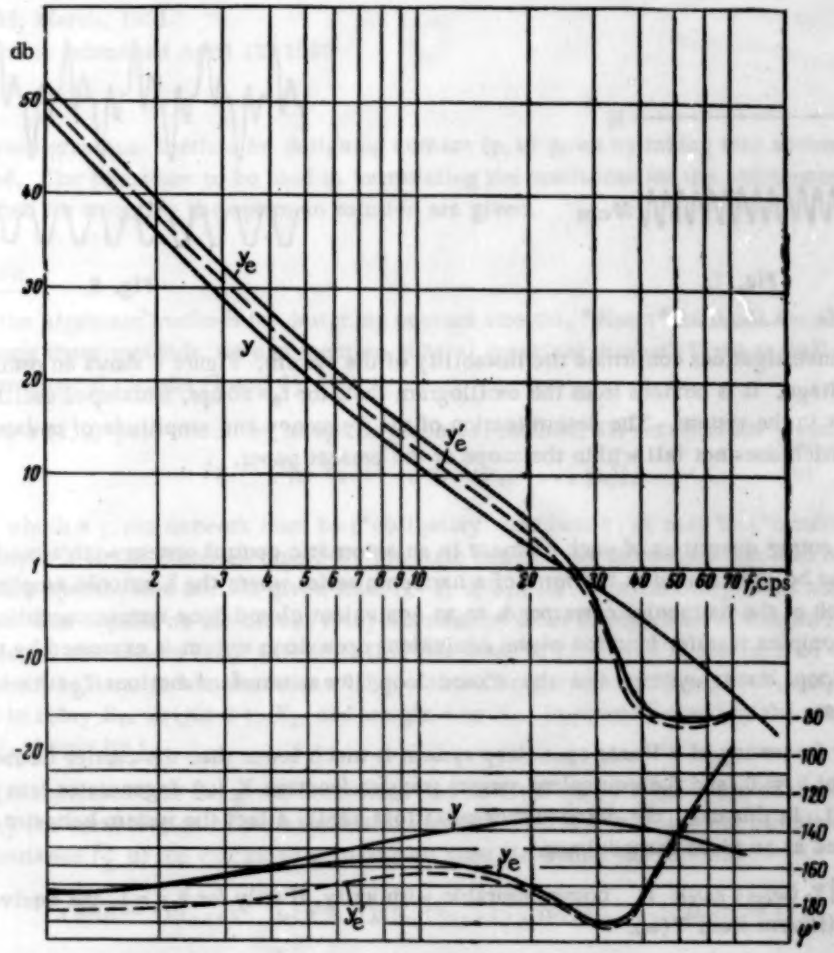

Fig. 6.

The open-loop system logarithmic amplitude and phase responses are given in Fig. 6 (curves Y). It follows from these curves that, for the crossover frequency $f_{co} = 25$ cps, a phase margin $\Delta\varphi = 46°$ is available, which secures adequate damping of the closed-loop system free oscillations [2].

If the selsyns are fed from a line with the frequency $f_0 = 400$ cps, then $f_{co} - f_0 = -375$ cps, and $f_{co} + f_0 = 425$ cps. For these frequencies, the open-loop transfer function is considerably less than unity, and the transfer function $Y_e(\omega)$ of the equivalent open-loop system degenerates into $Y(\omega)$. For the line frequency $f_0 = 400$ cps, the servosystem will behave as a continuous-control system with the frequency responses marked by Y in Fig. 6.

Experimental investigations showed that the system is stable for $f_0 = 400$ cps. An oscillogram of the tachometer generator voltage when the servosystem processes a jump-like mismatching of $\theta° = 5°$ is shown in Fig. 7.

If the selsyns are fed from a line with the frequency $f_0 = 50$ cps, $f_{co} - f_0 = -25$ cps, and $f_{co} + f_0 = 75$ cps. As follows from the Y curves in Fig. 6, the modulus of $Y(\omega)$ in the vicinity of $f_{co} - f_0$ is close to unity, and, consequently, the transfer function $Y_e(\omega)$ of the equivalent open-loop system will differ from the transfer function $Y(\omega)$ of the linear open-loop system.

Figure 6 shows the logarithmic plots of the amplitude and phase responses that correspond to the transfer function $Y_e(\omega)$ of the equivalent open-loop system, which was calculated by using Eqs. (38) and (36) (curves Y_e). The same figure shows the response curves corresponding to the simplified expression for the transfer function $Y'_e(\omega)$, which was calculated by using Eqs. (38) and (41). It follows from these graphs that the equivalent system will be unstable. In the vicinity of the crossover frequency, the $Y_e(\omega)$ and $Y'_e(\omega)$ curves are rather close to each other.

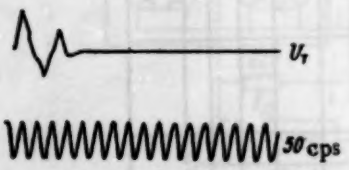

Fig. 7.

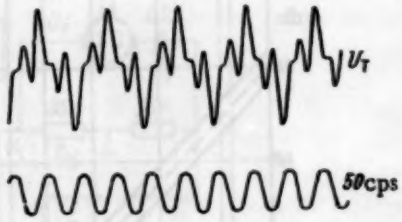

Fig. 8.

Experimental investigations confirmed the instability of the system. Figure 8 shows an oscillogram of the tachometer generator voltage. It is obvious from the oscillogram that, for $f_0 = 50$ cps, undamped oscillations with a 25-cps frequency are present in the system. The determination of the frequency and amplitude of undamped oscillations is a nonlinear problem which does not fall within the scope of the present paper.

5. Conclusion

The input and output quantities of each element in an automatic control system with a modulator and a half-wave demodulator can be represented in the form of a harmonic series where the harmonic amplitudes vary in time. The amplitude of each of the harmonics corresponds to an equivalent closed-loop system consisting of continuous linear elements. The complex transfer function of the equivalent open-loop system is expressed by the transfer function $Y(\omega)$ of the open-loop linear system and the closed-loop linear transfer functions $Y_c(\omega + k\omega_0)$ with the harmonic side frequencies.

If the crossover frequency of a linear open-loop system is much lower than the carrier frequency, then $|Y_c(\omega_{co} + k\omega_0)| \ll 1$ for $k \neq 0$, and the equivalent system transfer function $Y_e(\omega)$ degenerates into the linear system transfer function $Y(\omega)$. In this case, the demodulator pulsations hardly affect the system behavior, and the demodulator can be considered as an ideal demodulator.

If the modulus $|Y_c(\omega_{co} + k\omega_0)|$ is commensurable with unity, if only for $k = -1$, the equivalent system transfer function will be different from $Y(\omega)$.

The theoretically predicted influence of a converter element consisting of a modulator and a half-wave demodulator on the transfer function of the system was qualitatively confirmed by experimental investigations. In the case under consideration, the system, which was satisfactorily stabilized for the modulator carrier frequency $f_0 = 400$ cps, became unstable for $f_0 = 50$ cps.

LITERATURE CITED

1. E. L. L'vov, "Determination of the complex transfer function of an automatic control step system by using the modulated harmonics method," Nauchn. Doklady Vysshei Shkoly, Electromechanics and Automation, 1 (1959).
2. V. A. Besekerskii (Editor), Design of Low-Power Servosystems [in Russian] (Sudpromgiz, 1957).

A GENERALIZED GRAPHICAL METHOD FOR DESIGNING CONTACT CIRCUITS

V. N. Roginskii

(Moscow)

Translated from Avtomatika i Telemekhanika, Vol. 22, No. 3,
pp. 350-358, March, 1961
Original article submitted April 12, 1960

A generalized graphical method for designing contact (p, k)-poles by taking into account bypass paths is described. The procedure to be used in formulating the conditions for the ambiguous solution cases and a method for selecting the optimum solution are given.

1. Introduction

Along with the algebraic methods for designing contact circuits, "direct" methods are also being presently developed; from among these methods, we can mention general graphical methods [1-4] as well as methods for the particular case of symmetrical circuits [1 and 5].

For designing a (1, k)-pole circuit by using the graphical method, all networks are given as number sets

$$f_X = (\eta_1, \eta_2, \ldots, \eta_r, (\mu_1, \ldots, \mu_s))_B \tag{1}$$

of those states for which a given network must be ("obligatory" numbers η) or may be ("conditional" numbers μ) closed from the output X to the common input. By the state number, we understand the sum of "weights" $q_i = 2^{i-1}$ of those relays which operate in a certain given state (i = 1, 2, 3, . . . , n is the relay index number). The numbers belonging to the set also depend on the circuit relay numeration order (assignment of weights). For n relays, there can be n! such orders. The chosen order will be called the "base" B and noted in the form of the set index, while the relays in the base will be arranged in the order of their diminishing weights. Thus, $B = X_3X_2X_1$ signifies that weight 1 has been assigned to relay X_1, weight 2 to X_2, and weight 4 to X_3. In order to simplify the notation, we shall denote the base $X_i \ldots X_1$ simply by $\underline{i}$.

Expression (1) indicates that the given conditions can be satisfied by 2^s different contact circuits, which differ from each other by the combination of the numbers of conditional states in which the circuit will be closed. Thus, the structural admittance f_X^* of the circuit to be designed must lie within the interval

$$f_X\min = (\eta_1, \ldots, \eta_r)_B \leqslant f_X^* \leqslant (\eta_1, \ldots, \eta_r, \mu_1, \ldots, \mu_s)_B = |f_X|. \tag{2}$$

A set which includes the weight of 2^i numbers (for the $\underline{i}$ base) will be called a complete set, while, if the conditional numbers are not present in this set, such a set will correspond to a permanently closed circuit, i.e., $\{0, 1, \ldots, 2^i - 1\}_{\underline{i}} \equiv 1$. A set without compulsory numbers will be called an empty set. In the case where even the conditional numbers are absent, the set will correspond to a permanently open circuit, i.e., $\{-\} = 0$.

The sets where all compulsory numbers of any set are contained in each of the remaining ones, even if among the conditional numbers, will be called coincident sets. This means that, for all pairs of coincident sets f_g and $f_h (g \neq h)$, the following inequalities must be satisfied:

$$\begin{aligned} f_g\min &\leqslant |f_h|, \\ f_g\min &\leqslant |f_g|. \end{aligned} \tag{3}$$

The number of states which are not contained in the compulsory and the conditional portions of the set will be called forbidden numbers.

In using the graphical method of designing a (1, k)-pole circuit in the manner described in [1-3], the following operations are performed: Relay contacts are successively introduced in the circuit, the numbers are suitably converted, and the points with the coincident sets on individual circuit "sections" are combined. However, the presence of "direct lead-outs" can result in alternate path circuits, which may not satisfy the assigned conditions.

The possibility of obtaining an alternate path can be explained by considering the network $f_X = f_X(a_1, \ldots, a_n)$ in a circuit of n relays $A_1, \ldots, A_n$ [6]. We shall assume that one of the branches in this network, $f'_X \leq f_X$, at the point t_1 of section l is combined (Fig. 1) with some other network passing through the direct lead-out at the contact of relay A_m ($n \geq m > l \geq 1$) (before the contacts of relay A_l have been introduced into the circuit).

Fig. 1.

In this, besides the basic network $f'_X = \omega\psi_1\varphi_1$, where $\omega = \omega(a_{m+1}, \ldots, a_n)$, $\psi = \psi(a_{l+1}, \ldots, a_m)$, and $\varphi = \varphi(a_1, \ldots, a_l)$, also the bypass network $\omega\psi_1\psi_2\varphi_2$ will be present.

The necessary and sufficient condition which has to be satisfied if the alternate path is not to form a circuit contradicting the assigned conditions is given by the following inequality:

$$\omega\psi_1\psi_2\varphi_2 \leqslant |f'_X|. \tag{4}$$

In the particular case, this inequality is satisfied by the relation $\psi_2 \equiv 0$ or $\psi_1\psi_2 \equiv 0$, i.e., the presence of two unlike contacts of at least a single relay from $A_{l+1}, \ldots, A_m$ in circuit ψ_2 or $\psi_1\psi_2$. If $\psi_1\psi_2 \not\equiv 0$, the state of network φ_1 is of no consequence for those states of the circuit where the network $\omega\psi_1\psi_2\varphi_2$ is closed.

In this, if

$$f_{X\min} \leqslant \omega\psi_1\psi_2\varphi_2 \leqslant |f_X|, \tag{5}$$

network φ_1 as well as other parallel paths from X to the input can be entirely eliminated.

The present article offers a general number conversion method for use with the graphical method of circuit design where bypass networks are taken into account.

1. Operations with Sets

For the transformations necessary in graphical circuit design, we shall introduce the following operations with sets that are reduced to a single base: +(addition), ·(multiplication), ○(combination), −(subtraction), and ¯(inversion). If we denote by 1 the presence of a given number in the compulsory portion, by ½ its presence in the conditional portion, and by 0 its presence in the forbidden portion, the first four of these operations are defined in Table 1.

TABLE 1

x	y	x+y	x·y	x○y	x−y*	x	y	x+y	x·y	x○y	x−y*
0	0	0	0	0	0	1/2	1	1	1/2	1	1/2
0	1/2	1/2	0	0	—	1	0	1	0	0	1
0	1	1	0	0	—	1	1/2	1	1/2	1	1
1/2	0	1/2	0	0	1/2	1	1	1	1	1	1/2
1/2	1/2	1/2	1/2	1/2	1/2						

*Operation x−y can be performed only if the condition $|x| \geq |y|$ is satisfied.

The inversion operation is defined by Table 2.

TABLE 2

x	0	1/2	1
$\bar{x}$	1	1/2	0

Besides these operations, which are similar to three-value logic operations, we shall also introduce the following set transformation operations, a portion of which is connected with changes in the base.

Operation P_i of set division with respect to the contacts of relay A_i. By $P_i(f)$, we shall denote the operation of selecting from set f the numbers of those states for which relay A_i operates, and by $\bar{P}_i(f)$, we shall denote a similar operation for the case where the relay is inoperative.

Thus, for instance, $P_3\{0, 2, 5, (3,6)\}_3 = \{0, 2, (3)\}_3$, $\bar{P}_3\{0, 2, 5, (3,6)\}_3 = \{5, (6)\}_3$.

Hence, it follows that $P_2 1_3 = P_2\{0, 1, 2, 3, 4, 5, 6, 7\}_3 = \{2, 3, 6, 7\}_3$.

It can readily be seen that

$$P_i(f) + \overline{P}_i(f) = f, \quad P_i(f)\,\overline{P}_i(f) = 0. \tag{6}$$

Operation H_n^i of determining the "derivatives" of numbers in passing from base $A_i, \ldots, A_1$ to base $A_n, \ldots, A_1$, where $n > i \geq 1$. In this operation, the number χ is transformed into 2^{n-i} numbers by adding to this number all the possible weight combinations $q_{i+1}, q_{i+2}, \ldots, q_n$. For instance, for $n = 5$, we obtain

$$H_5^3\{5, (0)\}_3 = \{5, 13, 21, 29, (0, 8, 16, 24)\}_5.$$

It can be shown that

$$H_5^3(f) = H_n^{n-1} H_{n-1}^{n-2} \ldots H_{i+1}^i(f). \tag{7}$$

Operation C_i^n of "reducing" the base from $A_n, \ldots, A_1$ to $A_i, \ldots, A_1$. For this, the following relationship holds:

$$C_i^n(f) = C_i^{i+1} C_{i+1}^{i+2} \ldots C_{n-1}^n(f). \tag{8}$$

In the case of switching over from base i to base $i-1$, the number of states for which relay A_i operates is reduced by the relay weight q_i, while the remaining numbers do not change:

$$C_{i-1}^i(\chi)_i = \begin{cases} = \chi & \text{for } \chi < q_i, \\ = \chi - q_i & \text{for } \chi \geq q_i. \end{cases} \tag{9}$$

For instance, for $i = 3$ ($q_i = 4$)

$$C_2^3\{0, 2, 4, 3, 6\}_3 = \{0, 2, 0\,(3, 2)\}_2 = \{0, 2, (3)\}_2.$$

On the basis of the above definitions, it can be shown that

$$C_i^n H_n^i(f) = f, \quad H_n^i C_i^n(f) \geq f. \tag{10}$$

3. Transformation of Sets in Circuit Design

In the process of circuit design, each point a at the l section will be assigned three sets which will characterize the requirements imposed on the network from this point to the input as well as the possibility of obtaining alternate paths.

The "basic set" f_a is a set of compulsory and conditional numbers, reduced to the base l, which indicates for which states the given point will be or could be connected to the input.

The "bypass set" Φ_a is a set of compulsory and conditional numbers that are reduced to the base n of the entire circuit, which indicate for which states the given point will be or could be connected to the input along the alternate path.

The "forbidden set" Z_a is the set of the numbers reduced to the base n of the entire circuit of those states for which the given point must not be connected to the input.

The following relation holds in this case:

$$|f_a| = \overline{C_l^n\,|Z_a|}. \tag{11}$$

It follows from (11) that, for instance, the conditional portion of the basic set does not have to be assigned for a given forbidden set.

For the output point X, the basic set f_X corresponds to the assigned structural admittance between the given output and the common input, and the forbidden set includes all numbers that do not belong to the basic set, i.e., $Z_X = \overline{|f_X|}$, while the bypass set is absent: $\Phi_X = 0$.

In order that the two points a and b at the section l may be combined, it is necessary and sufficient that: a) The sets be coincident, $f_a \sim f_b$, and b) that the bypass set of a single point do not contain numbers belonging to the forbidden set of the second point, i. e.,

$$Z_a|\Phi_b| = 0, \quad Z_b|\Phi_a| = 0.$$

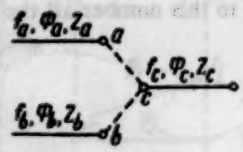

Fig. 2.

In combining the two points a and b with the common point c (Fig. 2), the following sets are assigned: the basic set

$$f_c = f_a \circ f_b; \tag{12}$$

the bypass set Φ_C, which is equal to the sum of the bypass sets of the points to be combined,

$$\Phi_c = \Phi_a + \Phi_b; \tag{13}$$

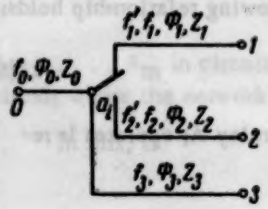

Fig. 3.

the forbidden set Z_C, which is equal to the sum of the forbidden sets of the points to be combined,

$$Z_c = Z_a + Z_b. \tag{14}$$

In passing from the lth section to the $(l-1)$th section, the contact between relay Al with the weight q_l and the direct lead-out is added to the initial point 0 with the sets f_0, Z_0, and Φ_0 (Fig. 3), and the sets are transformed according to the following rules.

A. The basic sets f_1' and f_2' of the opening and closing contact lead-outs are determined and reduced to the new base $l-1$:

$$f_1' = C_{l-1}^{l}\,\overline{P}_l(f_0), \quad f_2' = C_{l-1}^{l}\,P_l(f_0). \tag{15}$$

B. The direct lead-out set f_3 is found:

$$f_3 = f_1' \circ f_2'. \tag{16}$$

C. In the basic sets f_1' and f_2', the compulsory numbers belonging to the direct lead-out set are transformed into conditional numbers, as a result of which we obtain the following sets:

$$f_1 = f_1' - f_3, \quad f_2 = f_2' - f_3. \tag{17}$$

The lead-out h, whose set will be empty, is erased in correspondence with the graphical method.

D. The bypass sets are composed of the corresponding initial-point bypass numbers and of the new numbers which appear on account of networks passing through the given contact direct lead-out:

$$\begin{aligned}
\Phi_1 &= \overline{P}_l(\Phi_0) + \xi_3 \overline{P}_l H_n^{l-1}(f_3), \\
\Phi_2 &= P_l(\Phi_0) + \xi_3 P_l H_{ln}^{-1}(f_3), \\
\Phi_3 &= \Phi_0 + \xi_1 \overline{P}_l H_n^{l-1}(f_1) + \xi_2 P_l H_n^{l-1}(f_2),
\end{aligned} \tag{18}$$

where

$\xi_h = \begin{cases} 1 \text{ if the lead-out with the number h remains in the circuit,} \\ 0 \text{ if the lead-out with the number h is erased } (f_h \text{ is the empty set}). \end{cases}$

E. The following forbidden sets are composed:

$$\begin{aligned}
Z_1 &= \overline{P}_l(Z_0) + \xi_3 [H_n^l C_l^n \overline{P}_l(Z_0)]\overline{|\Phi_0|}, \\
Z_2 &= P_l(Z_0) + \xi_3 [H_n^l C_l^n P_l(Z_0)]\overline{|\Phi_0|}, \\
Z_3 &= Z_0 + [\xi_1 H_n^l C_l^n \overline{P}_l(Z_0) + \\
&\qquad \xi_2 H_n^l C_l^n P_l(Z_0)]\overline{|\Phi_0|}.
\end{aligned} \tag{19}$$

Here, the first term corresponds to the requirement that the appearance of new networks directed toward the circuit outputs is inadmissible, and the following terms correspond to the appearance of new bypass numbers in other lead-outs from the contact in question.

Figure 4a (the number sets pertaining to each of the points x_i, t_i, and u_i are given in Table 3) shows an example of synthesizing a (1,3)-pole circuit whose networks are defined by the following sets (this example was taken from a paper by F. Svoboda [7]):

$$f_{X_1} = \{2, 3, 6\}_3,$$
$$f_{X_2} = \{0, 1, 3, 6, (2,5)\}_3,$$
$$f_{X_3} = \{2, 3, 4, (1)\}_3.$$

When circuits are designed by using the above method, the possibility of creating spurious bypass networks is eliminated, while, at each instant of time, the operations are performed only with sets of points in a single contact group or a single section.

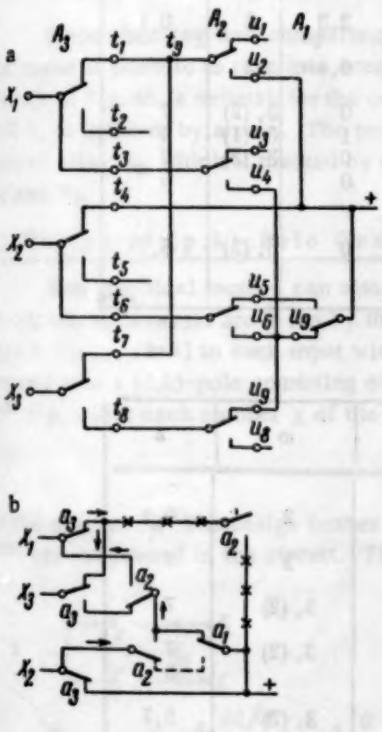

Fig. 4.

It should also be noted that, in the obtained circuits, the possibility of network breakdown during the transient periods of the actuation or the drop-out of individual relays is eliminated. At the same time, the method described above does not provide the possibility of using alternate paths. Neither does this method take into account the fact that, in forming the direct lead-out, it may happen that not all of the possible numbers which are contained in the set obtained according to Eq. (16) are assigned to this lead-out; a portion of these numbers can be left as compulsory numbers in sets f_1 and f_2. Thus, the process of assigning numbers to the direct lead-out is not well defined [1].

It should be noted that sets Φ and Z cannot be composed always, but only in the case where it is necessary to determine the possibility of effecting a combination in the presence of direct lead-outs.

Let us now consider some additional transformations which could lead to a simplified circuit.

4. Selection of Direct Lead-Out Variants

For selecting the set variant of the direct lead-out, we shall, in forming the latter, assign the Boolean coefficients $\alpha_1, \alpha_2, \ldots$ to all the compulsory numbers contained in its set, which is obtained by using Eq. (16). Instead of this, the inversions of the above coefficients ($\bar{\alpha}_1, \bar{\alpha}_2, \ldots$) will be assigned to the numbers in the compulsory portions of sets f_1' and f_2', which, in correspondence with (17), must be transformed into conditional numbers. The same coefficients will also be assigned to the corresponding numbers appearing in the bypass sets Φ_1 and Φ_2, and their inversions will be assigned to the numbers in the set Φ_3, which is obtained according to Eqs. (18) (if a certain given number belongs to set Φ_0, no coefficient should be assigned to it). Similarly, coefficients $\beta_1, \beta_2, \ldots$ are assigned to the numbers for the direct lead-out at the second contact, etc.

We shall further assign the values 0 or 1 to these coefficients. The value 1 signifies that the number to which a certain given coefficient is assigned remains a compulsory number, and the value 0 means that this number must be transferred to the conditional portion of the set (enclosed in parentheses). If the value 1 is assigned to a certain coefficient $\tilde{\alpha}_i$ ($\tilde{\alpha}_i$ indicates that the α_i coefficient without inversion as well as the $\bar{\alpha}_i$ coefficient with inversion can be taken), then the 1 value must also be assigned to all other coefficients in the section under consideration, while the 0 value must be assigned to the inverse coefficients, and conversely.

The coefficient values are decided upon while comparing the sets and combinations. At the present time, there are still no clearly defined rules indicating what values are to be assigned to the coefficients, and only the following considerations can be given:

a) If one of the sets that are being compared contains such a number with a coefficient that the transfer of this number into the conditional portion makes the sets coincident, the 0 value must be assigned to this coefficient in order that the unification can be performed.

b) If, in the case of two coincident sets, the number χ in one of them is a compulsory number and in the other set this number has a coefficient, then the 1 value is assigned to this coefficient, which also makes unification possible.

c) If all the compulsory numbers of a certain lead-out have coefficients, the 0 value can be assigned to all these coefficients, which makes it possible to erase the given lead-out.

d) If a number with a coefficient belongs to the complete set, it is convenient to assign the 1 value to this coefficient.

TABLE 3

	f'	f	Φ	Z		f'	f	Φ	Z
X_1	2,3,6			0,1,4,5,7	t_9		2,3	2	0,1
X_2	0,1,3,6, (2,5)			4,7	u_1				
X_3	2,3,4, (1)			0,5,6,7	u_2	0,1	0,1	2	
t_1	2,3	3, (2)	2	0,1	u_3				
t_2	2	(2)			u_4	0	0	3, (2)	7
t_3		2	3, (2)	0,1,4,5,7	u_5	1	1	0, (1)	4
t_4	0,1,3, (2)	0,3, (1,2)	1,2		u_6	0	0	3, (2)	7
t_5	2, (1)	(1,2)			u_7	0	0		5
t_6		1,2	0,3, (1,2)	4,7	u_8				
t_7	2,3,(1)	2,3,(1)		0	u_9		0	3, (2)	5,7
t_8	0	0		5,6,7					

TABLE 4

	f	Φ	Z		f	Φ	Z
X_1	2,3,6		0,1,4,5,7	t_9	3, (2)	2	0,1
X_2	0,1,3,6,(2,5)		4,7	u_1			
X_3	2,3,4, (1)		0,5,6,7	u_2	1, (0)	2	7
t_1	$\bar{\alpha}$2,3	α 2	0,1	u_3			
t_2	$\bar{\alpha}$2	α 6	4,5,7	u_4	0	3, (2)	7
t_3	α2	$\bar{\alpha}$2,3,$\bar{\alpha}$6	0,1,4,5,7	u_5	(1)		
t_4	0,$\bar{\beta}_1$1,3, (2)	$\beta_1$1, $\beta_2$2		u_6	0	3, (2)	7
t_5	$\bar{\beta}_2$2, (1)	$\beta_1$5, $\beta_2$6	4,7	u_7	0		5
t_6	$\beta_1$1, $\beta_2$2	0,$\bar{\beta}_1$1,3, $\bar{\beta}_2$6, (2,5)	4,7	u_8			
t_7	2,3, (1)		0	u_9	0	3, (2)	5,7
t_8	0		5,6,7				

In set transformations, the assigned coefficients are also ascribed to all numbers derived from the given number. If, in combining, a certain number has different coefficients in the two sets, the sum of these coefficients is used as the coefficient of this number in the combined set.

5. Use of Alternate Paths

The circuit can be further simplified by using bypass networks. This is possible if the following two conditions are observed in combining:

1) Among the compulsory bypass numbers of one of the points to be combined, there is a number χ' (or a group of numbers) which is equal to the compulsory number η' of output X that is connected to the second point to be combined.

2) The given bypass number χ' has not been obtained as a result of the direct lead-out that is connected to the second of the points to be combined.

If these conditions are observed, the number η'' of the second point set, obtained from the number η' of the output X in designing the circuit, can be transformed into a conditional number if it has not been obtained by a combination with any other compulsory number.

Thus, for establishing the possibility of using bypass networks, it is also necessary to know from which lead-out numbers the basic set numbers have been obtained and due to which direct lead-outs the bypass numbers have been obtained.

Under the above conditions, the coefficients $\alpha, \beta, \ldots$ carry such information, or any indices indicating the appurtenance to a certain given direct lead-out can be assigned to the numbers.

Table 4 shows sets pertinent to the circuit given in Fig. 4a.

Since checking and comparison of sets are performed each time only for one circuit section, this method does not make it possible to take into account alternate paths which pass through several direct lead-outs. Thus, in the circuit of Fig. 4b, a network for the output X_3 is formed through two direct lead-outs in the states with the numbers 2 and 3, as is shown by arrows. The presence of such a path makes it possible to eliminate the network with the contact of relay A_2, which is marked by crosses, and to leave only one opening contact of relay A_3 between the outputs X_1 and X_3.

6. Design of (p,k)-Pole Contact Circuits

The graphical method can also be used for designing contact (p,k)-poles which are separable on the output side [1-3], whose networks are given by the (p,k)-sets f_{ji}, which correspond to networks from each output with the number $\underline{j}$ ($j = 0, 1, \ldots, k-1$) to each input with the number $\underline{i}$ ($i = 0, 1, \ldots, p-1$). For design purposes, the (p,k)-pole is transformed into a (1,k)-pole consisting of n+m relay contacts, where $\underline{m}$ is the smallest integer satisfying the inequality $2^m \geq p$, while each number χ of the set f_{ji} is transformed into the number

$$\chi' = \chi 2^m + i \qquad (20)$$

of the new set f_j. The design further progresses along the usual lines until the contacts of relay A_{m-1} (with the weight 2^m) are introduced in the circuit. The numbers at the obtained ends will indicate the input numbers $\underline{i}$.

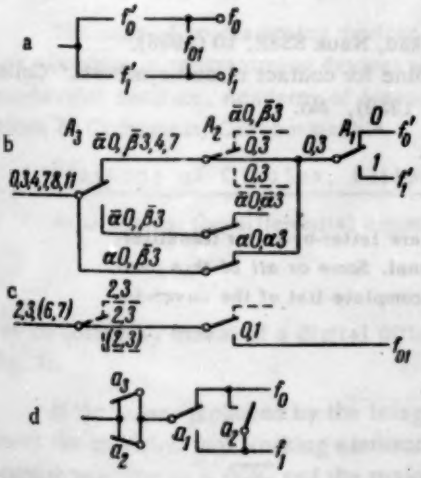

Fig. 5.

This approach can yield positive results also in designing (1,k)-poles under the condition that no equal compulsory numbers be contained in any of the output sets (the separability condition). In certain cases, a similar approach can be used for designing (1,2)-poles where the separability condition is absent, as is recommended in [4]. For this, sets f_0 and f_1 are transformed in such a manner that each number that is present in both sets remains only in one of them. For the obtained sets f_0' and f_1', a (1,2)-pole is constructed beginning from the input, for which the numbers of these sets are transformed into a single set according to (20). After this, the f_{01} network is constructed, whose set comprises the above-indicated numbers as the compulsory numbers which are common for both sets f_0 and f_1, while the numbers of the unused states and the forbidden numbers which are common for the f_0 and f_1 sets enter the network f_{01} set as conditional numbers. This network is connected between the outputs of the constructed (1,2)-pole (Fig. 5a).

For instance, if the following sets are given [4]:

$$f_0 = \{0, 2, 3, 4\}_3, \quad f_1 = \{1, 2, 3, 5\}_3,$$

then, by excluding the numbers 2 and 3 (this exclusion can be secured in different ways; at the present time, no clear indications are available about the procedure to be followed in order to obtain optimum results), we obtain

$$f_0' = (0, 2, 4)_3, \qquad f_1' = (1, 3, 5)_3.$$

Hence,

$$f_{01} = (2, 3, (6, 7))_3.$$

Since, for the given case, m = 1, we obtain the set

$$f = (0, 3, 4, 7, 8, 11)_4.$$

The construction of this circuit is shown in Fig. 5b, the construction of network f_{01} is shown in Fig. 5c, and the resulting circuit is given in Fig. 5d.

CONCLUSION

The graphical method makes it possible to design H-class circuits while automatically taking into account the unused states and bypass networks, which cannot be achieved by using the regular methods. Experience shows that, in most cases, the designed circuits are simpler than the same circuits designed by other methods, while the amount of work involved is considerably reduced. The simplicity of operations and their identity made it possible to use this method for designing an original machine for synthesizing relay circuits [1, 8, and 9].

LITERATURE CITED

1. V. N. Roginskii, Fundamentals of the Structural Synthesis of Relay Control Circuits [in Russian] (AN SSSR Press, 1959).
2. V. N. Roginskii, "A graphical method for synthesizing contact circuits," Élektrosvyaz', 11 (1957).
3. V. N. Roginskii, A Graphical Method for Synthesis of Multiterminal Contact Networks. Proc. of an Intern. Symposium on the Theory of Switching. Part II. Harvard Univ. Press, 1959.
4. A. H. Scheinman, The Numerical-Graphical Method in the Design of Multiterminal Switching Circuits. Comm. and Electronics, No. 6, 1959.
5. G. N. Povarov, "The problem of the structural synthesis of symmetric contact circuits," Avtomatika, Kiev, 4 (1956).
6. V. N. Roginskii, "A graphical strip-chart method for designing contact (1,k)-poles." Collection: Information Transmission Problems [in Russian] (AN SSSR Press, 1960), No. 6.
7. F. Svoboda, Užití neurčité dvouhodnove Booleovy funkce na synthesu jednotaktnich hradlovych schemat. Stroje na zpacování informací, II, Praha, 1954.
8. V. N. Roginskii, "A machine for designing relay circuits," Vestnik Akad. Nauk SSSR, 10 (1958).
9. A. A. Arkhangel'skaya, V. G. Lazarev, and V. N. Roginskii, "A machine for contact circuit synthesis." Collection: Information Transmission Problems [in Russian] (AN SSSR Press, 1959), No. 1.

All abbreviations of periodicals in the above bibliography are letter-by-letter transliterations of the abbreviations as given in the original Russian journal. *Some or all of this periodical literature may well be available in English translation.* A complete list of the cover-to-cover English translations appears at the back of this issue.

A DIGITAL COMPUTER FOR PROGRAMMING SECOND-DEGREE CURVES

Yang Hsi-jêng

(Peking)

Translated from Avtomatika i Telemekhanika, Vol. 22, No. 3,
pp. 359-368, March, 1961
Original article submitted June 20, 1960

The present article is concerned with the algorithm and the block diagram of a specialized digital computer for machine tools for cutting profiles consisting of sections of straight lines and second-power curves. The device errors are investigated and the results obtained in accuracy investigations on a universal computer are given.

The programs for metal-cutting tools with digital programming control are composed by means of universal computers, specialized computers, or manual calculators.

The program obtained in these machines is transformed into unitary code.

The extremely large volume of intermediate memory constitutes a disadvantage of programming by means of universal computers. Moreover, some enterprises which use machine tools with digital programming control are not in a position to acquire a universal computer. Therefore, a number of specialized computers for these purposes were developed in recent years.

Specialized programming devices can be designed on the basis of a digital differential analyzer where binary multipliers are used as digital integrators. In this case, the character of the interpolation curve will be determined by the number of integrating units in the digital differential analyzer and by their intercoupling circuit. Examples of such devices are given in [1 and 3]. Their disadvantage is the relatively nonuniform distribution of output pulses, which impairs the operation of digital follow-up systems and causes relatively large calculation errors. Thus, in reproducing a linear function, the error of an interpolator with a binary multiplier attains the following value under certain conditions:

$$\frac{1}{6}\left[n+\frac{1}{3}\left(10\pm\frac{1}{2^n}\right)\right],$$

where n+1 is the number of places in the binary multiplier [5 and 6].

The error of programming devices consisting of several intercoupled binary multipliers can be even larger.

The error of programming devices where increment summators are used as integrators is much smaller. We can cite examples of programming devices with parallel increment summators, which have been developed at the Electromechanical Institute, Academy of Sciences, USSR, and sequential summators, which have been developed at the Institute of Computers, Czechoslovakia.

Calculations of Circles, Ellipses, and Hyperbolas

As is known, the differential equation

$$\ddot{x}+\omega_0^2 x=0$$

can be solved by means of a digital differential analyzer where the integrators are coupled in the manner shown in Fig. 1a.

If the pulses produced by the integrators are fed through scaling circuits to digital follow-up systems which move the machine tool working element along the y and x axes, this element will move along an ellipse with the angular velocity $\omega_0=\sqrt{k_1k_2}$ and the major to minor axis ratio k_1/k_2. Here, k_1 and k_2 are the scaling factors of the scaling circuits. If these factors are so chosen that $k_1=k_2$, the working element will move along a circle.

Similarly, the hyperbola equation $\ddot{x}-\omega_0^2 x=0$ can be solved by means of a digital differential analyzer with the same circuit, but with positive feedback (Fig. 1b). The working element motion trajectory is in this case a hyperbola whose asymptote slope is equal to k_1/k_2.

Let us find the algorithms for calculating these curves. Consider a number of discrete points on an ellipse which are arranged in such a manner that the parameters of the adjacent points differ by δ.

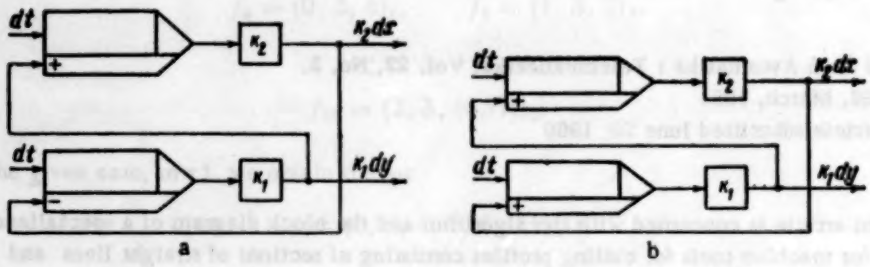

Fig. 1.

Let the i point coordinates, calculated from the ellipse parametric equations, be

$$x_i = \rho \sin(\theta + \delta), \qquad y_i = \frac{\rho}{a}\cos(\theta + \delta)$$

or

$$x_i = \rho \sin\theta\cos\delta + \rho\cos\theta\sin\delta, \tag{1}$$

$$y_i = \frac{\rho}{a}\cos\theta\cos\delta - \frac{\rho}{a}\sin\theta\sin\delta. \tag{2}$$

The coordinates of the adjacent (i-1)th point will be

$$x_{i-1} = \rho\sin\theta, \tag{3}$$

$$y_{i-1} = \frac{\rho}{a}\cos\theta. \tag{4}$$

By substituting (3) and (4) in Eqs. (1) and (2), we obtain

$$x_i = x_{i-1}\cos\delta + ay_{i-1}\sin\delta, \tag{5}$$

$$y_i = y_{i-1}\cos\delta - \frac{x_{i-1}}{a}\sin\delta. \tag{6}$$

Similarly

$$x_{i+1} = x_i\cos\delta + ay_i\sin\delta, \tag{7}$$

$$y_{i+1} = y_i\cos\delta - \frac{x_i}{a}\sin\delta; \tag{8}$$

$$x_{i+2} = x_{i+1}\cos\delta + ay_{i+1}\sin\delta, \tag{9}$$

$$y_{i+2} = y_{i+1}\cos\delta - \frac{x_{i+1}}{a}\sin\delta. \tag{10}$$

By taking into account relation (5), we have from Eqs. (6) and (8)

$$y_{i+1} = y_i\cos\delta - \frac{x_i}{a}\sin\delta = \left(y_{i-1}\cos\delta - \frac{x_{i-1}}{a}\sin\delta\right)\cos\delta - \frac{x_i}{a}\sin\delta =$$
$$= y_{i-1}\cos^2\delta + y_{i-1}\sin^2\delta - 2\frac{x_i}{a}\sin\delta = y_{i-1} - 2\frac{x_i}{a}\sin\delta. \tag{11}$$

Similarly, by taking into account relation (9), we obtain from Eqs. (7) and (8)

$$x_{i+2} = x_i + 2ay_{i+1}\sin\delta. \tag{12}$$

In the same fashion, we can find the algorithm for calculating the hyperbola.

Let the hyperbola equation be given by $x^2 - a^2y^2 = \rho^2$. We shall express the coordinates in the following manner:

$$x_i = \rho \operatorname{ch}(\theta + \delta) = \rho \operatorname{ch}\theta \operatorname{ch}\delta + \rho \operatorname{ch}\theta \operatorname{sh}\delta = x_{i-1} \operatorname{ch}\delta + a y_{i-1} \operatorname{sh}\delta, \tag{13}$$

$$y_i = \frac{\rho}{a} \operatorname{sh}(\theta + \delta) = \frac{\rho}{a} \operatorname{sh}\theta \operatorname{ch}\delta + \frac{\rho}{a} \operatorname{ch}\theta \operatorname{sh}\delta = y_{i-1} \operatorname{ch}\delta + \frac{x_{i-1}}{a} \operatorname{sh}\delta. \tag{14}$$

Similarly

$$x_{i+1} = x_i \operatorname{ch}\delta + a y_i \operatorname{sh}\delta, \tag{15}$$

$$y_{i+1} = y_i \operatorname{ch}\delta + \frac{x_i}{a} \operatorname{sh}\delta; \tag{16}$$

$$x_{i+2} = x_{i+1} \operatorname{ch}\delta + a y_{i+1} \operatorname{sh}\delta, \tag{17}$$

$$y_{i+2} = y_{i+1} \operatorname{ch}\delta + \frac{x_{i+1}}{a} \operatorname{sh}\delta. \tag{18}$$

Considering that $\operatorname{ch}^2\delta - \operatorname{sh}^2\delta = 1$, we obtain from Eqs. (13), (14), and (16)

$$y_{i+1} = y_{i-1} + 2\frac{x_i}{a} \operatorname{sh}\delta. \tag{19}$$

From Eqs. (15), (16), and (17), we obtain

$$x_{i+2} = x_i + 2a y_{i+1} \operatorname{sh}\delta. \tag{20}$$

It is obvious from Eqs. (11), (12), (19), and (20) that the values of $\sin\delta$ and $\operatorname{ch}\delta$ are independent of the values of coordinates $\underline{x}$ and $\underline{y}$ and that they are parameters which are determined by the argument increment for each iteration cycle. By substituting ω for $2\sin\delta$ and $2\operatorname{sh}\delta$, we obtain the final definition of the algorithms for calculating the ellipse and hyperbola coordinates in the form of difference equations:

$$y_{i+1} = y_{i-1} - \frac{\omega}{a} x_i, \tag{21}$$

$$x_{i+2} = x_i + a\omega y_{i+1} \tag{22}$$

for the ellipse, and

$$y_{i+1} = y_{i-1} + \frac{\omega}{a} x_i, \tag{23}$$

$$x_{i+2} = x_i + a\omega y_{i+1} \tag{24}$$

for the hyperbola.

For the processing of the obtained algorithms, we can suggest computer circuits with parallel and sequential increment summators. Consider a parallel circuit consisting of two registers, R_x and R_y, and two summators, C_x and C_y, as is shown in Fig. 2. The R_x and R_y registers consist of reversive counters.

The y_{i-1} value, obtained from the preceding iteration, is preserved in R_y and C_y, while the x_i value, obtained in the preceding iteration, is preserved in R_x and C_x.

Each iteration consists of two cycles. In the first cycle, the number contained in R_x is subtracted from the number contained by C_y; during the second cycle, the number in C_x is added to the number of R_y. The k_1 and k_2 units consist of multipliers. The multiplication factors are chosen in such a manner that $k_2 = \omega/a$ and $k_1 = a\omega$ (k_1 and k_2 are always smaller than unity). After passing through the k_1 unit, the summator C_y overfilling pulses are fed to counter R_y and are subtracted from the number contained in the counter. After passing through the k_2 unit, the summator C_x overfilling pulses are fed to counter R_x and are added to its contents.

Thus, iterations $y_{i+1} = y_{i-1} - \frac{\omega}{a} x_i$ and $x_{i+2} = x_i + a\omega y_{i+1}$ are performed. The pulses leaving units k_1 and k_2 are the output pulses Δy and Δx, respectively. The mobile element, which is driven by the two digital follow-up systems that are controlled by these pulses, moves in chessboard order, i.e., it first attains the position y_{i+1}, then x_{i+2}, then again y_{i+3}, etc. In the circuit [4] constructed at the Institute of Electromechanics, Academy of Sciences, USSR, this movement is secured by introducing a lag line into one of the channels.

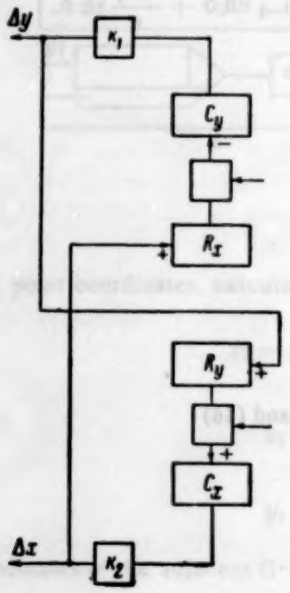

Fig. 2.

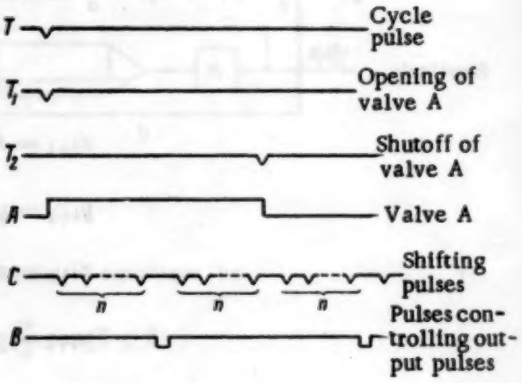

Fig. 4.

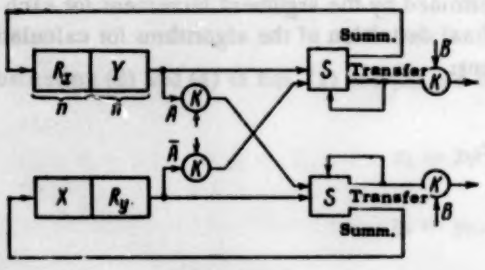

Fig. 3.

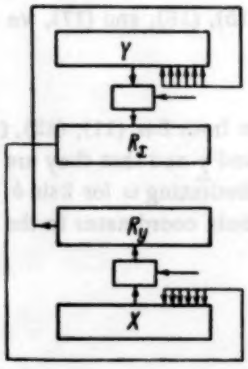

Fig. 5.

Moreover, a computer circuit with sequential increment summators can be used (Fig. 3). The circuit consists of two shifting registers R_X, Y and X, R_Y and of other single-place summators S, which can perform the addition and subtraction operations. The time diagram explaining the circuit operation is shown in Fig. 4. Such a circuit was used in the digital computer which was developed in Czechoslovakia [2].

Error of the Device

In order to determine the error magnitude, we shall first find some intermediate expressions. From (21) and (22), the present coordinates can be expressed in the following manner:

$$y_1 = y_{-1} - \frac{\omega}{a} x_0,$$

$$x_2 = x_0(1 - \omega^2) + a\omega y_{-1},$$

$$y_3 = y_{-1}(1 - \omega^2) - \frac{x_0}{a}(2\omega - \omega^3),$$

$$x_4 = x_0(1 - 3\omega^2 + \omega) + a\omega y_{-1}(2\omega - \omega^3),$$

. . . . . .

$$y_{2i-1} = y_{-1}\left[1 - \frac{i(i-1)}{2!}\omega^2 + \frac{(i+1)\,i\,(i-1)\,(i-2)}{4!}\omega^4 - \ldots\right.$$

$$\left. \ldots + (-1)^{i-1}\omega^{2(i+1)}\right] - \frac{x_0}{a}\left[i\omega - \frac{(i-1)\,i\,(i+1)}{3!}\omega^3 + \ldots (-1)^{i-1}\omega^{2i-1}\right] =$$

$$= y_{-1}\sum_{j=0}^{i-1}[(-1)^j C_{i+j-1}^{2j}\omega^{2j}] - \frac{x_0}{a}\sum_{j=1}^{i}[(-1)^{j-1}C_{i+j-1}^{2j-1}\omega^{2j-1}],$$

$$x_{2i} = x_0\left[1 - \frac{i(i+1)}{2!}\omega^2 + \frac{(i+2)\,(i+1)\,i\,(i-1)}{4!}\omega^4 - \ldots + (-1)^i\omega^{2i}\right] +$$

$$+ ay_{-1}\left[i\omega - \frac{(i+1)\,i\,(i-1)}{3!}\omega^3 + \ldots + (-1)^{i-1}\omega^{2i-1}\right] =$$

$$= x_0\sum_{j=1}^{i}[(-1)^j C_{i+j}^{2j}\omega^{2j}] + ay_{-1}\sum_{j=1}^{i}[(-1)^{j-1}C_{i+j-1}^{2j-1}\omega^{2j-1}].$$

This can be written as

$$y_{2i-1} = \xi_{2i-1}y_{-1} - \frac{1}{a}\eta_{2i}x_0, \tag{25}$$

$$x_{2i} = \xi_{2i+1}x_0 + a\eta_{2i}y_{-1}, \tag{26}$$

where

$$\xi_{2i-1} = \sum_{j=0}^{i-1}[(-1)^j C_{i+j-1}^{2j}\omega^{2j}], \tag{27}$$

$$\xi_{2i+1} = \sum_{j=0}^{i}[(-1)^j C_{i+j}^{2j}\omega^{2j}], \tag{28}$$

$$\eta_{2i} = \sum_{j=1}^{i}[(-1)^{i-1}C_{i+j-1}^{2j-1}\omega^{2j-1}]. \tag{29}$$

From the definition, it follows that

$$x_0 = \rho\sin\theta, \tag{30}$$

$$y_{-1} = \frac{\rho}{a}\cos(\theta - \delta), \tag{31}$$

and

$$x_{2i} = \rho\sin(\theta + 2i\delta), \tag{32}$$

$$y_{2i-1} = \frac{\rho}{a}\cos[\theta + (2i-1)\,\delta]. \tag{33}$$

From Eqs. (30) and (31), we obtain

$$\rho\sin\theta = x_0;$$

$$\frac{\rho}{a}\cos\theta = y_{-1} - \frac{x_0}{a}\sin\delta\,, \quad \rho\cos\theta = ay_{-1} - x_0\sin\delta.$$

By substituting these expressions in Eqs. (32) and (33), we obtain after simplification

$$y_{2i-1} = y_{-1}\cos(2i-1)\,\delta - \frac{x_0}{a}[\sin\delta\cos(2i-1)\,\delta + \sin(2i-1)\,\delta],$$

$$x_{2i} = x_0[\cos 2i\delta - \sin\delta\sin 2i\delta] + ay_{-1}\sin 2i\delta.$$

For very small δ values, which are actually used in practice, the latter equations can be replaced by the approximate equations

$$y_{2i-1} = y_{-1} \cos(2i-1)\delta - \frac{x_0}{a} \sin 2i\delta \tag{34}$$

and

$$x_{2i} = x_0 \cos(2i+1)\delta + a y_{-1} \sin 2i\delta. \tag{35}$$

By comparing (34) and (25) with (35) and (26), we find:

$$\xi_{2i-1} = \cos(2i-1)\delta, \tag{36}$$

$$\xi_{2i+1} = \cos(2i+1)\delta \tag{37}$$

and

$$\eta_{2i} = \sin 2i\delta. \tag{38}$$

The Device Errors in Calculating Ellipses and Circles

The following operation must be performed for each iteration in calculating ellipses and circles:

$$y_{2i-1} = y_{2i-3} - \frac{\omega}{2} x_{2i-2}, \qquad x_{2i} = x_{2i-2} + a\omega y_{2i-1}.$$

In practice, however, the numbers $\underline{x}$ and $\underline{y}$ are divided into two portions. The integer portions of $\underline{x}$ and $\underline{y}$ are contained in R_x and R_y, while the fractional portions are contained in C_x–unit k_2 and C_y–unit k_1, respectively. During the iteration process, only the integer portions of the numbers are added. The fractions are rejected, and an error arises. We shall call this the rounding-off error.

We shall denote the exact coordinate values by the capital letters X and Y, while their actual values will be denoted by the small letters $\underline{x}$ and $\underline{y}$. The numbers contained in R_x and R_y will be denoted by $[x]_{in}$ and $[y]_{in}$, while the numbers in C_x and C_y will be denoted by x_g and y_g, respectively. Thus, we can write

$$\begin{aligned} y_{-1} &= Y_{-1} + \varepsilon_{-1}, \\ x_0 &= X_0 + \mu_0, \\ &\cdots\cdots \\ y_{2i-1} &= Y_{2i-1} + \varepsilon_{2i-1}, \\ x_{2i} &= X_{2i} + \mu_{2i}, \end{aligned} \tag{39}$$

where ε_{-1} and μ_0 are errors caused by the inaccurate assignment of initial conditions, and x_0 and y_{-1} are the initial values of the $\underline{x}$ and $\underline{y}$ variables,

$$\begin{aligned} Y_{2i-1} &= Y_{2i-3} - \frac{\omega}{a} X_{2i-2}, \\ X_{2i} &= X_{2i-2} + a\omega Y_{2i-1}, \end{aligned} \tag{40}$$

and

$$\varepsilon_1 = \varepsilon_{-1} - \frac{\mu_0}{a}\omega + \frac{x_{0g}}{a}\omega, \tag{41}$$

$$\mu_2 = \mu_0(1-\omega^2) + a\omega\varepsilon_{-1} + \omega^2 x_{0g} - a\omega y_{1g},$$

$$\cdots\cdots\cdots\cdots\cdots\cdots\cdots\cdots$$

$$\varepsilon_{2i-1} = \xi_{2i-1}\varepsilon_{-1} - \frac{\eta_{2i}}{a}\mu_0 + \frac{\omega}{a}\sum_{k=0}^{i-1} \xi_{2k+1} x_{2(i-k-1)g} + \omega \sum_{k=1}^{i-1} \eta_{2k} y_{[2(i-k-1)+1]g}, \tag{42}$$

$$\mu_{2i} = \xi_{2i+1}\mu_0 + a\eta_{2i}\varepsilon_{-1} + \omega \sum_{k=1}^{i} \eta_{2k} x_{2(i-k)g} - a\omega \sum_{k=0}^{i-1} \xi_{2k+1} y_{[2(i-k)-1]g}. \tag{43}$$

The expressions for the errors (42) and (43) consist of two portions. The first two terms of these expressions represent the error arising due to the inaccuracy in assigning the initial conditions, and the last two terms are the rounding-off errors.

In order to find the exact error value, it is necessary to know all values x_{0f} of the fractional portions for each iteration:

$$x_{2g}, \ldots, x_{2ig}, y_{1g}, y_{2g}, \ldots, y_{(2i-1)g}, \text{ etc.}$$

This is impossible in practice, since the rejected fractional portions x_{kg} and y_{kg} will have different values for different initial conditions in different ω; generally speaking, they can be considered as random functions. However, for a very large number of iterations with a sufficiently high degree of accuracy, we can use the average value of the rejected fractional portions instead of their instantaneous random values in error calculation.

By denoting the average values of the fractional portions x_g and y_g by $\bar{x}_g$ and $\bar{y}_g$ and by substituting them in Eqs. (42) and (43), we obtain

$$\varepsilon_{2i-1} = \xi_{2i-1}\varepsilon_{-1} - \frac{\eta_{2i}}{a}\mu_0 + \frac{\bar{x}_g}{a}\omega\sum_{k=1}^{i-1}\xi_{2k+1} + \bar{y}_g\omega\sum_{k=1}^{i-1}\eta_{2k}, \tag{44}$$

$$\mu_{2i} = \xi_{2i+1}\mu_0 + a\eta_{2i}\varepsilon_{-1} + \bar{x}_g\omega\sum_{k=1}^{i}\eta_{2k} - a\bar{y}_g\omega\sum_{k=0}^{i-1}\xi_{2k+1}. \tag{45}$$

On the basis of (27)-(29), it can be shown that

$$\omega\sum_{k=0}^{i-1}\xi_{2k+1} = \eta_{2i}, \quad \omega\sum_{k=0}^{i-1}\eta_{2k} = 1 - \xi_{2i-1}, \quad \omega\sum_{k=1}^{i}\eta_{2k} = 1 - \xi_{2i+1}. \tag{46}$$

By taking into account (36)-(38) and by substituting (46) and (45), we obtain

$$\varepsilon_{2i-1} = \varepsilon_{-1}\cos(2i-1)\delta - \frac{\mu_0}{a}\sin 2i\delta + \frac{\bar{x}_g}{a}\sin 2i\delta + \bar{y}_g[1 - \cos(2i-1)\delta], \tag{47}$$

$$\mu_{2i} = \mu_0\cos(2i+1)\delta + a\varepsilon_{-1}\sin 2i\delta + \bar{x}_g[1 - \cos(2i+1)\delta] - a\bar{y}_g\sin 2i\delta. \tag{48}$$

If the initial values x_0 and y_{-1} are given accurately, ε_{-1} and μ_0 are equal to zero. Then, expressions (47) and (48) assume the following form:

$$\varepsilon_{2i-1} = \frac{\bar{x}_g}{a}\sin 2i\delta + \bar{y}_g[1 - \cos(2i-1)\delta], \tag{49}$$

$$\mu_{2i} = \bar{x}_g[1 - \cos(2i+1)\delta] - a\bar{y}_g\sin 2i\delta. \tag{50}$$

If we consider that $\bar{x}_g$ and $\bar{y}_g$ can assume any of the possible values between zero and unity with equal probability, 0.5 should be taken as their average value. The validity of this assumption has been confirmed by many calculations.

In order to obtain the maximum rounding-off error, $\bar{x}_g = \bar{y}_g = 1$ (instead of $\frac{1}{2}$) must be substituted in Eqs. (49) and (50); the maximum error value will then be twice as large as that calculated with respect to the arithmetical mean value.

It should be noted that the maximum error actually can never arise, since it is impossible to specify such conditions for which all the rejected fractional portions x_g and y_g are equal to unity. Thus, this estimate will definitely give a higher value. From an analysis of Eqs. (49) and (50) and also from the data obtained in testing a parallel circuit, the following conclusions can be drawn:

1. The rounding-off error is independent of the ellipse axis length or of the circle radius; it depends only on the value of a, i.e., the ratio of the major axis to the minor axis.

2. For $a > 1$, the error ε is always less than 1, while the error μ increases with an increase in a and has a negative value.

3. For $a < 1$, the error μ is always less than 1, while the error ε increases with a decrease in a and has a positive value.

4. In circle calculations, the error μ is always less than unity, and ε attains unity for $\theta = \frac{\pi}{2}$. If, in processing the curve, the residues in the registers are rejected and the initial conditions are again established each time y passes through zero, the error will not exceed unity in processing the entire ellipse.

5. In order to reduce the rounding-off error, it is sufficient to reduce the $\bar{x}_g$ and $\bar{y}_g$ values.

0		0		π/2		π		3π/2		2π	
R		integer	fractional	i	f	i	f	i	f	i	f
$R = 74$ (60)	i	0	—	146	—	145	—	145	—	145	—
	x	00	00	74	01	00	74	74	01	00	10
	y	74	00	00	10	74	00	00	10	74	00
$R = 764$ (500)	i	0	—	1445	—	1444	—	1444	—	1444	—
	x	000	000	764	006	000	764	764	006	000	764
	y	764	000	000	607	764	000	000	607	764	000
$R = 5670$ (3000)	i	0	—	14443	—	14442	—				
	x	0000	0000	5670	0013	0000	5670				
	y	5670	0000	0000	5027	5670	0000				

Remarks. 1. All numbers are given in the octuple system (decimal system numbers are in parentheses). 2. Here, the i value denotes the number of iterations for every $\pi/2$. For instance, i = 145 for $Q = 3\pi/2$ to 2π for R = 60.

For the sequential circuit, the calculations for circle computation were performed by means of the "Ural 1" universal computer by solving the difference equations (21) and (22) directly. The results indicate (see table) that the following values are obtained for $\theta = \pi/2$ and $\theta = 2\pi$: y = 0, x = 60, 100, 500, 3000, and x = 0, y = 60, 100, 500, 3000, respectively (for the initial conditions $x_0 = 0$, y = 60, 100, 500, 3000). Thus, it is not necessary to discard the residues in the register and to reestablish the initial conditions when y passes through zero.

A Method for Reducing the Rounding-Off Error

For reducing the rounding-off error, we propose an arrangement (Fig. 5) where the numbers to be carried over from the first places of the registers R_y and R_x are returned to the (n-i)-places of registers Y and x, respectively. In such circuits, the rounding-off error is the smaller, the larger the scaling factor 2^{-i}. It is obvious from Eqs. (49) and (50) that the rounding-off error is proportional to the value of a and to the average values $\bar{x}_g$ and $\bar{y}_g$ of the fractional portions. If a scaling factor larger than or equal to a is used in the proposed circuit, the average values of the fractional portions $\bar{x}_g$ and $\bar{y}_g$ will be equal to or less than $1/2a$. It is obvious from Eqs. (49) and (50) that μ and ε will always be less than unity. A circuit with such a correction will be called a circuit with a small rounding-off error in comparison with the circuit where the transfers are effected from the ith place of the R_y and R_x registers, respectively.

Experimental Check

The operation of the described parallel-type device was simulated in a "Ural 1" universal digital computer. Over ten circles with different radii and ellipses with different major and minor axes were computed. Programs were composed for determining the maximum positive and negative errors in calculating circles.

The calculation data indicate that the rounding-off error for all curves can become larger than unity. This is explained by the fact that the author took into account the intermediate points for each iteration. Actually, the curves do not pass through these points due to the fact that the time interval between two successive operations in each iteration is extremely small, while the servosystem angular momentum is relatively large.

LITERATURE CITED

1. A. A. Voronov and G. N. Sokolov, "A device based on digital integrators for the programming of second-power curves," Avtomatika i Telemekhanika, 20, 2 (1959).

2. Morton Nidler, Final Report on Project Digital Differential Analyzer NUDA Institute of Computing and Calculation Machines, Academy of Sciences of Czechoslovakia.
3. Yngvar Lundh. Digital Techniques for Small Computation. Journal of British Institute of Radio Engineering, vol. I, No. 1 (1959).
4. A. A. Voronov, B. L. Ermilov, G. G. Kornitenko, and G. N. Sokolov, "A machine-tool digital computer for processing second-power curves." Collection: Maching Automation in Leningrad Industry [in Russian](Mashgiz, 1959).
5. Yang Hsi-jêng, "Determination of the maximum error of binary multipliers," Avtomatika i Telemekhanika, 21, 7 (1960).
6. A. A. Voronov, A. R. Garbuzov, B. L. Ermilov, M. B. Ignat'ev, G. G. Kornitenko, G. N. Sokolov, and Yang Hsi-jêng, Digital Analogs for Automatic Control Systems [in Russian] (AN SSSR Press, 1960).

THE USE OF SEMICONDUCTOR DIODES IN MAKING OF SYMMETRICAL NONLINEAR RESISTANCES

Tai Tzŭ-hsin

(Moscow)

Translated from Avtomatika i Telemekhanika, Vol. 22, No. 3, pp. 369-375, March, 1961
Original article submitted May 27, 1960

An analysis of the factors is made which influence the stability of symmetrical nonlinear resistances composed of semiconductor diodes connected in a bridge circuit. Examples are given for determination of the sensing threshold of a magnetic amplifier using such resistances for selective rectification of even harmonics of output voltages. It is shown that silicon diodes are suitable for construction of symmetrical nonlinear resistors to be used in magnetic amplifiers of high sensitivity.

In magnetic amplifiers in which four harmonics are rectified by means of a symmetrical nonlinear resistance [1, 2], the latter can be made up either of carborundum resistors, or of two diodes connected in series or in parallel with opposite polarities, or of a number of diodes connected in a bridge scheme. The carborundum resistors are stable, but are subject to high losses [3]. When two diodes of opposite polarities are used, it is very difficult to construct a nonlinear resistance having a good symmetry of the voltampere characteristic around a selected point, because the individual diode specimens differ a great deal in their characteristics. The symmetrical nonlinear resistance produced by four electronic valves connected to a common cutoff voltage (Fig. 1) [4] also has its shortcomings; these are: first, the necessity of employing for the cutoff a battery or other source of constant dc voltage; second, the great losses introduced by the high resistance of this voltage source, especially if it is of low power; and third, the eventual presence of a so-called "zero current," that is, a current in the output when no voltage is applied to the a, b terminals of such a symmetrical nonlinear resistance.

Fig. 1.

Of great interest is a bridge scheme (Fig. 2) which has in its diagonal branch a "stabilitron" voltage regulator consisting of a silicon breakdown or zener diode of one of the D808-D813 types.* Potentiometer rheostat or slide wire R_p serves to adjust the bridge to symmetrical output. Such a bridge has low impedance and small physical dimensions. In obtaining of symmetrical nonlinear resistances of high stability, the determining factors are the magnitude and stability of the forward resistances and of the reverse currents (or reverse resistances) of the rectifying diodes in the bridge arms.

*It has been proven that at higher voltages—say, above 5-6 v—an avalanche breakdown rather than the Zener phenomenon is responsible for the operation; therefore, there is at present among semiconductor engineers a tendency to use the term "breakdown diode," rather than "zener diode," as the generic term. In this translation, as well as in the original Russian text, the name "zener diode" is not used [Translator's note].

In Tables 1 and 2 are presented characteristics of germanium diodes of type DGTs-27 and of silicon diodes of type D202, all obtained experimentally. The diodes were chosen to have peak inverse voltages u_{inv} of 16 v, which is much higher than the highest possible breakdown voltage in the bridge diagonal; in that case the reverse voltages normally applied to each of the rectifying diodes in the bridge arms are approximately equal to the rated voltage output from the type D808-813 silicon stabilitron. The data of Table 1 show that the reverse currents with a potential of 16 v applied to DGTs-27 germanium diodes reach tens and hundreds of microamperes at elevated temperatures. Farther below in this paper it will be shown that in a typical magnetic amplifier for measurement purposes which is to have sufficient sensitivity for sensing an input of 10^{-12} w, the highest permissible "zero" current (output current with zero input to the amplifier) must be less than 3.5 μa. The high reverse currents and the large scattering of the characteristics of DGTs-27 germanium diodes make it impossible to use them for construction of a bridge of the type under discussion. In addition, in the DGTs-27 diodes after application of the reverse potential, a change of the reverse current with time is observed as illustrated in Fig. 3. This phenomenon is especially conspicuous at elevated temperatures. At 55°C also a lack of constancy, or reproducibility of the reverse currents in the very same DGTs-27 diode in successive tests, is observed: the reverse current varies by several microamperes from test to test.

TABLE 1

Characteristics of DGTs-27 Germanium Diodes

No. of diode	Reverse current with 16 v applied reverse voltage, μa		Forward resistance for 2 ma forward current, ohms	No. of diode	Reverse current with 16 v applied reverse voltage, μa		Forward resistance for 2 ma forward current, ohms
	20°C	55°C	20°C		20°C	55°C	20°C
1	8.9	92	92.4	6	17.8	134	92.0
2	14.8	109	99.0	7	18.0	240	97.3
3	20.0	256	90.5	8	19.1	126	91.3
4	15.2	193	101.0	9	14.8	134	98.2
5	10.0	74	94.1	10	12.0	184	93.0

TABLE 2

Characteristics of D202 Silicon Diodes

No.	Reverse current with 16 v applied in reverse direction, μa		Forward resistance (ohms) at forward current of			
			2 ma		20 ma	
	20°C	90°C	20°C	90°C	20°C	90°C
1	0.05	0.29	322	264.5	37.8	33.55
2	0.00	0.40	318	260.0	36.8	32.45
3	0.00	0.41	320	261.0	37.1	32.85
4	0.05	0.70	320	270.5	38.4	34.40
5	0.00	1.85	310	251.0	36.2	36.90
6	0.00	0.15	318	259.5	37.1	33.25
7	0.20	2.88	318	262.5	37.0	33.40
8	0.10	1.90	320		37.5	

Let us consider the possibility of using silicon diodes of type D202 in this bridge. The forward resistance of these diodes is about three times as large as that of the DGTs-27 germanium diodes, but it varies much less from specimen to specimen at a given temperature. The reverse current in the D202 diodes is very small even at 90°C (Table 2); however, here the forward resistance of the diodes is of much more importance than the reverse current: it is the forward resistance which practically determines the sensing threshold (minimum of detectability) in a magnetic amplifier when the bridge discussed here is used. In view of the above, ultimately silicon diodes of types D202-205 were chosen as rectifiers for the arms of our bridge.

In Fig. 4 a static voltampere curve of the bridge is shown when the silicon diodes were used in the bridge arms, and a silicon "stabilitron" in the bridge diagonal. The dynamic resistance at a current of 20 ma is

$$R_d = \frac{\Delta u}{\Delta i} = \frac{11.5 - 10.6}{(20 - 0.11)\,10^{-3}} = 45.1 \text{ ohm.}$$

The breakdown diode in the bridge diagonal has no influence on the symmetry of the bridge when all four diodes in the bridge arms are equal, because the bridge is being opened for passage of current at the same applied voltage regardless of the latter's polarity. Sources of asymmetry are inequalities of forward resistances and of reverse currents of the rectifying diodes in the bridge arms.

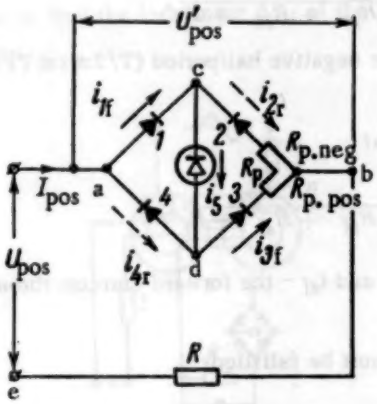

Fig. 2.

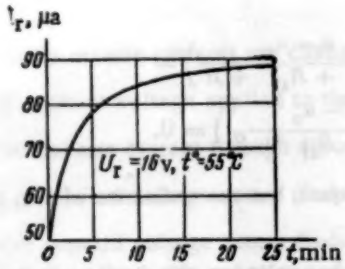

Fig. 3.

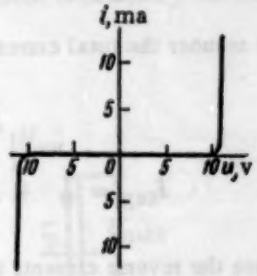

Fig. 4.

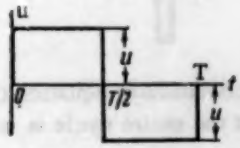

Fig. 5.

Let us first examine how the bridge symmetry is affected by the forward resistances of the arms, or, in other words, how the sensing threshold of a magnetic amplifier using such a bridge is affected by these arm resistances.

We assume that a rectangular ac voltage as shown in Fig. 5 is applied to the a and e terminals of the bridge circuit of Fig. 2. The character of operations of the circuit of Fig. 2 is not changed thereby.

During the positive halfperiod the total current passed through the bridge (see Fig. 2) is

$$I_{pos} = i_{1f} + i_{4r} = i_{3f} + i_{2r}, \tag{1}$$

where i_{1f} and i_{3f} are the forward currents through diodes 1 and 3, and i_{4r} and i_{2r} – the reverse currents through diodes 4 and 2.

It is assumed that during the halfperiod under consideration the currents in diagonally opposite arms of the bridge are equal, that is, that

$$i_{4r} = i_{2r} \tag{2}$$

and

$$i_{1f} = i_{3f} = \frac{u - (u_o + i_{1f} R_d)}{R_{1f} + R_{3f} + R}, \tag{3}$$

where u is the voltage applied to the bridge during the period of time t between 0 and T/2 ($0 \le t \le T/2$), u_o – the breakdown blocking voltage of the diode in the bridge diagonal, R_{1f} and R_{3f} – the forward resistances of diodes 1 and 3,

R – the sum of all active resistances in the output circuit including $R_{p\,pos}$, which is the resistance of the part of potentiometer R_p in series with R_{3f} still inside the bridge (Fig. 2).

When $i_{1f}R_d \ll u - u_0$, equation (3) is simplified to the following:

$$i_{1f} = i_{3f} = \frac{u - u_0}{R_{1f} + R_{3f} + R}. \tag{4}$$

From (4), (2), and (1) we obtain the total current through the bridge at $0 \leq t \leq T/2$:

$$I_{pos} = i_{4r} + \frac{u - u_0}{R_{1f} + R_{3f} + R} = i_{2r} + \frac{u - u_0}{R_{1f} + R_{3f} + R}. \tag{5}$$

In a similar manner the total current through the bridge during the negative halfperiod ($T/2 \leq t \leq T$) is obtained, which is

$$I_{neg} = i_{3r} + i_{3f} = i_{1r} + i_{4f},$$

$$I_{neg} = i_{3r} + \frac{u - u_0}{R_{3f} + R_{4f} + R} = i_{1r} + \frac{u - u_0}{R_{2f} + R_{4f} + R}, \tag{6}$$

where i_{1r} and i_{3r} are the reverse currents through diodes 1 and 3, and i_{2f} and i_{4f} – the forward currents through diodes 2 and 4.

In order that the bridge be symmetrical, the following condition must be fulfilled:

$$R_{1f} + R_{3f} = R_{2f} + R_{4f}. \tag{7}$$

When the condition of equation (7) is fulfilled, and in addition the reverse currents in the arms are equal, the dc component for the entire cycle is equal to zero, that is,

$$I_0 = i_{2r} + \frac{u - u_0}{R_{1f} + R_{3f} + R} - \left(i_{3r} + \frac{u - u_0}{R_{2f} + R_{4f} + R}\right) =$$

$$= i_{4r} + \frac{u - u_0}{R_{1f} + R_{3f} + R} - \left(i_{1r} + \frac{u - u_0}{R_{2f} + R_{4f} + R}\right) = 0.$$

Let us now assume that the forward resistances of three diodes are equal, but the resistance of arm one has changed by a quantity ΔR_{1f}.

When there is a change in the forward resistance, the reverse voltages applied to the diodes are changed only insignificantly; therefore, it is possible to disregard the changes in the reverse currents caused by the resistance change ΔR_{1f}. Then, for the deviation of the "zero" current from actual zero, that is, for the dc component, we have

$$\Delta I_0 = \frac{u - u_0}{R_{1f} - \Delta R_{1f} + R_{3f} + R} - \frac{u - u_0}{R_{1f} + R_{3f} + R} \approx \frac{(u - u_0)\,\Delta R_{1f}}{(R_{1f} + R_{3f} + R)^2}. \tag{8}$$

By means of (8) it is possible to find the highest permissible variation in the forward resistances of the bridge arm diodes corresponding to any given acceptable sensitivity level.

When to an arrangement according to the circuit diagram of Fig. 6 a symmetrical sinusoidal potential is applied, which is sufficiently high for magnetic saturation of the cores during the major part of each halfperiod, then the output voltages have the shapes of pulses [1]. For the sake of simplicity, let us assume that these pulses have rectangular shapes, that is, that the potentials at the terminals of the output winding maintain constant values for the entire duration of the halfperiod T_p of the pulse (Fig. 7). In this case quantity ΔI_0 is determined by the following formula:

$$\Delta I_0 = \frac{1}{T}\left[T_p \frac{(u - u_0)\,\Delta R_{1f}}{(R_{1f} + R_{3f} + R)^2}\right]. \tag{9}$$

From this it follows that, to have a desired threshold ΔI_0 of current sensitivity, the permissible variation of the forward resistance is

$$\Delta R_{1f} = \Delta I_0 \frac{T}{T_p} \frac{(R_{1f} + R_{3f} + R)^2}{u - u_0}. \tag{10}$$

Let us now examine how the reverse currents in the bridge arms affect the symmetry of the bridge. We make the following assumptions: 1) the reverse currents of three diodes remain unchanged and are all equal to each other, while the reverse current of the fourth diode is changed by Δi_{4r}; 2) the change of the forward resistances produced by the change Δi_{4r} can be disregarded. Throughout $T/2 \leq t \leq T$ the total I_{neg} current through the bridge remains unchanged at the value specified by equation (6). The change of the reverse current of the fourth diode which takes place at $0 \leq t \leq T/2$ causes a deviation of the "zero," that is, the appearance of a constant dc component ΔI_0 in the output of the bridge. Because, when i_{4r} is changed, i_{1f} is also changed, the zero deviation is

$$\Delta I_0 = I'_{pos} - I_{pos} = (i'_{4r} + i'_{1f}) - (i_{4r} + i_{1f}) = \Delta i_{4r} - \Delta i_{1f}. \tag{11}$$

Let us find the increment Δi_{1f} of the forward current of diode one which is caused by the change of the reverse current i_{4r}.

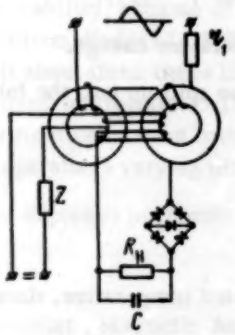

Fig. 6.

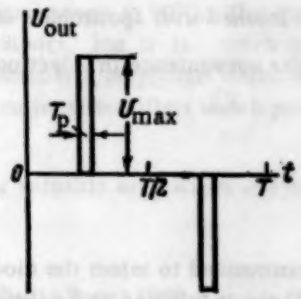

Fig. 7.

When the reverse currents are changed, the voltage at the bridge terminals a, b remains practically unchanged.

With constant voltage applied to the bridge terminals a–b, the following changes take place simultaneously:

1. The reverse current through diode 4 increases from i_{4r} to i'_{4r}; the voltage applied to it decreases by Δu_4.

2. The forward voltage across diode 3 increases by Δu_3, the forward current through it by Δi_{3f}.

3. The forward voltage across diode one is decreased by Δu_1; and, assuming that the voltage across the diode in the bridge diagonal remains constant and equal to u_0, the forward current through diode one is decreased by $\Delta i_{1f} = i'_{1f} - i_{1f}$.

4. The reverse voltage across diode 2 is increased by Δu_2, but the current through it remains unchanged.

The reverse voltage across the diodes is in a section of the characteristics where the reverse current is independent of the applied reverse voltage. Therefore, when the reverse voltage applied to diode 2 is increased by Δu_2, the reverse current remains unchanged.

The current through the diode in the bridge diagonal i_5 is decreased by an amount Δi_5 which is equal to the change of the current in diode one (according to the first networks law of Kirchhoff applied to the currents meeting at point c, Fig. 2). For point d (Fig. 2) we have

$$|\Delta i_{4r}| = |\Delta i_{1f}| + |\Delta i_{3f}|. \tag{12a}$$

When the voltage across the a–b terminals of the bridge is constant, and the breakdown voltage u_0 of the diode in the bridge diagonal also is constant, the voltage increase across diode one is equal in absolute value to the voltage decrease across diode 3, that is, $|\Delta u_1| = |\Delta u_3|$. Therefore, since diodes one and 3 have identical characteristics, the variations of their forward currents are also equal in absolute value, that is,

$$|\Delta i_{1f}| = |\Delta i_{3f}|. \tag{12b}$$

From (12a) and (12b) we have

$$|\Delta i_{4r}| = 2\,|\Delta i_{1f}|. \tag{12c}$$

Substituting (12c) into (11), we obtain the following expression for the zero shift caused by a change in the reverse current of one of the four bridge arms diodes:

$$\Delta I_o = \frac{\Delta i_{4r}}{2}. \tag{13}$$

Thus, we see that the change in the total bridge current is smaller than the change of the reverse current of one of the diodes.

Temperature changes do not cause an asymmetry of the bridge, provided the following equation prevails:

$$(i'_{4r} - i_{4r}) + (i'_{2r} - i_{2r}) = (i'_{3r} - i_{3r}) + (i'_{1r} - i_{1r}), \tag{14}$$

wherein the i's marked with apostrophes designate the currents after the temperature change.

For greater convenience in selection of the diodes, equation (14) may be split up into the following two equations:

$$i_{4r} + i_{2r} = i_{3r} + i_{1r}, \tag{15}$$

$$i'_{4r} + i'_{2r} = i'_{3r} + i'_{1r}. \tag{16}$$

It is recommended to select the diodes to fit equation (16) for an elevated temperature, since in that case usually equation (15) too is fulfilled as a natural consequence.

In conclusion it can be stated that with respect to the reverse currents the diodes must be selected in such a way that, first, the sum of the reverse currents in one pair of diametrically opposite bridge arms is equal to the sum of the reverse currents in the other pair of bridge arms, and, second, that the highest values of the reverse currents occurring within the range of operational temperatures are taken into account for establishment of this equality.

TABLE 3

R_c, ohms	R_{1f}, ohms	R_{3f}, ohms	R, ohms	k_I	P, w	ΔI_0, μa	ΔR_f, ohms
400	300	300	300	70	10^{-14}	0.35	0.35
400	300	300	300	70	10^{-12}	3.5	3.5

Let us evolve the relationships between the sensing threshold and the "zero" current when the forward resistance in one of the arms of a nonlinear symmetrical bridge, connected to the output of a magnetic amplifier (Fig. 6), is changed.

Designating the lower threshold of sensing (minimum detectable quantity) of the magnetic amplifier, in terms of power, by P, and the shift in "zero" current at the amplifier output by ΔI_0, we have [1]

$$P = \left(\frac{\Delta I_o}{k_I}\right)^2 R_c \quad \text{or} \quad \Delta I_o = \sqrt{\frac{P}{R_c}}\, k_I, \tag{17}$$

where k_I is the current amplification and R_c – the sum of all active resistances in the control circuit.

From (10) and (17) we obtain an expression for the highest admissible variation of the forward resistance for a given sensing threshold, which is as follows:

$$\Delta R_f = \sqrt{\frac{P}{R_c}}\, k_I \frac{(R_{1f} + R_{3f} + R)^2}{u - u_o} \frac{T}{T_v}. \tag{18}$$

From (17) and (18) we can find for any required sensing threshold the corresponding highest permissible variation in "zero" current ΔI_0 and the corresponding highest permissible variation of the forward resistance. For example, when typical specification data for an instrumental magnetic amplifier with low sensing thresholds, built according to the diagram of Fig. 6, are substituted into formulas (17) and (18), the data of Table 3 are obtained. It was assumed that $T_v = T/20$, $u = 20$ v, and $u_0 = 10$ v.

From the calculated values of permissible increments of the "zero" current given in Table 3 and the data presented in Tables 1 and 2 we come to the conclusion that using germanium diodes it is impossible to create a symmetrical nonlinear resistance whose "zero" current would be smaller than 3.5 μa.

CONCLUSIONS

It is shown that inclusion of a stabilitron voltage regulator, consisting of a breakdown silicon diode, in the bridge diagonal makes it possible to obtain nonlinear resistances having uneven voltampere characteristics. The customary use of germanium diodes in the bridge arms is very little suitable for creation of symmetrical nonlinear resistances of high stability, because of the high and variable reverse currents of these diodes, especially at elevated temperatures. Silicon diodes of D202-205 types have high reverse resistances even at 90°C. The forward resistance of these diodes is about three times higher than those of the germanium diodes, but it is much more uniform and invariable at a fixed temperature. Their use makes it possible to build magnetic amplifiers which operate on the principle of rectification of even harmonics, by means of symmetrical nonlinear rectifiers which possess low sensing thresholds at temperatures varying within wide limits.

The author expresses his thanks to M. A. Rozenblat for a number of valuable suggestions and comments.

LITERATURE CITED

1. M. A. Rozenblat, Magnetic Amplifiers, v. II [in Russian], Soviet Radio Press, 1960.
2. B. A. Mazzeo, "A low-level, high-accuracy dc magnetic amplifier," Electrical Manufacturing, 62, No. 5, Nov. 1958.
3. M. A. Rozenblat, "Fundamentals of theory and design of selective rectifiers using nonlinear symmetrical resistances," Avtomatika i Telemekhanika, 15, No. 4, 1954.
4. R. Ya. Berkman, "A phase detector using multiple frequencies," Avtomatika i Telemekhanika, 19, No. 4, 1958.

SENSITIVE MAGNETIC MODULATOR WITH TWO-PHASE INPUT

F. I. Kerbnikov and M. A. Rozenblat

(Moscow)

Translated from Avtomatika i Telemekhanika, Vol. 22, No. 3,
pp. 376-382, March, 1961
Original article submitted June 1, 1960

Circuit and theory are presented of a two-phase magnetic modulator which uses perpendicular to each other magnetic fields and is supplied with power from a source of rectangular voltage pulses. It is shown that such a modulator has substantial advantages over other, more widely used types of modulators.

Results of an experimental investigation of this modulator also are presented.

It is known that of all types of magnetic modulators the modulators operating on the principle of frequency doubling have the lowest sensing threshold [1]. The limit of sensitivity of such modulators is set by the magnetic noises and is within the range of 10^{-19} to 10^{-17} w.

However, such a low sensing threshold can be assured only by the use of complicated schemes for removal of even harmonics from the supply voltage and suppression of the disturbance voltages (uneven harmonics) in the modu-

lator output. Another shortcoming of the frequency doubling modulator is the necessity of connecting into the circuit a blocking filter or a large inductance to eliminate the shunting action of the low resistance signal source with respect to the modulator output.

Use of modulators with perpendicular to each other fields [2] makes it possible to some extent to eliminate the mentioned shortcomings of modulators with frequency doubling by substantially lowering the parasitic disturbance voltages in the modulator output.

There are further improvements possible in the characteristics of magnetic modulators using frequency doubling such as: decrease of the disturbance voltages, lowering of the sensing threshold, improvement of the curve shape of the output voltage, and elimination of the necessity of having a blocking filter in the control circuit loop; these improvements can be achieved by the use of two similar modulators each with two perpendicular to each other fields, supplied by a two-phase voltage of rectangular shape.

The present article is devoted to a presentation of the results of an investigation of the modulation scheme using a two-phase supply voltage, suggested by the authors.

1. Scheme of the Modulator

The magnetic modulator consists of two ferrite cores 1 (Fig. 1), each of which is provided with an excitation winding W_1 which serves for production of the transverse alternating magnetic field, a control winding W_c, and an output winding W_2 [2].

As an electric power supply, a two-phase magnetic transistor generator-converter is used, consisting of two identical dc to ac converters and an arrangement for synchronization of these two converters [3].

This scheme (Fig. 2) is distinguished by the feature that there are in the output two rectangularly shaped voltages U_1, U_2 which differ from each other by 90° in phase. The generator has high efficiency, and its output voltage has only a very small content of even harmonics. Moreover, these harmonics can be practically reduced to zero by adjustment of a variable resistor R_θ.

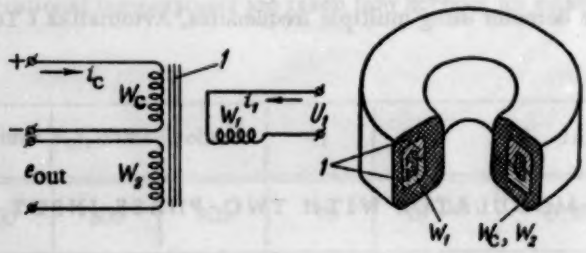

Fig. 1.

The rectangular shape of the voltage supply pulses makes it possible, as will be shown, to obtain practically sinusoidally shaped voltages in the modulator output.

In the scheme of Fig. 2 the voltages of doubled frequency, which are produced by induction in the control windings W_c when a signal is present, mutually compensate each other. Therefore, there is no need any more for a special filter or inductance in the control circuit loop for elimination of these double frequency voltages.

2. Operation of the Modulator When in the Idling State

Let us examine one of the excitation circuits of the modulator shown in Fig. 2, when to the excitation winding W_1 an excitation potential of rectangular shape is applied, while in the control winding W_c there is only a very small signal applied.

During one halfperiod of the supply voltage ($0 \leq t \leq T/2$), the process in the excitation circuit is described by the equation

$$W_1 S_\perp 10^{-8} \frac{dB_\perp}{dt} + Ri_1 = U_1, \qquad (1)$$

where U_1 is the amplitude of the supply voltage, R – the resistance of the W_1 winding, $S_\perp$ – the cross-sectional area for the excitation flux.

When the resistance of the excitation circuit loop is sufficiently small, the Ri_1 component in equation (1) can be considered negligible for the major part of the halfperiod under examination. Neglecting Ri_1, integration of (1) gives

$$B_\perp = -B_0 + \frac{10^8 U_1}{W_1 S_\perp} t, \tag{2}$$

wherein $-B_0$ is the value of the magnetic induction $B_\perp$ at the moment $t = 0$.

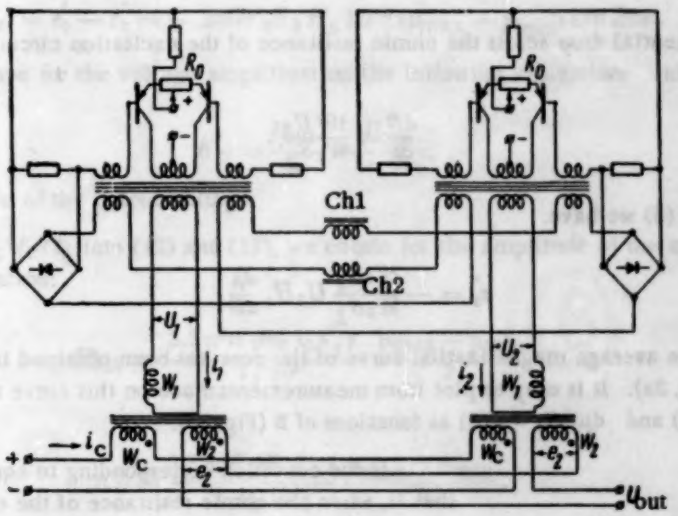

Fig. 2.

It follows from the symmetry condition that, when a steady state of operation has been reached, at $t = T/2$ there must be $B_\perp = B_0$. Hence we have

$$B_0 = \frac{10^8 U_1}{4W_1 S_\perp} T = \frac{10^8 U_1}{4fW_1 S_\perp}, \tag{3}$$

where f is the frequency of the excitation voltage.

Considering the material of the core to be magnetically isotropic we have

$$\frac{B_\parallel}{H_\parallel} = \frac{B_\perp}{H_\perp} = \frac{B}{H},$$

where $B = \sqrt{B_\parallel^2 + B_\perp^2}$, $H = \sqrt{H_\parallel^2 + H_\perp^2}$. $B_\parallel$ and $H_\parallel$ here are respectively the induction and field strength (magnetizing force) in the longitudinal direction, and $B_\perp$ and $H_\perp$ – the induction and field intensity in the transverse direction.

Under the influence of a signal i_C in the control winding, a longitudinal field strength $H_0 = 0.4\pi i_C w_C / l_\parallel$ is produced, to which an induction in the longitudinal direction corresponds which is

$$B_\parallel = H_0 \frac{B_\perp}{H_\perp} = H_0 \mu, \tag{4}$$

where μ is the static magnetic permeability of the core material.

Under these conditions on the terminals of output winding W_2 of the modulator under examination the following emf will appear:

$$e_2' = -W_2 S_\parallel 10^{-8} \frac{dB_\parallel}{dt} = -W_2 S_\parallel H_0 10^{-8} \frac{d\mu}{dt}. \tag{5}$$

We must point out that the μ used here must be determined from measurements on the so-called "average" magnetization curve, which is the curve located midway between the ascending and descending branches of the hysteresis loop.

If we limit our examination only to small signals, we can assume that the law according to which μ varies with time is univalently determined exclusively by the variation with time of the transverse inductance component $B_\perp$, and practically does not depend at all upon the magnitude of the signal. Therefore, expression (5) can be rewritten as follows:

$$e_2' = -W_2 S_\parallel H_0 10^{-8} \frac{d\mu}{dB}\frac{dB}{dt}, \tag{6}$$

where $B = B_\perp$.

If we neglect the potential drop across the ohmic resistance of the excitation circuit, then for $B_\perp$ formula (2) is valid, and from it we obtain

$$\frac{dB}{dt} = \frac{10^8 U_1}{W_1 S_\perp}. \tag{7}$$

Substituting this into (6) we have

$$e_2' = -\frac{W_2 S_\parallel}{W_1 S_\perp} U_1 H_0 \frac{d\mu}{dB}. \tag{8}$$

Let us assume that the average magnetization curve of the core has been obtained in graphic form by means of suitable measurements (Fig. 3a). It is easy to plot from measurements made on this curve the curves expressing the quantities $\mu = B_\perp / H_\perp = f(B)$ and $d\mu/dB = \varphi(B)$ as functions of B (Fig. 3b).

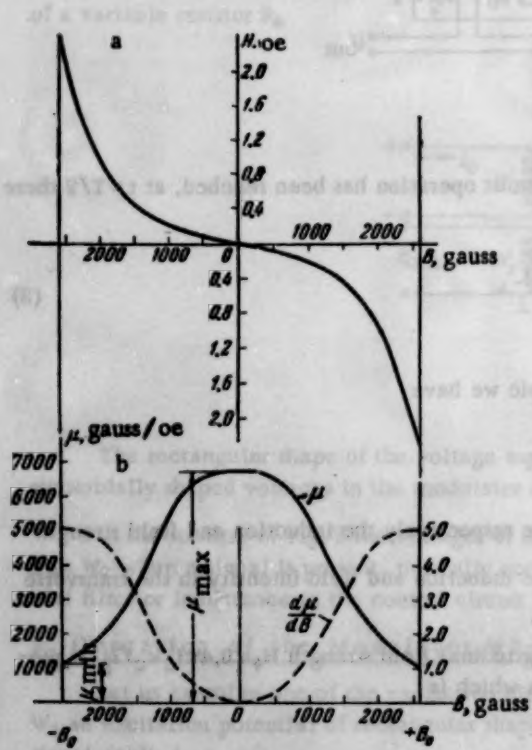

Fig. 3.

If the condition corresponding to equations (2) and (8) prevails, that is, when the ohmic resistance of the excitation loop is practically zero, the curve of the output of the modulator e_2' will coincide with the curve $d\mu/dB = \varphi(B)$ within the limits from $B = -B_0$ to $B = +B_0$. Experience has shown that it is not difficult, when using ferrite cores, to select such a value for B_0 (by a suitable choice of supply voltage), that $\varphi(B) = d\mu/dB$ will be close to a harmonic function.

That means that within the indicated range of B, the relationship between B and μ can practically be represented as follows:

$$\mu = \frac{\mu_{max} + \mu_{min}}{2} + \frac{\mu_{max} - \mu_{min}}{2} \cos\frac{B}{B_0}\pi, \tag{9}$$

where B is determined by formula (2), B_0—by formula (3), and μ_{min} is the value of the magnetic permeability at $B = \pm B_0$. Substituting this value of μ into (8) and taking into account (3), we obtain

$$e_2' = -\omega W_2 S_\parallel H_0 10^{-8} (\mu_{max} - \mu_{min}) \sin 2\omega t. \tag{10}$$

Thus, for determination of the amplitude of the output voltage it is sufficient to know the maximum value of the permeability from the average magnetization curve, and the minimum value of permeability μ_{min} which corresponds to $B = \pm B_0$. Since usually $\mu_{min} \ll \mu_{max}$, for approximate calculations it is sufficient to know the value of μ_{max}.

Let us point out that the presence of a finite ohmic resistance in the excitation circuit has an effect only when B approaches the values of $\pm B_0$, that is, in the region of saturation of the core. Moreover, the ohmic resistance plays a part favoring a sinusoidal shape for the output voltage e_2', since because of it at $B = \pm B_0$ practically $dB/dt \approx 0$. Therefore, even in the case that the derivative $d\mu/dB \neq 0$ at $B = \pm B_0$, the emf e_2' becomes equal to 0 because $dB/dt \approx 0$ [see formula (6)].

In the next halfperiod when the supply voltage changes from $+U_1$ to $-U_1$, we obtain for the emf in the output of the first modulator core an expression which is exactly the same as expression (10) obtained for the first halfperiod, because $\mu(t+T/2) = \mu(t)$.

Taking into account the $\pi/2$ phase shift between the supply voltages of the two core windings, we obtain the following expression for the output voltage from the second core of the modulator:

$$e_2''(\omega t) = -e_2'\left(\omega t + \frac{\pi}{2}\right) = \omega W_2 S_{\parallel} H_0 10^{-8} (\mu_{max} - \mu_{min}) \sin 2\omega t. \tag{11}$$

When the output windings of the two modulator cores are connected with each other in series opposition the overall output voltage is

$$e_{out} = e_2' - e_2'' = -2\omega W_2 S_{\parallel} H_0 10^{-8} (\mu_{max} - \mu_{min}) \sin 2\omega t. \tag{12}$$

Since $U_c = R_c i_c$ we have for the voltage amplification the following expression:

$$K_U = \frac{U_{out}}{U_c} = \frac{U_{out}}{i_c R_c}, \tag{13}$$

where U_{out} is the amplitude of the output voltage.

Substituting $H_0 = 0.4\pi i_c W_c / l_{\parallel}$ into (12) and (13), we obtain for the amplitude of the modulator output voltage, and for the voltage amplification:

$$U_{out} = \frac{3.2\pi^2 W_2 W_c i_c S_{\parallel} f}{l_{\parallel} 10^8} \frac{\mu_{max} - \mu_{min}}{2} \tag{14}$$

and

$$K_U = \frac{3.2\pi^2 W_2 W_c S_{\parallel} f}{R_c l_{\parallel} 10^8} \frac{\mu_{max} - \mu_{min}}{2}, \tag{15}$$

where $l_{\parallel}$ is the average length of the core.

3. Time Constant of the Modulator

Under the influence of a signal in the core a dc component of the induction is established which is.

$$B_{0\parallel} = \frac{1}{2\pi} \int_0^{2\pi} B_{\parallel} d\omega t = \frac{1}{2\pi} \int_0^{2\pi} \mu H_0 d\omega t. \tag{16}$$

Substituting μ from (9) and carrying out the integration, we find that B_0 parallels $\mu_0 H_0$, where μ_0 is the magnetic permeability of the core for the dc induction component, which is determined by the formula

$$\mu_0 = \frac{\mu_{max} + \mu_{min}}{2}. \tag{17}$$

The inductance of the control winding is

$$L_c = \frac{0.8\pi W_c^2 S_{\parallel}}{l_{\parallel} 10^8} \frac{\mu_{max} - \mu_{min}}{2}. \tag{18}$$

The time constant of the control circuit can be calculated by means of the fundamental formula for charge or discharge of an inductance: $\tau = L_c/R_c$ where R_c is the overall resistance of the control circuit.

4. Operation of the Modulator under Load

An exact account of the effects of the load resistance leads to cumbersome calculations. However, for the type of modulator under discussion an approximate account of its behavior under a load R_L is possible by the use of the following simplified method [4]. The modulator is considered to be a generator of an emf $= U_{out}$ of doubled frequency having an internal inductive impedance $Z_i = 2\omega L_i$. In this approximate computation we neglect the variation of U_{out} and L_i with magnitude of load current. The L_i considered here is the average value during a period of the inductance of the output winding W_2, and therefore can be calculated in a manner similar to that of the inductance

L_C. Thus we have

$$L_i = \frac{W_2^2}{W_C^2} L_C = \frac{0.8\pi W_2^2 S_{\parallel}}{l_{\parallel} 10^8} \frac{\mu_{max} + \mu_{min}}{2}. \quad (19)$$

The amplitude of the second harmonic in the voltage across the load resistance is

$$U_{Lm} = \frac{U_{out}}{\sqrt{R_L^2 + (2\omega L_i)^2}}. \quad (20)$$

Taking into account (14), (18), and (20) we have

$$U_{Lm} = \frac{1.6\pi^2 W_2 W_C S_{\parallel} f i_C R_L (\mu_{max} + \mu_{min})}{l_{\parallel} 10^8 \sqrt{R_L^2 + 2.56\pi^4 \left[\frac{f W_2^2 S_{\parallel} (\mu_{max} + \mu_{min})}{l_{\parallel} 10^8}\right]^2}}. \quad (21)$$

It is evident that the output power reaches its maximum when the load resistance is

$$R_L = 2\omega L_i \approx 2\omega \frac{W_2^2}{W_C^2} L_C = \frac{1.6\pi^2 W_2^2 S_{\parallel} f (\mu_{max} + \mu_{min})}{l_{\parallel} 10^8}. \quad (22)$$

5. Results of Experimental Investigation

An experimental investigation of a modulator with cores as described was carried out for the purpose of comparing the actual characteristics with the theoretical, and for determination of the lowest sensing threshold. The results of this investigation are presented in the accompanying table.

μ_{max}, gauss/oe	μ_{min}, gauss/oe	B_s, gauss	H_c, oe	$S_{\parallel}$, cm^2	$l_{\parallel}$, cm	T_k, °C
6700	1100	2670	0.1	0.68	7.53	80

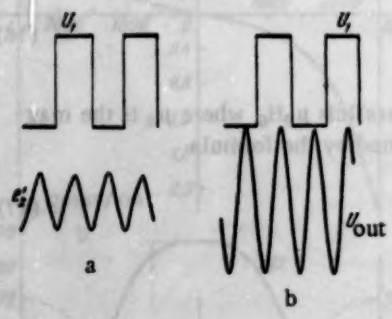

Fig. 4.

The windings on the cores of the modulator which was used in these tests had the following parameters: $W_1 = 100$, $W_2 = 1500$, $W_C = 1000$ turns; $R_C = 155$ ohms.

The oscillograms of the output voltage are shown in Fig. 4. The oscillogram in Fig. 4a is the one obtained from a single core with a signal of 10^{-10} w, and the oscillogram in Fig. 4b is the one obtained when both cores were used. It can be seen that the shape of the output voltage is already practically sinusoidal when a single-phase modulator is used; with a two-phase modulator, the amplitude of the output voltage is twice as large, and the content of higher harmonics is decreased.

The voltage amplification K_U, computed by formula (15) for the idling state, was 386. The maximum value of voltage amplification K_U actually measured at $f = 500$ cps with a high resistance load, in idling condition, was 368. The voltage of the parasitic second harmonic in the modulator output was found to equal an input signal of the order of $4 \cdot 10^{-16}$ w.

As is well known [2], a single-phase modulator with transverse fields makes it possible to obtain a sensing threshold of the order of 10^{-14} w. In Fig. 5 are presented the experimental curve (dashed line) and the curve computed by means of formula (21) (drawn-out line) for the relationship between the load resistance and the voltage across it at a current of $1 \cdot 10^{-6}$ amp on the control winding. The experimental curve practically coincides with the theoretical curve.

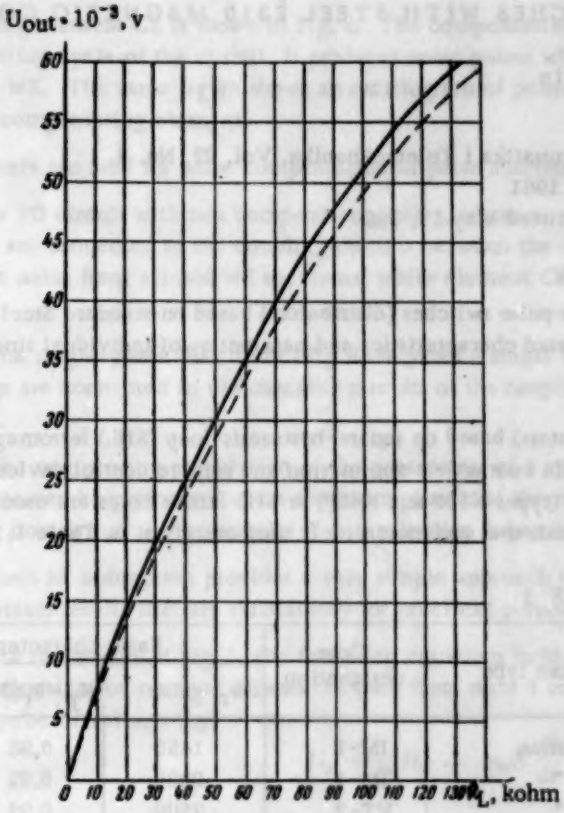

Fig. 5.

CONCLUSIONS

The proposed scheme of a modulator with two transverse fields using two rectangular pulses shifted in phase by 90° for voltage supply makes it possible: a) to obtain lower thresholds of detectable power, that is, higher sensitivity, than by a modulator with a single core; b) considerably to simplify the circuit of the amplifier in which the magnetic modulator is used, since there is no more need for filters in the control and power supply circuits; and c) to obtain a practically pure sinusoidal shape of the output voltage.

LITERATURE CITED

1. M. A. Rozenblat, Magnetic Amplifiers [in Russian], Soviet Radio Press, 1956.
2. F. I. Kerbnikov and M. A. Rozenblat, Magnetic modulators with transverse excitation. Avtomatika i Telemekhanika, 19, No. 9, 1958.
3. W. E. Jewett and P. Z. Schmidt, A more stable three-phase transistor-core power inverter, Proc. C.M.A. A.I.E.E., 1958.
4. M. A. Rozenblat, Magnetic Amplifiers [in Russian], Soviet Radio Press, 1960.

All abbreviations of periodicals in the above bibliography are letter-by-letter transliterations of the abbreviations as given in the original Russian journal. *Some or all of this periodical literature may well be available in English translation.* A complete list of the cover-to-cover English translations appears at the back of this issue.

CONTACTLESS SWITCHES WITH STEEL É310 MAGNETIC CORES

K. G. Mityushkin

(Moscow)

Translated from Avtomatika i Telemekhanika, Vol. 22, No. 3,
pp. 383-392, March, 1961
Original article submitted May 12, 1960

Magnetic contactless pulse switches (distributors) based on standard Steel É310 (KhVP) cores are described. The calculated characteristics and parameters of individual single- and double-throw distributors are given.

Pulse switches (distributors) based on square-hysteresis-loop (SHL) ferromagnetic components are presently used to an ever increasing extent in contactless automation and remote control devices [1-4]. Either metallic (laminated) cores made of special alloys (types N50P and N65P) or SHL ferrite cores are used in these components. The magneti characteristics of SHL materials that are most widely used are given in Table 1.

TABLE 1

Core type	Core designation	Basic characteristics		
		B_r, gauss	$K_p = B_r/B_s$	H_c, oe
Ferrite	IM-1	1450	0.96	1.1
"	IM-4	2000	0.92	0.3
"	VT-2	2500	0.93	0.8
"	VT-1	2300	0.93	1.25
"	VT-5	2700	0.93	0.15
Metallic	N-50P	15000	0.98	0.1
"	N-65P	13500	0.98	0.05

This article is concerned with the possibility of equipping contactless switches with standard laminated toroidal cores that are made of Steel É310 (GOST 5021-55), which are widely used in various electronic devices as intermediate and output low-frequency transformers.

The production technology of these cores is much simpler than that required for SHL alloys, and their cost is considerably lower.

The hysteresis loop of a Steel É310 core which was plotted for 50-cps alternating current is shown in Fig. 1. Although the É310 alloy does not belong to the group of SHL alloys, experiments indicate that these cores can be used in all known pulse distributor circuits which use SHL magnetic components. In this, the following advantages of distributors with laminated cores are preserved: the high specific power of the output pulse per unit volume of the material, the high temperature stability, and the possibility of making cores of any size required in electrocommunications practice* (the outside diameter of anchor rings can attain a few hundreds of millimeters). Due to this, it is possible to obtain pulses with a considerable amount of energy at the distributor (switch) output, which often makes it unnecessary to use the intermediate amplifying units that connect the distributor to the load.

Due to the nonrectangularity of the hysteresis loop of É310 cores, compensating elements, which serve for compensating the noise** arising in the working components, must be used in distributor circuits.

*It should be noted that the maximum outside diameter of SHL ferrite rings that are produced by the industry does not exceed 10 mm. For technological reasons, this diameter cannot be greatly increased.

**Emf noise arises due to departures from the rectangular shape of the hysteresis characteristic in shifting the operating point along saturation segments 0–0' and 1–1' (Fig. 1).

The circuit of the compensating element CE is shown in Fig. 2. The compensating element does not have a control winding, and, for each operating cycle of the circuit, it produces noise pulses which are in opposition to the noise pulses of the working element WE. The same figure shows an oscillogram of pulses in the load circuit in the absence (a) and presence (b) of the compensating element.

Common compensating elements are used for noise compensation in pulse distributor (PD) circuits.

Figure 3 shows a double-throw PD circuit with two compensating cores, where one core is provided for each phase. The compensating windings are connected to the coupling circuits between the elements and to the load circuits. Element CE_1 compensates the noise from all odd WE elements, while element CE_2 compensates the noise from all even WE elements.

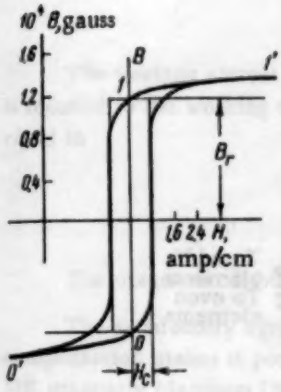

Fig. 1.

The single-phase PD circuit (Fig. 4) requires a single compensating element, whose windings are connected to the charging circuits of the coupling capacitors and to the load circuits.

The engineering calculation of the parameters of a single magnetic element with an E310 core can be performed under the assumption that the resulting hysteresis loop of the working core is strictly rectangular if compensation is provided (thin line contour in Fig. 1).

Such an assumption provides a very simple approach to the solution of this problem, and it yields results that are satisfactory for practical purposes.

For the circuit of Fig. 5, the following equations hold under the assumption that the core magnetization reversal follows the path from state 1 to state 0 under the action of a square pulse of voltage U_w:

$$U_w = i_w R_w + w_w S \frac{dB}{dt} 10^{-8}, \tag{1}$$

$$e_L = - w_L S \frac{dB}{dt} 10^{-8} = i_L R_L, \tag{2}$$

$$i_w w_w - i_L w_L = H_c l. \tag{3}$$

The initial core state is characterized by the point 1, and its final state is given by point 0 (Fig. 5).

By simultaneously solving this system of equations, we obtain the following expression for the variation of magnetic induction in time:

$$B_t = B_r - \frac{H_c l (k_{fo} - 1) R_L' t}{w_w^2 S 10^{-8} \left(1 + \frac{R_L'}{R_w}\right)}, \tag{4}$$

where $R_L' = R_L \left(\frac{w_w}{w_L}\right)^2$ is the load resistance, which is reduced to the working circuit, $k_{fo} = \frac{U_w}{I_c R_w}$ is the forcing coefficient under the operating conditions, and $I_c = \frac{H_c l}{w_w}$.

The total core magnetization reversal time (from point 1 to the point 0) is found from (1) for $B_t = -B_r$:

$$t_s = \frac{2B_r \, w_w^2 S 10^{-8} \left(1 + \frac{R_L'}{R_w}\right)}{H_c l R_L' (k_{fo} - 1)}. \tag{5}$$

It is clear that, for a total magnetization reversal in the core, it is necessary that the operating pulse time t_p be not less than t_s.

According to (2), the load current amplitude is equal to

$$I_L = \frac{w_L S}{R_L} \frac{dB}{dt} 10^{-8} = \frac{w_L S}{R_L} \frac{2B_r}{t}. \tag{6}$$

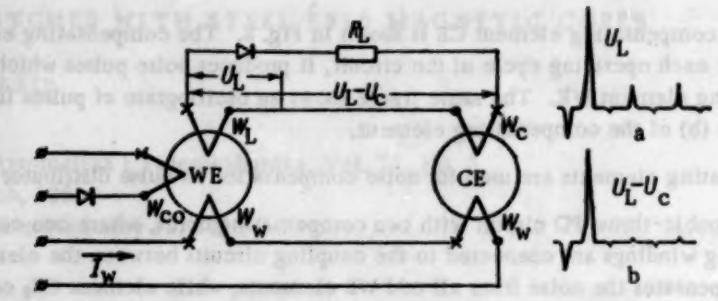

Fig. 2. W_w) working windings; W_{CO}) control winding; W_L and W_C) load and compensating winding, respectively; R_L) load resistance.

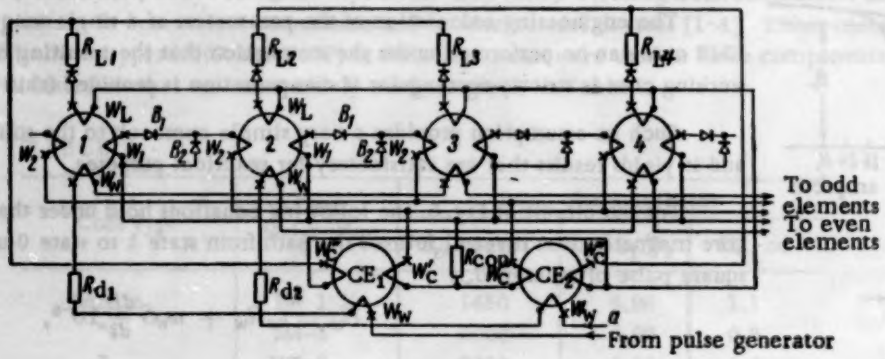

Fig. 3.

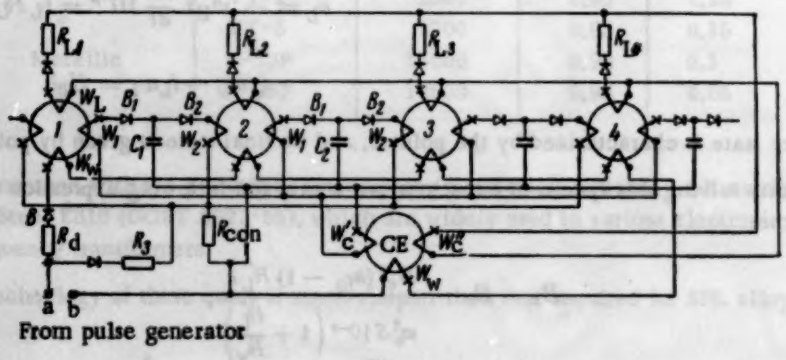

Fig. 4.

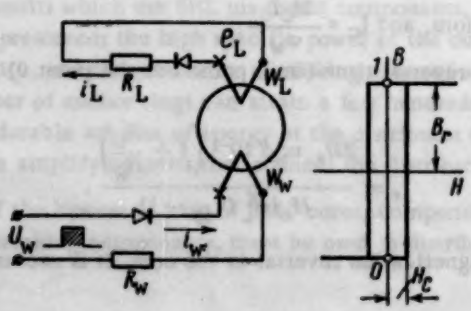

Fig. 5.

By substituting in this expression the value of dB/dt, which is found from (4), we obtain the following expression after some transformations:

$$I_L = \frac{H_c l}{w_L} \frac{(k_{fo} - 1)}{\left(1 + \frac{R_L'}{R_w}\right)}. \quad (7)$$

The current through the working winding during the magnetization reversal process is found from (3) by taking into account (7):

$$I_w = I_{NL}\left[\frac{k_{fo} - 1}{1 + \frac{R_L'}{R_w}} + 1\right]. \quad (8)$$

The working circuit current consists of two components: the no-load current I_{NL} and the load current I_L, which is reduced to the working circuit. After the magnetization reversal is completed, the working circuit current becomes equal to

$$I_w = I_{wm} = \frac{U_w}{R_w}. \quad (9)$$

The diagrams of the magnetic induction and of the load and working circuit currents are given in Fig. 6.

The satisfactory agreement between experimental and calculated data for a single magnetic element with compensation makes it possible to use the well-known method for calculating the parameters of pulse distributors for SHL magnetic elements [3 and 4] when Ė310 cores are used in these circuits.

Example 1. By using the above equations, we shall determine the parameters of a magnetic element that secures a current equal to $I_L = 1$ amp in the load winding for the resistance $R_L = 5$ ohms and a pulse duration of 5 msec.

The core dimensions are 30 × 20 × 6 mm, the remanent induction is $B_r = 12{,}000$ gauss, and $H_c = 0.8$ amp/cm. The core cross-sectional area is $S = 0.30\ cm^2$, and the median line length is $l = 7.8$ cm.

By substituting in Eq. (5) the expression for the difference $k_{fo} - 1$ found from (7), we obtain

$$t_s = \frac{2B_r w_L S\ 10^{-8}}{I_L R_L}. \quad (10)$$

Hence, $w_L = 350$.

We shall find the forced-conditions coefficient from expression (7):

$$k_{fo} = \frac{I_L w_L \left(1 + \frac{R_L'}{R_w}\right)}{H_c l} + 1.$$

For a pulse source that is close to a current source, $R_w \gg R_L'$. Therefore, the expression in brackets can be assumed to be equal to unity. Then, $k_{fo} = 56$.

The operating current amplitude is found from expression (8). By taking into account that $R_L' \ll R_w$, we have

$$I_w = \frac{H_c l}{w_w} k_{fo} = 3.5 \text{ amp}.$$

In calculating I_w, the number of turns in the operating winding was assumed to be 100.

As was shown by suitable experiments, the pulse in the load winding of an element with an Ė310 core of this size is equal to 0.95 amp for $w_L = 350$ and $w_w = 100$ and a duration of 5.1 msec.

Example 2. By using the method described in [3], we shall determine the parameters of a double-throw pulse distributor that is loaded directly with an output RÉS-6 electromagnetic relay. The schematic diagram is shown in Fig. 7.

The output relay data are the following: The actuation current is 70 ma, the winding resistance is R = 135 ohms, and the actuation time for the voltage U_L = 18 v is 7.8 msec. The actuation factor of assurance for U_L = 18 v is k_{as} = = 2.05.

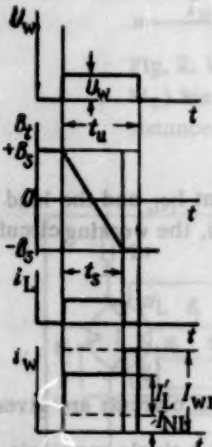

Fig. 6. U_w) Operating pulse source voltage; B_t) core induction; i_L) load circuit current; i_w) working circuit current.

Consequently, the output pulse from the distributor element must have a power of the order of 2.5 w and a duration of approximately 8.0 msec.

For determining the core dimensions, we shall find the product $w_L S$ from expression (10):

$$w_L S = U_L \frac{t_s}{2B_r \cdot 10^{-8}} = 600.$$

We shall choose two 30 × 20 × 6 mm cores with an overall cross-sectional area of S = 0.6 cm^2. Then, w_L = 1000 turns.

The power P_μ spent on the core magnetization reversal during its actuation is calculated by using the equation

$$P_\mu = \frac{VA_h \cdot 10^{-8}}{2t_s}, \qquad (11)$$

where V is the magnetic core volume (cm^3), and A_h is the hysteresis loop area (gauss $\frac{amp}{cm}$). The values of V and A_h are equal to

$$V = Sl_{av} = 4.7 \text{ cm}^3,$$

$$A_h = 4B_r H_c = 38.4 \cdot 10^3 \text{ gauss } \frac{amp}{cm}.$$

For this, P_μ = 0.112 w.

We shall now determine the resistance of the distributor coupling circuit by using the equation

$$R_{12} = \frac{(k_w - 1) P_\mu}{\left(\frac{H_c l}{w_2}\right)}. \qquad (12)$$

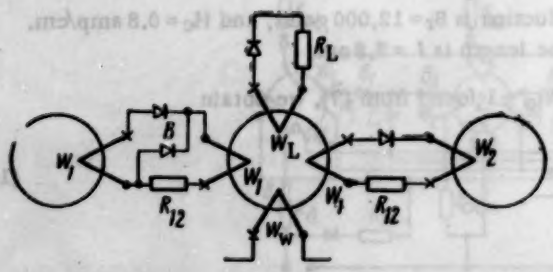

Fig. 7.

Here, $k_w = w_1/w_2$ is the ratio of the number of turns in the transmitting winding to the number of turns in the receiving winding in the PD coupling circuits. Under optimum conditions with respect to power consumption, the coefficient k_w is assumed to be equal to 2. However, in order to reduce the so-called "reverse information," it is convenient to use larger k_w values.

"Reverse information" can be characterized as the ratio of the transmission factors of the "reverse" and "forward" magnetic fluxes during the operation of a given magnetic element:

$$k_B^r = \frac{\Delta B_2}{\Delta B}, \quad k_B^{for} = \frac{\Delta B_1}{\Delta B},$$

where ΔB_1 and ΔB_2 are the magnetic induction variations in the subsequent and the preceding distributor elements, respectively, which are caused by the change in the operating element magnetic induction.

We shall designate the reverse information coefficient by ξ. It can be shown that, in the absence of shunting rectifiers in the coupling circuits, this coefficient is determined by the value of k_w:

$$\xi = \frac{k_B^r}{k_B^{for}} = \frac{1}{k_w^2}.$$

Thus, by choosing, for instance, $k_w = 4$, we can secure a sufficiently reliable PD operation ($\xi = 1/16$) without using additional shunting rectifiers. If $k_w = 4$ and the number of turns in the receiving winding is $w_2 = 50$, we obtain $R_{12} = 21.5$ ohms from expression (12).

The obtained resistance R_{12} must be several times larger than the forward resistance of the coupling circuit rectifier. For D-7 junction-type diodes, the forward resistance r_f does not exceed 1 ohm under operating conditions. From this point of view, the obtained resistance R_{12} can be considered as acceptable. In the opposite case, different w_2 and k_w values must be assigned.

If, for any reason, the reverse information coefficient is not satisfactory, shunting rectifiers are installed, in which case the coefficient ξ is calculated from the equation

$$\xi = \frac{1}{\left(1 + \frac{R_{12}}{r_f}\right) k_w^2}.$$

By substituting $R_{12} = 21.5$ ohms, $r_f = 1$ ohm, and $k_w = 4$, we obtain $\xi = 1/300$.

In order to determine the pulse source current and voltage, we shall compose an equivalent circuit for the operating PD cell (Fig. 8). The equivalent circuit is constructed in correspondence with the wiring diagram of a double-throw PD with shunting rectifiers for the limitation of "reverse information." The forward resistances of all rectifiers are assumed to be equal to zero. In this circuit, R_{c1} is the resistance of the element magnetization reversal in operation:

$$R_{c1} = \frac{Sw_w^2 2B_r \cdot 10^{-8}}{H_c l t_s} \quad \text{or} \quad R_{c1} = \frac{P_\mu}{\left(\frac{H_c l}{w_w}\right)^2}; \tag{13}$$

R_{c2} is the magnetization reversal resistance of the subsequent element:

$$R_{c2} = \frac{P_\mu}{\left(\frac{H_c l}{w_2}\right)^2}. \tag{14}$$

The power dissipated in resistor R_{c2} is equal to P_μ.

In the equivalent circuit of Fig. 8, all resistances are reduced to the working winding, and, therefore,

$$R'_{c2} = R_{c2}\left(\frac{w_w}{w_1}\right)^2 = R_{c1}\frac{1}{k_w^2}.$$

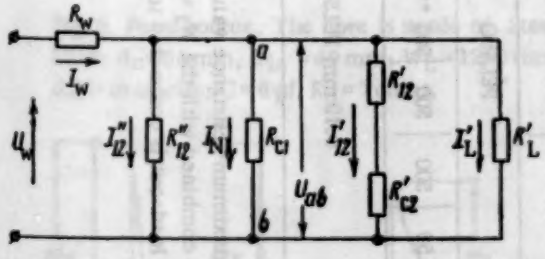

Fig. 8.

$R'_{12} = R_{12}\left(\frac{w_w}{w_1}\right)^2$ is the reduced resistance of the subsequent element coupling circuit. By taking into account expressions (12) and (13), we obtain

$$R'_{12} = R_{c1}\frac{k_w - 1}{k_w^2}.$$

The power dissipated in resistor R_{12} is calculated according to the equation $P_{R'_{12}} = (k_w - 1)P_\mu$. $R''_{12} = R_{c1}(k_w - 1)$ is the reduced resistance of the preceding element coupling circuit. The power dissipated in this resistor is calculated by using the equation $P_{R''_{12}} = \frac{P_\mu}{k_w - 1}$. $R'_L = R_L\left(\frac{w_w}{w_L}\right)^2$ is the reduced load resistance.

By using the above equations, we shall calculate the equivalent circuit parameters. For the determination of R_{c1}, the number of turns w_w must be given. In this, it is necessary to take into account the presence of the winding space as well as the fact that the required current from the pulse source decreases with an increase in w_w. If $w_w = 100$, $R_{c1} = 28.7$ ohms.

TABLE 2

Parameters of Pulse Distributors with Cores Made of Steel É310

Distributor	PD type	Winding data						Circuit parameters					Supply source type	Motion pulse parameters	Output pulses
		W_w	W_1	W_s	W_L	W_c'	W_c''	R^*_{con}, ohm	C_{con}, ohm	R_d, ohm	R_s, ohm	R_L, ohm			
1	Double-throw circuit (Fig. 3)	100	200	50	250	200	250	20—50	—	10	—	4	Multivibrator with amplifier	$I_{wm} = 2.5$amp $t_p = 6$ msec	see Fig. 10
		0.41 mm PÉLShO													
2	Single-throw circuit (Fig. 4)	250	700	450	700 **	—	700	2000—4000	2	100	2400	>300	50-cps industrial frequency line	$I_{wm} = 1.2$amp I_{wNL} 0.4amp	see Fig. 11
		0.25 mm		0.14 mm		—	0.14 mm								
		PÉLShO													
3	"	50	500	500	500 **	500	500	1000—4500	1	7	0	>300	Ferroresonance pulse source (Fig. 9)***	$U_{\sim} = 100$ v $I_{wm} = 3$amp $t_p = 1.5$ msec	see Fig. 12
		0.19 mm PÉLShO													

* The minimum and maximum resistance values are indicated.

** The W_L winding is combined with the W_1 winding.

*** The pulse source lead-out is connected to the terminals c and b of the pulse distributor of Fig. 4. Jumper ac is removed.

Correspondingly, we determine the other parameters:

$$R'_{c2} = 1.8\,\text{ohm}, R'_{12} = 5.4\,\text{ohm}, R''_{12} = 86.1\,\text{ohm}, R'_L = 1.25\,\text{ohm}.$$

Since, with the exception of R_w, all resistances in the equivalent circuit as well as the power dissipated in these resistances are known, the current I_w through resistor R_w can be readily calculated. This current is necessary for the operation of the distributor cell in the circuit of Fig. 7. The current values in the equivalent circuit networks, reduced to the primary (working) winding, are given below:

$$I'_L = \sqrt{\frac{P_L}{R'_L}} = 1.4\,\text{amp}, I_{NL} = \frac{H_c l}{w_w} = 0.0625\,\text{amp},$$

$$I'_{12} = I_{c2}\frac{w_1}{w_2} = 0.25\,\text{amp}, I''_{12} = \sqrt{\frac{P_{R'_{12}}}{R''_{12}}} = 0.0208\,\text{amp}.$$

In order to check the calculations for the equivalent circuit, voltage U_{ab} must be determined with respect to the known resistances and currents in the branches; this voltage must be of course equal for all the branches. In the case under consideration, $U_{ab} \approx 1.7$ v.

The total current is $I_w = I''_{12} + I_{NL} + I'_{12} + I''_L = 1.73\,\text{amp}$.

Assuming that the working pulse source voltage is equal to 24 v, we find the resistance of the distributor motion circuit:

$$R_w = \frac{U_w - I_w R_\Sigma}{I_w} = 13.2\,\text{ohm}.$$

In the latter equation, $R_\Sigma = 0.645$ ohm is the resistance of the equivalent circuit parallel branches. The resistance R_w comprises the ohmic resistances of all the W_w windings that are connected in series and the additional resistance R_{ad}.

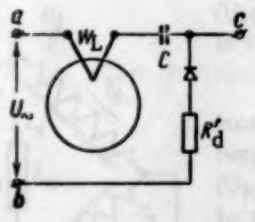

Fig. 9. Pulse source. The core is made of Steel E310; $d_o = 60$ mm, $d_{in} = 40$ mm; $W_L = 1200$ turns of 0.35-mm wire; C = 6 μf, $R'_d = 7$ ohms.

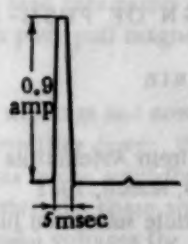

Fig. 10. Output pulse in the double-throw PD circuit of Fig. 3 (the current through the $R_L = 40$ ohm load).

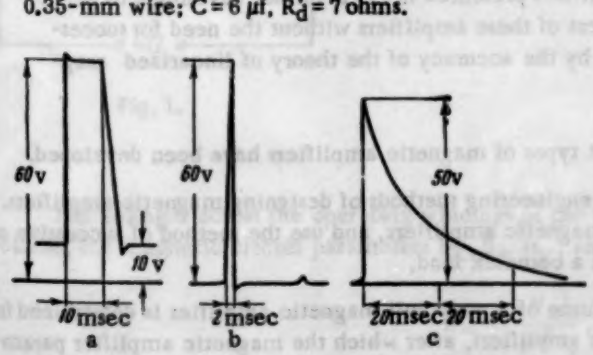

Fig. 11. Oscillograms of pulses in the single-throw PD circuit (Fig. 4). a) Voltage across capacitor C_{con}; b) voltage across the $R_L = 2300$ ohms load; c) voltage across the $R_L = 6000$ ohms load and across the $C_L = 2$ μf capacitor, which is connected in parallel.

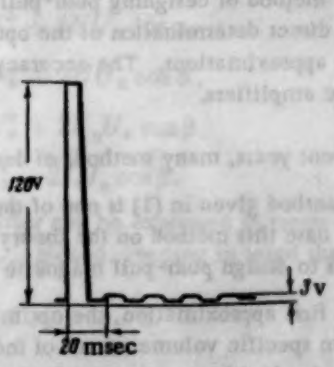

Fig. 12. Output pulse in the single-throw PD circuit of Fig. 4 (voltage across the C_{con} capacitor for $R_L = \infty$).

In conclusion, we shall give here the characteristics of some pulse distributors based on the circuits shown in Figs.3 and 4 and using É310 cores (Table 2).

In all cases, 30 × 20 × 6 mm cores are used. The rectifiers in the circuits are of the D7D type.

The pulse distributors whose parameters are given in Table 2 allow considerable voltage fluctuations in the supply sources (of the order of 50% of the rated value).

The temperature tests, which were performed on a distributor based on the data in item 1 of Table 2, proved that the operation of this distributor is stable at temperatures attaining 100°C.

As was shown by suitable experiments, the use of pulse distributors with magnetic cores made of Steel É310 in remote control devices with time separation of channels in using a synchronous 50-cps line as the supply source makes it possible to dispense entirely with intermediate amplifiers between the distributor and the output final units (MKU-48 relays, commutator incandescent lamps, etc.), which lowers the costs and makes the entire remote control device more simple.

LITERATURE CITED

1. V. A. Zhozhikashvili and K. G. Mityushkin, Remote Control and Remote Signalization (RC—RS) Contactless Devices [in Russian] (VINITI AN SSSR Branch Press, 1957).
2. V. A. Zhozhikashvili and K. G. Mityushkin, "Single-throw pulse distributor with square-loop elements," Tr. VNIIÉ [in Russian] (Goséenergoizdat, 1958), No. 7.
3. V. A. Zhozhikashvili and K. G. Mityushkin, "Calculation of full-wave pulse distributors with hysteresis elements." Industrial Remote Control [in Russian] (AN SSSR Press, 1960).
4. N. V. Korol'kov, "High-speed magnetic pulse relay elements," Automatic Control and Computer Techniques [in Russian] (Mashgiz, 1958).

ON THE DESIGN OF PUSH-PULL MAGNETIC AMPLIFIERS

V. L. Benin

(Khar'kov)

Translated from Avtomatika i Telemekhanika, Vol. 22, No. 3,
pp. 393-399, March, 1961
Original article submitted July 22, 1960

The method of designing push-pull magnetic amplifiers presented in [1] is further developed to permit direct determination of the optimum parameters of these amplifiers without the need for successive approximations. The accuracy is determined by the accuracy of the theory of linearized magnetic amplifiers.

In recent years, many methods of designing different types of magnetic amplifiers have been developed.

The method given in [1] is one of the most rational engineering methods of designing magnetic amplifiers. The authors base this method on the theory of linearized magnetic amplifiers, and use the method of successive approximations to design push-pull magnetic amplifiers with a complex load.

In the first approximation, the optimum specific volume of a push-pull magnetic amplifier is determined from the minimum specific volume curves of inductor magnetic amplifiers, after which the magnetic amplifier parameters are obtained with greater precision, according to [1].

The error of the first approximation can be significant, especially if the load is active and the current multiples are $k < 5$, and thus one or two approximations must be made in order to get the required design accuracy. In

this work, the design method given in [1] is further developed to permit direct determination of the optimum parameters of push-pull magnetic amplifiers without successive approximations. The accuracy of this method is determined by the accuracy of the theory of linearized magnetic amplifiers.

1. Specific Volume of the Steel in a Push-Pull Magnetic Amplifier

The circuit diagram of a push-pull bridge magnetic amplifier is shown in Fig. 1.

According to [1], the volume of the steel in one core of a push-pull magnetic amplifier is found from the formula

$$V_c = 2I_н^2 Z_н \left\{ \frac{10^8 \left[\sin\varphi \left(B_к - \frac{B_0}{k} \right) + \sqrt{\sin^2\varphi \left(B_к - \frac{B_0}{k} \right)^2 + \left(1 - \frac{1}{k^2} \right)(B_0^2 - B_к^2)} \right]}{\omega H_к (B_0^2 - B_к^2)} \right\} = 2I_н^2 Z_н v_1, \quad (1)$$

where

$$v_1 = \frac{V_{CI}}{P} = \frac{10^8 \left[\sin\varphi \left(B_к - \frac{B_0}{k} \right) + \sqrt{\sin^2\varphi \left(B_к - \frac{B_0}{k} \right)^2 + \left(1 - \frac{1}{k^2} \right)(B_0^2 - B_к^2)} \right]}{\omega H_к (B_0^2 - B_к^2)}. \quad (2)$$

The following designations are introduced in these expressions: P—the apparent load power in volt-amps, V_{CI}—the volume of one core of an inductor magnetic amplifier, in cm^3, v_1—the specific volume of one core of an inductor magnetic amplifier in cm^3/volt-amp, Z_H—load impedance in ohms, I_K—effective value of the current in the magnetizing inductor winding of a push-pull magnetic amplifier, in amps, B_K and B_0—the magnitudes of the alternating flux density components in the magnetizing and demagnetizing cores of the amplifier, in gauss, H_K—the alternating component of the magnetic field strength in the magnetizing core, in amps/cm, $k = I_K/I_0 = H_K/H_0$—ratio of the alternating operating currents in the magnetizing and demagnetizing windings of the cores (the current change multiple), φ—the phase angle between the voltage U_H and current I_H in the amplifier load, and $\omega = 2\pi f$—the angular frequency of the supply voltage.

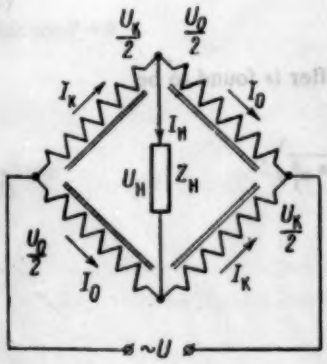

Fig. 1.

To determine the current I_K from the load parameters given in the design (U_H and I_H), we use the vector diagram of a push-pull magnetic amplifier shown in Fig. 2.

When the resistances of the operating windings and core losses can be neglected, as is usually assumed in magnetic amplifier design, the phase angle between the corresponding currents and voltages in the amplifier working windings (U_K, I_K, U_0, I_0) is equal to 90°. In view of this, the phase angle between currents I_K and I_0 is equal to the phase angle β between voltages U_K and U_0.

It is easy to obtain the following equations from the vector diagram of Fig. 2:

$$U_0^2 = U^2 + U_н^2 + 2UU_н \cos\alpha, \quad (3)$$

$$U_к^2 = U^2 + U_н^2 - 2UU_н \cos\alpha, \quad (4)$$

$$4U^2 = U_0^2 + U_к^2 + 2U_0 U_н \cos\beta, \quad (5)$$

$$I_к^2 = I_н^2 + I_0^2 - 2I_н I_0 \cos\beta. \quad (6)$$

The voltages across the operating windings of the magnetic amplifier can be expressed in terms of the core volume, the magnetic circuit parameters B_K, B_0, H_K, and the current I_K. Indeed, keeping in mind that

$$w_\sim = \frac{H_к l}{\sqrt{2} I_к}, \quad V_c = ql,$$

where $w_\sim$ is the number of turns in one coil of the operating winding, and l and q are the mean length and cross section of one core, we find that

$$U_н = \sqrt{2}\,\omega B_н q w_\sim 10^{-8} = \omega B_н H_к \frac{V_c}{I_к} 10^{-8}, \quad (7)$$

$$U_0 = \sqrt{2}\,\omega B_0 q w_\sim 10^{-8} = \omega B_0 H_н \frac{V_c}{I_н} 10^{-8}. \tag{8}$$

Solving equations (3)-(8) simultaneously, and keeping in mind that

$$I_0 = \frac{I_н}{k}, \tag{9}$$

we get the equation

$$I_н^4 + \frac{1}{4} kV_c^2 B_0 B_н H_н^2 \omega^2 \frac{10^{-16}}{U_н^2}\left[1 + \frac{1}{k^2} - \frac{1}{k}\left(\frac{B_0}{B_н} + \frac{B_н}{B_0}\right)\right] I_н^2 -$$

$$- \frac{1}{4} kV_c^2 B_0 B_н H_н^2 \omega^2 10^{-16} \frac{I_н^2}{U_н^2} = 0, \tag{10}$$

from which we determine the current in the operating winding of the magnetizing core, I_K:

$$I_к^2 = \sqrt{\frac{1}{4} A^2 \frac{V_c^4}{U_н^4}\left[1 + \frac{1}{k^2} - \frac{1}{k}\left(\frac{B_0}{B_н} + \frac{B_н}{B_0}\right)\right]^2 + AV_c^2 \frac{I_н^2}{U_н^2}} -$$

$$- \frac{1}{2} A \frac{V_c^2}{U_н^2}\left[1 + \frac{1}{k^2} - \frac{1}{k}\left(\frac{B_0}{B_н} + \frac{B_н}{B_0}\right)\right], \tag{11}$$

where

$$A = \frac{1}{4} kB_0 B_н H_н^2 \omega^2 10^{-16}. \tag{12}$$

Substituting (11) into (1), we find the volume of the steel in one core of the push-pull magnetic amplifier, after certain transformations,

$$V_c = \frac{2Z_н I_н^2 v_1}{1 + \frac{1}{k^2} - \frac{1}{k}\left(\frac{B_0}{B_н} + \frac{B_н}{B_0}\right)}\left(1 - \frac{1}{k\omega^2 B_0 B_н H_н^2 10^{-16} v_1^2}\right). \tag{13}$$

The specific volume of the steel in one core of the push-pull magnetic amplifier is found to be

$$v_2 = \frac{V_c}{Z_н I_н^2} = \frac{2v_1}{1 + \frac{1}{k^2} - \frac{1}{k}\left(\frac{B_0}{B_н} + \frac{B_н}{B_0}\right)}\left(1 - \frac{1}{k\omega^2 B_0 B_н H_н^2 10^{-16} v_1^2}\right). \tag{14}$$

Taking (2) into account, the specific volume of the steel in the core equals

$$v_2 = \frac{2v_1}{1 + \frac{1}{k^2} - \frac{1}{k}\left(\frac{B_0}{B_н} + \frac{B_н}{B_0}\right)}\left(1 - \frac{\frac{B_0}{B_н} - \frac{B_н}{B_0}}{k - \frac{1}{k}}\right). \tag{14a}$$

if the amplifier load is purely active ($\cos\varphi = 1$).

For a purely inductive amplifier load ($\cos\varphi = 0$),

$$v_2 = \frac{2v_1}{\left(1 - \frac{1}{k}\right)^2}. \tag{14b}$$

The last expression fully agrees with the formula derived in [1].

The specific volume of the steel in the core of a push-pull magnetic amplifier is found with the aid of formula (14) from the magnetization curves of a ferromagnetic material simultaneously by direct and alternating currents, and from the core steel specific volume curves of inductor magnetic amplifiers. In this case, as in [1], a current change multiple k must be chosen for each dc value in such a way that the specific volume of the steel will be minimized.

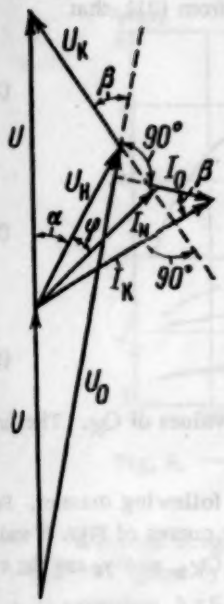

Fig. 2.

2. Choosing the Optimum Alternating Current Change Multiple

We use (14) to find the optimum ac current change multiple $\underline{k}$, from the viewpoint of minimum amplifier weight, having approximated the magnetization curve by an analytic function. It is known that the magnetization curves of transformer steels and a number of other magnetic materials can be adequately approximated by the hyperbolic sine

$$h = \alpha Sh\beta b, \tag{15}$$

where $\underline{h}$ is the instantaneous magnetic field strength in amps/cm, $\underline{b}$ – the instantaneous flux density in gauss, and α and β are coefficients characterizing the properties of the magnetic material.

The quantities α and β, computed from the magnetization curves of different materials given in [1], have the following values:

Material	α, amp/cm	β, 1/gauss
É-42	0.12	$4.2 \cdot 10^{-4}$
É-320	0.055	$2.9 \cdot 10^{-4}$
50-NP	0.005	$5 \cdot 10^{-4}$

Let us determine the optimum current change multiple $\underline{k}$ as a function of the dc magnetic field strength H_d for two extreme cases, $\cos\varphi = 1$, and $\cos\varphi = 0$. To do this, we will rewrite expressions (14a) and (14b) as dimensionless quantities, taking equation (2) into account also: for $\cos\varphi = 1$

$$\dot{v}_2 = \frac{2\sqrt{1-\frac{1}{k^2}}}{nQ_H\left[1+\frac{1}{k^2}-\frac{1}{k}\left(\gamma+\frac{1}{\gamma}\right)\right]}\left(1-\frac{\gamma-\frac{1}{\gamma}}{k-\frac{1}{k}}\right), \tag{16a}$$

for $\cos\varphi = 0$

$$\dot{v}_2 = \frac{2}{nQ_H(\gamma-1)\left(k-\frac{1}{k}\right)}, \tag{16b}$$

where

$$\dot{v}_2 = \frac{\alpha\omega a_d}{\beta} v_2 10^{-8}, \tag{17}$$

$$a_H = \frac{H_H}{\alpha}, \quad a_d = \frac{H_d}{\alpha}, \quad Q_H = \beta B_H, \quad Q_0 = \beta B_0, \tag{18}$$

$$\gamma = \frac{B_0}{B_H} = \frac{Q_0}{Q_H}, \tag{19}$$

$$n = \frac{H_H}{H_d} = \frac{a_H}{a_d}. \tag{20}$$

The optimum multiple $\underline{k}$ can be found if n, Q_K, and γ are known as functions of the term a_d. These dependencies are easily obtained from a normalized analytic expression of the simultaneous dc and ac magnetization curves of the core with free, even, current harmonics, the magnetization curve being approximated by (15) [2]:

$$a_H = \sqrt{\left[1+\frac{a_d^2}{I_0^2(Q_H)}\right][I_0(2Q_H)-1]}, \tag{21}$$

where $I_0(Q_K)$ is a Bessel function of the first kind, zero order, with a purely imaginary argument.

When $a_d > 50$, which is the case for transformer steels where $H_d > 5$ amps/cm, we find, from (21), that

$$n = \frac{a_K}{a_d} \approx \frac{1}{I_0(Q_K)} \sqrt{I_0(2Q_K) - 1}. \quad (22)$$

Setting $a_d = 0$ in (21), we find

$$a_K = a_0 = \frac{H_0}{\alpha} = \frac{n a_d}{k} = \sqrt{I_0(2Q_0) - 1}, \quad (23)$$

and we get the equation

$$\frac{a_d}{k} = I_0(Q_K) \sqrt{\frac{I_0(2\gamma Q_K) - 1}{I_0(2Q_K) - 1}} \quad (24)$$

from (22) and (23), from which the dependence $a_d/k = f_1(\gamma)$ can be constructed for different values of Q_K. The functions $n = f(Q_K)$, and $a_d/k = f_1(\gamma)$, derived from (22) and (24), are plotted in Figs. 3 and 4.

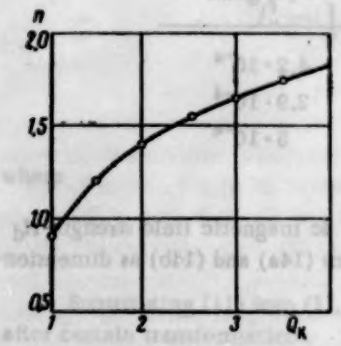

Fig. 3.

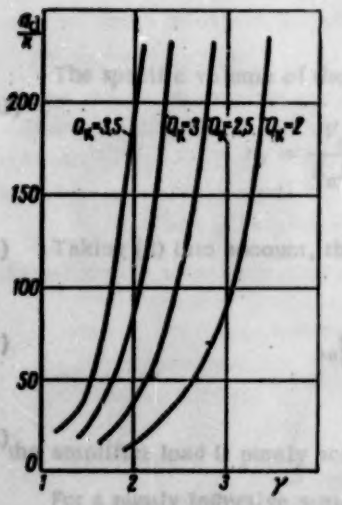

Fig. 4.

The optimum $\underline{k}$ for different a_d is determined in the following manner. For each a_d, and different $\underline{k}$ and Q_K, $\underline{n}$ and γ are found from the curves of Figs. 3 and 4, and v_2^* is found from expressions (16). The optimum k_0, n_0, Q_{K0}, and γ_0 are the values for which v_2^* is minimum.

Figure 5 shows the calculated dependencies of the optimum normalized parameters of push-pull amplifiers as a function of the relative dc magnetic field strength a_d. Since the values of k_0 almost agree for active and inductive loads, the function $R_0 = f(a_d)$ is shown only for $\cos\varphi = 1$ in Fig. 5. It can be seen from the curves of Fig. 5 that the optimum current change multiple $\underline{k}$ varies insignificantly over a wide range of dc magnetic field strengths, and when $a_d > 200$, $k_0 \approx 5$ (for É-42 steel, $H_d > 20$ amps/cm; for É-320 steel, $H_d > 11$ amps/cm; for NP-50 permalloy, $H_d > 1$ amp/cm). When $50 < a_d < 200$, the mean value of the optimum multiple can be taken as $k_0 = 4$.

The optimum n_0 over the whole range of a_d changes from 1.4 to 1.65, which agrees with the conclusions in [1].

Since the optimum $k_0 \leq 5$, the determination of the specific volume of the core steel in a push-pull magnetic amplifier from the relations in [1] is in error by a significant amount (more than 20%) when $\cos\varphi = 1$; this error is eliminated by successive approximations.

It therefore seems desirable to do the calculations with the formulas given in this article, setting $k_0 = 4 - 5$.

The optimum $\underline{k}$ for actual magnetization curves may differ somewhat from the values given in Fig. 5, but the specific volume of steel computed from (14) will differ insignificantly from the minimum.

3. Concerning the Design of a Push-Pull Magnetic Amplifier

The design of a push-pull magnetic amplifier can be done analytically with satisfactory accuracy. Figure 6 shows the curve of the minimum normalized specific volume of the steel in the core as a function of the dc magnetic field strength. This curve can be plotted in absolute magnitudes by using known values of α and β (for example, see [3]), and all of the parameters found by the method given in [1]. One need only remember that in finding the number of turns in the operating winding, the current in it, I_K, should be determined from formula (11) of this article, and the supply voltage U in (3) and (4) from the formula

$$U = \sqrt{\frac{U_0^2 + U_H^2}{2} - U_H^2}, \quad (25)$$

where U_0 and U_K are found from (7) and (8).

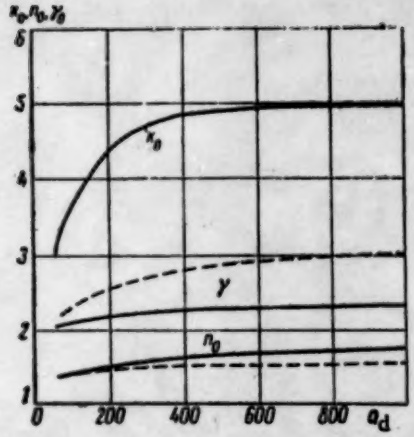

Fig. 5. —— $\cos\varphi = 1$, ---- $\cos\varphi = 0$.

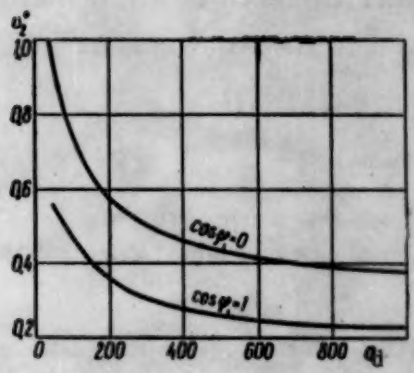

Fig. 6.

A bridge magnetic amplifier using Sh-32 cores made of É-42 transformer steel (α = 0,12 amps/cm, β = $= 4{,}2 \cdot 10^{-4}$ gauss^{-1}) was designed analytically from the given dependencies; the active load was 200 watts for H_d = = 25 amps/cm, k = 5. The difference between the computed and experimental values of load current was about 4%, for nominal values of U and H_d.

CONCLUSIONS

1. A push-pull magnetic amplifier can be designed without successive approximations, and with an accuracy determined by that of the theory of linearized magnetic amplifiers.

2. The optimum current multiple k = 4 – 5 for push-pull magnetic amplifiers, from the viewpoint of minimum weight. It is therefore desirable to design them from the dependencies given in this work, and not from the relations given in [1], which require successive approximations for such values of k.

LITERATURE CITED

1. N. P. Vasil'eva, O. A. Sedykh, and M. A. Boyarchenkov, The Design of Magnetic Amplifiers [in Russian] (Gosénergoizdat, 1959).
2. L. A. Bessonov, Electrical Circuits with Steel [in Russian] (Gosénergoizdat, 1948).
3. V. L. Benin, "Dimensionless parameters of inductor magnetic amplifiers" [in Russian], from the archives of the Electrotechnology Institute of the Academy of Sciences, Ukrainian SSR, 10th edition (1953).

NOMOGRAM FOR DETERMINING PHASE BY MEANS OF AN ASYMPTOTIC LOGARITHMIC AMPLITUDE-FREQUENCY CHARACTERISTIC

B. M. Menskii

(Moscow)

Translated from Avtomatika i Telemekhanika, Vol. 22, No. 3, pp. 400-402, March, 1961
Original article submitted October 5, 1960

It is known that a unique relation exists between the amplitude-frequency and phase-frequency characteristics in minimum phase systems and elements. The phase φ at frequency ω_0 can be computed from the formula

$$\varphi(\omega_0) = \frac{c}{\pi} \int_{-\infty}^{\infty} \frac{dA_L}{du} \ln \operatorname{cth} \left| \frac{u}{2} \right| du, \tag{1}$$

where $u = \ln \frac{\omega}{\omega_0}$, dA_L/du is the slope of the logarithmic amplitude-frequency characteristic, and c is a constant determined by the dimensionality of dA_L/du and φ.

However, it is difficult to compute phase from equation (1), even with the use of an asymptotic logarithmic amplitude-frequency characteristic. Therefore, different methods of simplifying the calculation have been developed. Using the graph $\ln \operatorname{cth} |u/2|$, which is given in [1], it is possible to evaluate the phase approximately at chosen points [2]. Approximate formulas are used in [3] and in other works. A method of plotting the phase-frequency characteristic by using auxiliary graphs was developed in [4]. The tables given in [5] can be used instead of these graphs.

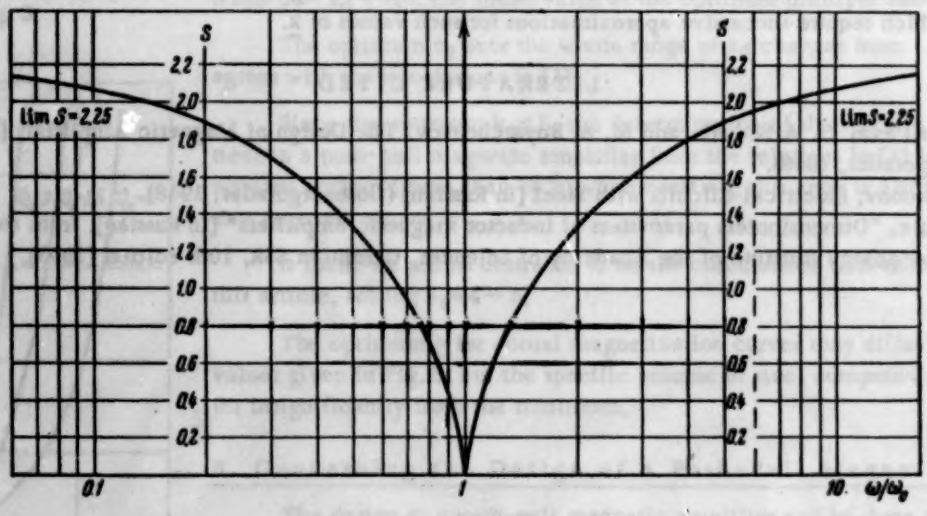

Fig. 1.

The phase at a chosen frequency can also be determined from an asymptotic amplitude-frequency characteristic by means of the nomogram given in Fig. 1.

The nomogram is a graph of an auxiliary function

$$S = \frac{c}{\pi} \int_{0}^{\omega/\omega_0} \ln \operatorname{cth} \left| \frac{u}{2} \right| du,$$

plotted on a logarithmic scale. The nomogram is symmetric about the line $\omega/\omega_0 = 1$. Computed values of S for

$$0{,}01 \leqslant \frac{\omega}{\omega_0} \leqslant 100$$

are given in the table, which was formed with the aid of the tables given in [5].

To find the phase at the chosen frequency ω_0, one must place the nomogram on the asymptotic characteristic so that the arrow on the nomogram coincides with this frequency (Fig. 2). The phase in degrees is found from the formula

$$\varphi^0(\omega_0) = \sum_{i=1}^{n} \nu_i \Delta S_i, \tag{2}$$

where ν_i is the slope of the i-th asymptote in db/decade (taking sign into account); ΔS_i – the change in the absolute value of S over the frequency range corresponding to the i-th asymptote; and n – the number of asymptotes in the frequency range covered by the nomogram.

ω/ω_0	S	ω/ω_0	S	ω/ω_0	S	ω/ω_0	S
1.00	0.000	3.5	1.724	1.00	0.000	0.30	1.697
1.05	0.210	4.0	1.791	0.96	0.182	0.25	1.791
1.10	0.351	5.0	1.884	0.92	0.318	0.20	1.884
1.15	0.467	6.0	1.945	0.88	0.437	0.17	1.939
1.20	0.565	7.0	1.989	0.84	0.547	0.14	1.994
1.30	0.726	8.0	2.022	0.80	0.650	0.12	2.030
1.40	0.855	10.0	2.068	0.70	0.877	0.10	2.068
1.60	1.052	20.0	2.154	0.64	1.020	0.05	2.154
1.80	1.197	30.0	2.188	0.56	1.188	0.03	2.195
2.00	1.310	50.0	2.214	0.50	1.310	0.02	2.214
2.50	1.507	80.0	2.227	0.40	1.507	0.015	2.223
3.00	1.634	100.0	2.232	0.35	1.603	0.010	2.232

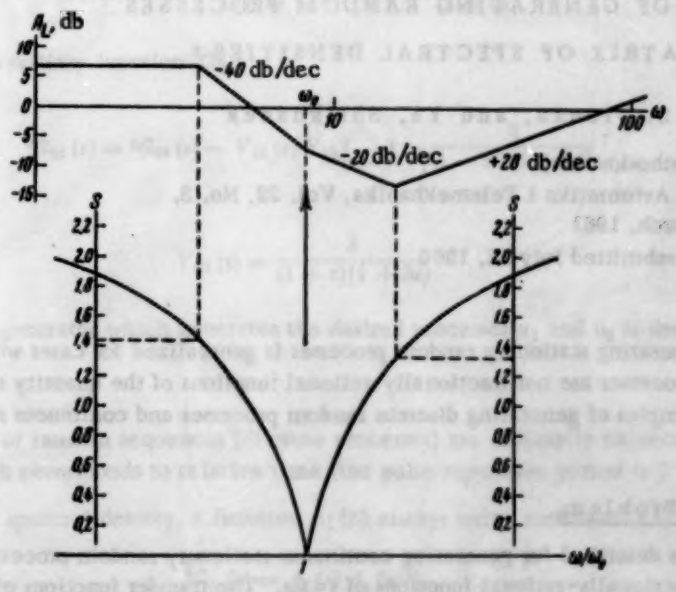

Fig. 2.

If the frequency ω_0 divides any asymptote into two parts, each of them must be considered as a separate asymptote.

The phase can be found approximately by using a nomogram plotted over a range of two decades (as is shown in Fig. 1). To increase accuracy, one must use a nomogram plotted, by means of the data in the table, over a four decade range.

Having found the phase for several frequencies, one can plot an approximate phase-frequency characteristic.

Example. Let us find the phase at $\omega_0=8$ from the asymptotic amplitude-frequency characteristic shown in Fig. 2:

$$\varphi^0(\omega_0) = [0(2.25-1.44)] + [-40(1.44-0)] + \\ + [-20(1.32-0)] + [20(2.25-1.32)] = -65.4°.$$

To check this value, we find that

$$\varphi^0(\omega_0) = -65.8°$$

for the same frequency, by using the tables given in [5].

LITERATURE CITED

1. H. W. Bode, "Relations between attenuation and phase in feed-back amplifier design," Bell System Technical Journal 19, 3, July (1940).
2. N. T. Kuzovkov, Automatic Control Theory Based on Frequency Methods [in Russian], Oborongiz (1957).
3. Fundamentals of Automatic Control. Theory [in Russian], edited by V. V. Solodovnikov, Mashgiz (1954).
4. H. W. Bode, Circuit Theory and Feed-back Amplifier Design [Russian translation from English], Foreign Literature Press (1948).
5. V. V. Solodovnikov, Introduction to the Statistical Dynamics of Automatic Control Systems [in Russian], State Press for Technical and Theoretical Literature (1952).

ON THE METHOD OF GENERATING RANDOM PROCESSES WITH A GIVEN MATRIX OF SPECTRAL DENSITIES

I. Matyash, L. Prouza, and Ya. Shilkhanek

(Pardubitse, Czechoslovakia)

Translated from Avtomatika i Telemekhanika, Vol. 22, No. 3,
pp. 403-405, March, 1961
Original article submitted July 22, 1960

A method of generating stationary random processes is generalized for cases when the spectral densities of the desired processes are not fractionally-rational functions of the quantity $s=j\omega$. The method is illustrated by examples of generating discrete random processes and continuous random processes with delay.

Statement of the Problem

In [1], a method is described for generating continuous stationary random processes whose direct and reciprocal spectral densities are fractionally-rational functions of $s=j\omega$. The transfer functions of the generator filters (the so-called shaping filters) in this case are fractionally-rational functions of a complex variable.

A method is described in this article for generating stationary random processes with any type of spectral density. The transfer functions of the shaping filters are determined in the same manner as in [1]; however, they are not fractionally-rational functions of s in the general case.

The generation of random processes by the method described in [1] is based on theorems about the properties of spectral density matrices (see the appendix in [1]). These theorems, evidently, are true for spectral densities of any arbitrary type in the class of stationary random processes, since their proofs are based only on the properties of Hermitic matrices.

The formulas defining the transfer functions of the shaping filters also hold for cases other than when they are fractionally-rational functions of $\underline{s}$. The restriction in [1] was made only so that the transfer functions of the shaping filters would be fractionally-rational functions of the complex variable $\underline{s}$.

By discarding this limitation, one can use the formulas given in [1] to find the transfer functions of shaping filters for generating random processes with arbitrary spectral densities.

Continuous Random Processes

All the statements and formulas of reference [1] remain true for any kind of spectral densities. Therefore, they are not stated here, but only examples of their application are given.

Example 1. Suppose it is necessary to generate continuous random processes u_1 and u_2, whose spectral densities have the form

$$^1G_{11}(s) = 4\frac{1-s^2}{1-4s^2}, \quad ^1G_{22}(s) = \frac{10-s^2}{(1-s^2)(1-9s^2)}, \quad ^1G_{12}(s) = 2e^{\tau s}\frac{1+s}{(1+3s)(1-2s)}.$$

From formulas (11) and (12) in [1], we get

$$Y_{11}(s) = 2\frac{1+s}{1+2s}H_1(s), \qquad Y_{12}(s) = e^{\tau s}\frac{1+s}{(1+3s)(1-s)}H_1(s).$$

The function $H_1(s)$ must be defined in such a way that Y_{11} and Y_{12} will be transfer functions of stable filters. It follows from this condition that

$$H_1(s) = e^{-\tau s}\frac{1-s}{1+s}.$$

By substitution, we get

$$Y_{11}(s) = 2e^{-\tau s}\frac{1-s}{1+2s}, \qquad Y_{12}(s) = \frac{1}{1+3s}.$$

Now we will find the auxiliary function $^2G_{22}$:

$$^2G_{22}(s) = {}^1G_{22}(s) - Y_{12}(s)\,Y_{12}(-s) = \frac{9}{(1-s^2)(1-9s^2)}$$

Whence

$$Y_{22}(s) = \frac{3}{(1+s)(1+3s)}$$

A block diagram of a generator which generates the desired processes u_1 and u_2 is shown in Fig. 1.

Random Sequences

The spectral densities of random sequences (discrete processes) are ordinarily expressed as functions of the quantity $z = e^s$ ($s = j\omega$), which corresponds to relative time (the pulse repetition period is $T = 1$).

If $^iG_{ii}(z)$ is the direct spectral density, a function $A_i(z)$ always exists such that

$$^iG_{ii}(z) = A_i(s)\,A_i(z^{-1}).$$

This equality is analogous to formulas (1) and (16) in [1], since $z^{-1} = e^{-s}$.

The generator diagram is completely analogous to the diagram in Fig. 1 of reference [1], where Q_i are generators of non-correlated "white" random sequences (discrete processes), and F_{ik} are discrete filters.

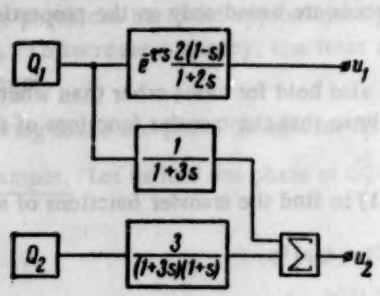

Fig. 1.

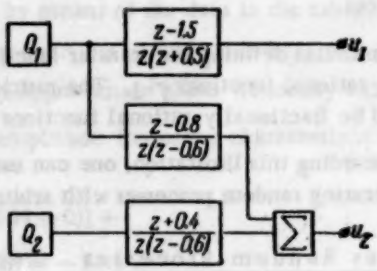

Fig. 2.

Ultimately, one can arrive at the conclusion given in [1]. In this case, the transfer functions $Y_{ik}(z)$ of the discrete shaping filters are found from the formula

$$Y_{ik}(z) = \frac{{}^{i}G_{ik}(z)}{A_i(z^{-1})} H_i(z).$$

The auxiliary spectral densities ${}^{i}G_{ik}$ are found from formula (13) in [1], and $H_i(z)$ are transfer functions of discrete phase filters; in general form

$$H_i(z) = \frac{f(z)}{f(z^{-1})}.$$

If the spectral densities of the required random sequences are fractionally-rational functions of z, the functions ${}^{i}G_{ik}$, A_i, H_i, and consequently Y_{ik}, will also be fractionally-rational functions of z. The transfer functions of the phase filters in this case assume the form

$$H_i(z) = \frac{1}{z^m} \prod_k \frac{1}{|z_k|} \frac{z - z_k}{z - z_k^{-1}} \qquad (m \geqslant 0,\ k = 1, 2 \ldots).$$

Example 2. Let it be necessary to generate discrete random processes u_1 and u_2, whose spectral densities are

$${}^{1}G_{11}(z) = \frac{-1.5 + 3.25z - 1.5z^2}{0.5 + 1.25z + 0.5z^2},$$

$${}^{1}G_{12}(z) = \frac{-0.8 + 2.2z - 1.5z^2}{-0.6 + 1.36z - 0.6z^2},$$

$${}^{1}G_{22}(z) = \frac{-0.4 + 2.8z - 0.4z^2}{-0.6 + 1.36z - 0.6z^2}.$$

One can obtain

$$Y_{11}(z) = \frac{2}{3} \frac{z - {}^{3}/_{2}}{z + {}^{1}/_{2}} H_1(z), \qquad Y_{12}(z) = \frac{2}{3} \frac{z - 0.8}{z - 0.6} \frac{1 - 1.5z}{1 - {}^{3}/_{2}z} H_1(z)$$

as transfer functions.

We find, from the condition that Y_{12} be a transfer function of a stable filter, that

$$H_1(z) = \frac{2}{3z} \frac{z - {}^{3}/_{2}}{z - {}^{2}/_{3}}.$$

Whence

$$Y_{11}(z) = \frac{z - 1.5}{z(z + 0.5)}, \qquad Y_{12}(z) = \frac{z - 0.8}{z(z - 0.6)}.$$

The auxiliary function ${}^{2}G_{22}(z)$ has the form

$${}^{2}G_{22}(z) = \frac{0.4 + 1.16z + 0.4z^2}{-0.6 + 1.36z - 0.6z^2},$$

so that

$$Y_{m1}(z) = \frac{z + 0.4}{z(z - 0.6)}.$$

A block diagram of a generator which generates the required processes u_1 and u_2 is shown in Fig. 2.

CONCLUSION

A generator of any number of stationary random processes whose spectral densities are fractionally-rational functions of $s = j\omega$ was described in [1]. This article gives a generalization of this method for cases when the spectral densities of the required processes have arbitrary form. In particular, it is possible to generate discrete random processes (random sequences) by means of this method, by using digital computers, for example.

LITERATURE CITED

1. I. Matyash and Ya. Shilkhanek, "A generator of random processes with a given matrix of spectral densities," Avtomatika i Telemekhanika 21, 1 (1960).

THE POSITIONING OF SENSING DEVICES IN A CONVERTER

A. I. Ivushkin

(Moscow)

Translated from Avtomatika i Telemekhanika, Vol. 22, No. 3,
pp. 406-408, March, 1961
Original article submitted June 7, 1960

Different methods of positioning sensing devices which operate on the V-reading principle in converters of angular rotation or linear displacement into digital form are examined. The use of these methods eases the construction of the converter. A method of deciphering the codes read off is described.

False codes can arise in converters of angular rotation or linear displacement, operating on the reading principle, into digital form. This occurs at scale points where the code changes by more than one digit, because of the finite size of the sensing devices, and the variation in their physical characteristics [1].

Certain methods of eliminating false codes exist. Converters are examined in this article which operate on the principle of a logical choice of the sensing devices, or according to the V-reading principle as it is frequently called.

According to this method, two sensors, placed symmetrically about a reference line, are put in each digit position, except zero; their orientation reminds one of the letter "V" (Fig. 1). The zero digit sensor V_0 is placed on the reference line. The displacement of the sensor relative to the reference line will be called λ_i, and the size of the i-th digit, x_i. The V_i sensors constitute the left group, and the V_i'—the right group. The striated portions of the scale designate code "0", and the clear portions—"1". Scale movement along the σ arrow increases the code read off.

The choice of sensors, in reading the code, is made according to the following logical rule. If the zero sensor V_0 reads "0", we choose the sensor in the right group, V_1', for the first digit x_1. If the zero sensor V_0 reads "1," we choose the sensor in the left group, V_1, for the first digit x_1. The figure read by the first digit sensor chosen is the criterion for an analogous choice of the sensor of the second digit x_2, etc.

The decoding operation, in connection with this type of logic, is done in a digital computer (Dig. Comp.) according to the diagram shown in Fig. 2. This circuit consists of two input registers (right and left), and two logic cells Inh. and "and." The registers consist of logic cells, each of which delays the information fed in for one operat-

ing cycle of the Dig. Comp. The logic cell Inh. inhibits when information is fed to the inhibit input. The "and" gate has an output only when both inputs are excited simultaneously.

The decoder works in the following way. The information in the converter is read out on command simultaneously at all digits, and is written in the appropriate cells of the right and left registers. Then this information is shifted from one cell of the register to the next after each operating cycle of the Dig. Comp. In this manner, the information from the converter is fed in the form of a sequential code to the logic cells. These cells do the decoding. This kind of decoder makes it possible to decrease the required number of logic cells, and to decrease the number of wires needed for transmitting information to the Dig. Comp. Let us examine the effect of the displacement of the sensing devices relative to the reference line on the performance of the converter. Converters having their sensors displaced by $\lambda_i = 0.25\,nx_i$, where $n = 1, 2, 3, \ldots$, are inoperative, since the code changes simultaneously by more than one digit at certain scale points. Also, converters will not operate reliably if their sensors are placed within a certain zone near these points. These "dead" zones are approximately two or three times wider than the sensitive zone of the sensor. The remaining zones are effective. If the sensors are placed within the effective zones, they will be operative. The location of the "dead" and effective zones is shown in Fig. 3.

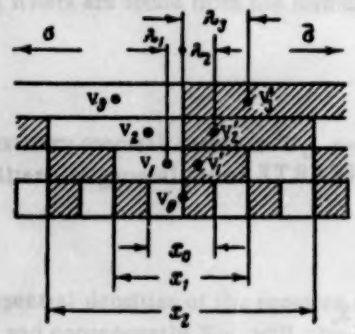

Fig. 1.

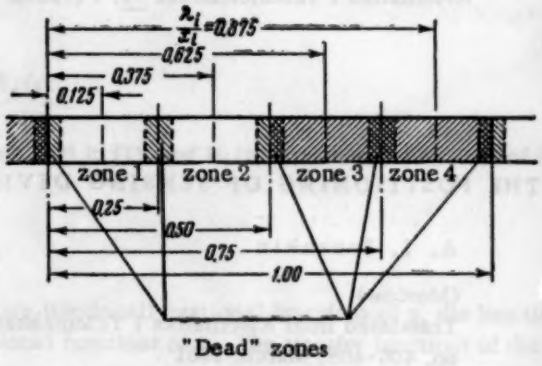

"Dead" zones

Fig. 3.

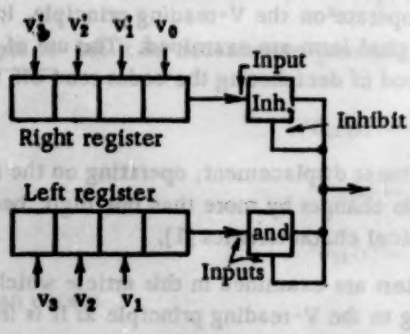

Fig. 2.

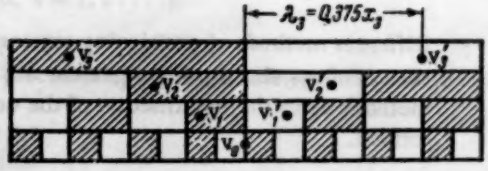

Fig. 4.

The center lines of the effective zones are the optimum locations for the sensors; their coordinates are equal to $0.125x_i$, $0.375x_i$, $0.625x_i$, $0.875x_i$, etc. The effective zone centered around the $0.125x_i$ line will be called zone 1, zone 2 has the $0.375x_i$ center line, zone 3 – $0.625x_i$, and zone 4 – $0.875x_i$.

Figure 1 shows the locations of the sensors in zone 1 ($\lambda_i = 0.125x_i$). The direct code is used for this case (all digits start from the dark areas), and decoding is done according to the diagram shown in Fig. 2.

The location of the sensors in zone 2 is shown in Fig. 4. An inverse code is used in this case for correct operation of the converter. The inverse code scale differs from the direct code scale in that white areas are replaced by dark, and dark by white. Decoding is done according to the diagram shown in Fig. 5.

For direct connection of the sensors, the left sensor V_i is connected to the left register, and the right sensor V_i' is connected to the right register. For inverse connection, the left sensor is connected to the right register, and the right sensor to the left register. The zero sensor is connected to the right register in all cases.

The location of sensors in zone 3 is shown in Fig. 6. The inverse code is used in this case. Decoding is done according to the diagram of Fig. 2. Direct connection of the sensors is required in this case.

Figure 7 shows the location of sensors in zone 4. The direct code is used, and decoding is done as in Fig. 5. Inverse connection of the sensors is required here.

The table shows the varieties of code, and the method of connecting the sensors, depending on their location.

Zone number	Relative displacement	Code	Sensor connection
1	0.125	direct	direct
2	0.375	inverse	inverse
3	0.625	inverse	direct
4	0.875	direct	inverse

One should keep in mind that in V-reading type converters sensors for each individual digit can be located in any zone which is most convenient for structural reasons. The code and method of connecting the sensors for each digit depend on which zone the sensors are in, in accordance with the table.

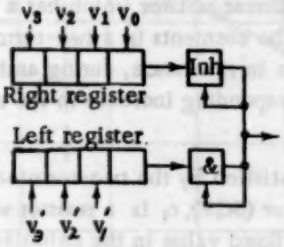

Fig. 5.

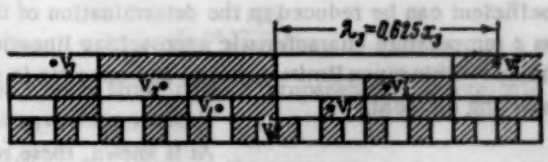

Fig. 6.

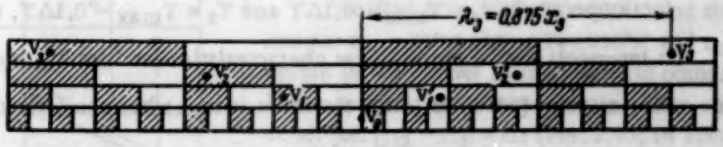

Fig. 7.

CONCLUSIONS

The sensing devices in a V-reading converter of angular rotation of linear displacement into digital form can be placed at any part of the scale, except "dead" zones, by placing two sensors symmetrically about a reference line for each digit in the code. The zero digit sensor is an exception. There is only one sensing device, and it is placed on the reference line.

For each digit except zero, there are four methods (or zones) of placing the sensors, depending on the amount by which they are displaced from the reference line. The coding and method of connecting the sensors to the registers depend on the zone of location.

Construction of a converter is a complex problem if the sensors are placed only in zone 1. The use of all zones for locating sensors significantly eases this problem.

LITERATURE CITED

1. A. D. Talantsev, "Converters of angular rotation and linear displacement into digital form," Avtomatika i Telemekhanika 20, 3 (1959).

THE CALCULATION OF A TWO-TERMINAL NETWORK WITH ONE SEMICONDUCTOR THERMISTOR OPERATING UNDER LINEAR CONDITIONS

N. P. Udalov

(Moscow)

Translated from Avtomatika i Telemekhanika, Vol. 22, No. 3,
pp. 409-412, March, 1961
Original article submitted May 23, 1960

The article presents the calculations for a two-terminal network with a semiconductor thermistor, operating under linear conditions, which can be applied in circuits with temperature compensation and microthermostats.

The calculation of a circuit for temperature compensation of a linear resistor which has a positive temperature coefficient can be reduced to the determination of the parameters of the elements in a two-terminal network which has a temperature characteristic approaching linearity, and an increase in resistance, during ambient temperature changes within given limits, equal to and opposite in sign from the corresponding increase in the resistance of the compensating element.

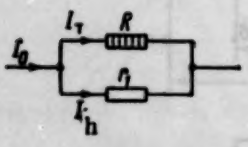

Fig. 1. Two-terminal network with one fixed resistor.

As is known, these requirements are satisfied by the two-terminal network shown in Fig. 1, where R is a semiconductor thermistor (SCT), r_1 is a resistor which changes very little with temperature and is considered of fixed value in the calculations. The temperature characteristic of such a two-terminal network in its best form approaches linearity if, for temperatures $T_1 = T_{min} + 0.1\Delta T$ and $T_2 = T_{max} - 0.1\Delta T$, where $\Delta T = T_{max} - T_{min}$, it intersects with a given linear characteristic, and for $T_{av} = \frac{T_1 + T_2}{2}$, it has a point of discontinuity [1]. The latter condition is met when the following equality is observed:

$$r_1 = \frac{B - 2T_{av}}{B + 2T_{av}} R_{av}, \tag{1}$$

where R_{av} is the SCT resistance at a temperature T_{av}, B is the coefficient of the SCT temperature characteristic, the value of which is determined from the values of the SCT resistances R_1 and R_2 at temperatures T_1 and T_2:

$$B = \frac{T_1 T_2}{T_2 - T_1} \ln \frac{R_1}{R_2}. \tag{2}$$

Inasmuch as the SCT operates under linear conditions in the circuits under examination, i.e., with currents which do not produce noticeable heating of the active part of the SCT, the quantities R_1, R_{av}, and R_2 may be expressed by the resistors of the two-terminal network, r_{k1}, $r_{k.av}$, and r_{k2}, corresponding to the temperatures T_1, T_{av}, and T_2:

$$R_1 = \frac{r_1 r_{k1}}{r_1 - r_{k1}}, \quad R_{av} = \frac{r_1 r_{k.av}}{r_1 - r_{k.av}}, \quad R_2 = \frac{r_1 r_{k2}}{r_1 - r_{k2}}. \tag{3}$$

After substituting expression (3) in (1) and (2), we obtain

$$B = 2T_{av} \frac{r_1}{2r_{k.av} - r_1}, \tag{4}$$

$$B = \frac{T_1 T_2}{T_2 - T_1} \ln \frac{r_{k1}(r_1 - r_{k2})}{r_{k2}(r_1 - r_{k1})}. \tag{5}$$

If the linear temperature characteristic of the two-terminal network is given (Fig. 2, a), then in expressions (4) and (5) there remain only two unknown quantities B and r_1, which can be determined simply by constructing graphs of the functions (4) and (5) with values for r_1 in the interval

$$r_{k1} < r_1 < 2r_{k.av}. \quad (6)$$

The coordinates of the intersection points of these graphs (Fig. 3) correspond to the values B and r_1, which we are seeking.

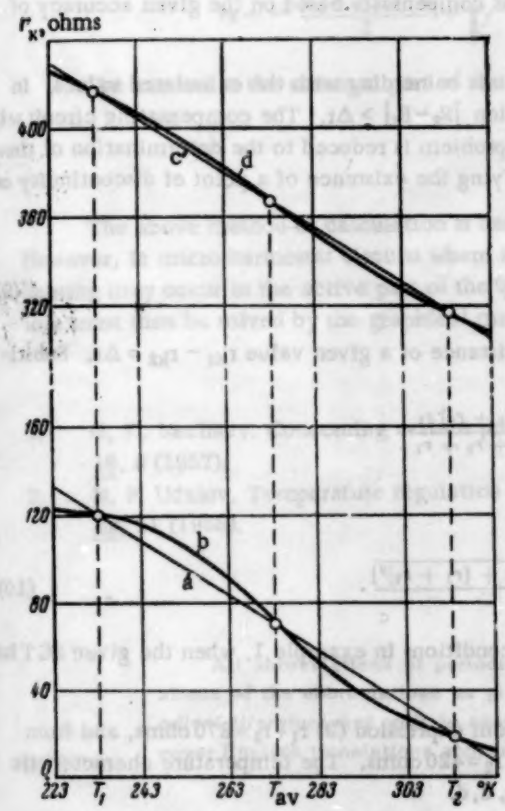

Fig. 2. Temperature characteristics of a two-terminal network: a, b apply to example 1; c, d–to example 2.

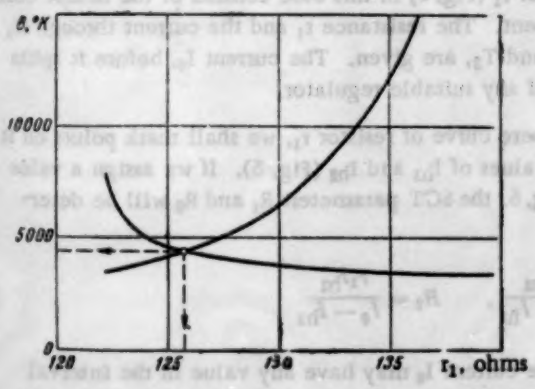

Fig. 3. Graphical solution of a system of equations (applying to example 1).

The temperature characteristic of the SCT is defined by the expression

$$R = R_{av}\exp\left(\frac{B}{T} - \frac{B}{T_{av}}\right). \quad (7)$$

The SCT parameter R_{av} inserted here may be found from one of the expressions in (3).

The temperature characteristic of the compensator (Fig. 2, b) may be constructed by substituting in the expression

$$r_k = \frac{r_1 R}{r_1 + R} \quad (8)$$

the values of R found from the SCT temperature characteristic for a series of temperature values.

Example 1. To calculate the compensator for a copper resistor $r_{c.\,av} = 300$ ohms (for $T_{av} = 273°K$) if $T_{min} = 223°K$, $T_{max} = 323°K$.

We find $\Delta T = 100°$, $T_1 = 233°K$ and the corresponding copper resistor $r_{c1} = 249.5$ ohms, $T_2 = 313°K$ and $r_{c2} = 350.5$ ohms. The increase in the copper resistor $\Delta r = 101$ ohms. Let us assume that the linear temperature characteristic of the compensator satisfies the condition $|r_{k2} - r_{k1}| = \Delta r$ (Fig. 2, a), in accordance with which $r_{k1} = 121$ ohms, $r_{k.av} = 70.5$ ohms, $r_{k2} = 20$ ohms.

Substituting the known values in (4) and (5), we obtain

$$B = 546\,\frac{r_1}{141 - r_1}, \quad B = 911.48 \ln\frac{6.05\,(r_1 - 20)}{(r_1 - 121)}.$$

Solving this system of equations graphically (Fig. 3), we find $r_1 = 125.6$ ohms, $B = 4500°K$ (the values for r_1 were taken in the interval $121 < r_1 < 141$ ohms). The SCT temperature characteristic in conformity with (7) is written in the form

$$R = 160\exp\left(\frac{4500}{T} - \frac{4500}{273}\right).$$

The temperature characteristic of the compensator is constructed in Fig. 2, b.

In the example under consideration the linear characteristic of the compensator was given in accordance with the requirements for minimum power consumption in the compensator (ideal from this viewpoint would be a compensator with zero resistance at T_{max}).

Let us assume that the given characteristic corresponds to Fig. 2, c. In this case, with the same conditions of the problem,

we shall obtain: $r_1 = 496$ ohms, $B = 1100°K$, $R_{av} = 1400$ ohms. The temperature characteristic of the compensator is shown in Fig. 2, d. Comparing curves b and d in Fig. 2, it is easy to note that the gain in power results in a decrease in quality of compensation, which may be determined by the maximum value of the relationship $\Delta/r_{c.\,av}$ (here Δ is the deviation of the compensator characteristic from the given linear relationship, and $r_{c.\,av}$ is the resistance of the compensating element at a temperature T_{av}). This value is 3.3% in the first variant of our problem, and 0.5% in the second.

It appears possible to find a quantitative relationship between the quantity $\Delta/r_{c.\,av}$ and the relationship of $r_{k.\,av}$ to $r_{c.\,av}$ which permits the use of a linear characteristic for the compensator based on the given accuracy of compensation.

In practice, it is not always possible to select SCT with parameters coinciding with the calculated values. In that case, any type of SCT may be selected which satisfies the condition $|R_2 - R_1| > \Delta r$. The compensating circuit will then contain two fixed resistors r_1 and r_2 (Fig. 4), and the calculation problem is reduced to the determination of these resistances. For its solution we shall make use of the condition specifying the existence of a point of discontinuity on the temperature characteristic of such a two-terminal network [1]:

$$r_1 + r_2 = \frac{B - 2T_{av}}{B + 2T_{av}} R_{av} \tag{9}$$

and the condition of equality of the increment in the compensator resistance of a given value $r_{k1} - r_{k2} = \Delta r$. Substituting here

$$r_{k1} = \frac{(R_1 + r_2) r_1}{R_1 + r_2 + r_1} \quad \text{and} \quad r_{k2} = \frac{(R_2 + r_2) r_1}{R_2 + r_2 + r_1}$$

and solving the latter equation with respect to r_1, we have

$$r_1 = \sqrt{\frac{\Delta r \left[R_1 R_2 + (R_1 + R_2)(r_1 + r_2) + (r_1 + r_2)^2\right]}{R_1 - R_2}}. \tag{10}$$

Example 2. To calculate the compensator in accordance with conditions in example 1, when the given SCT has a temperature characteristic $R = 1.57 \exp(1890/T)$.

We find $R_{av} = 1570$ ohms. From expression (9) $r_1 + r_2 = 870$ ohms, and from expression (10) $r_1 = 450$ ohms, i.e., $r_2 = 420$ ohms. The temperature characteristic of the compensator is shown in Fig. 2, d.

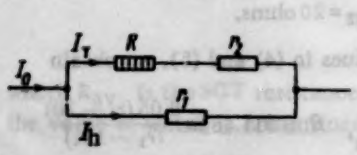

Fig. 4. Two-terminal network with one SCT and two fixed resistors.

The design of a simple microthermostat intended for the thermostatic control of separate circuit elements [2] involves the determination of the SCT parameters which, with a change in temperature of the medium within given limits, will produce a change in current through the resistance r_1 which conforms to a law approaching linearity. The resistor r_1 (Fig. 1) in this case consists of the heater coil located on the thermostat element. The resistance r_1 and the current through it, I_{h1} and I_{h2} at temperatures T_1 and T_2, are given. The current I_0, before it splits up, is held constant by means of any suitable regulator.

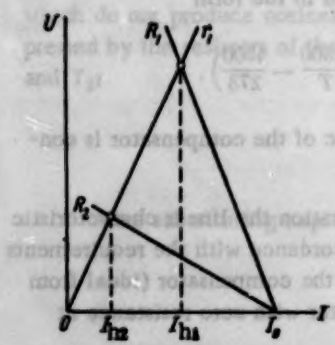

Fig. 5. The determination of the SCT parameters in a microthermostat circuit.

After constructing the volt-ampere curve of resistor r_1, we shall mark points on it which correspond to the given values of I_{h1} and I_{h2} (Fig. 5). If we assign a value for the current I_0, then from Fig. 5, the SCT parameters R_1 and R_2 will be determined from the expressions

$$R_1 = \frac{r_1 I_{h1}}{I_0 - I_{h1}}, \qquad R_2 = \frac{r_1 I_{h2}}{I_0 - I_{h2}}$$

It is quite obvious that the current I_0 may have any value in the interval $I_{h1} < I_0 < \infty$ and should be taken as small as possible. Since I_0 is always greater than I_{h1}, then the value of the SCT resistance at a temperature T_2 is also limited:

$$R_2 < \frac{I_{h2} r_1}{I_{h1} - I_{h2}}.$$

If the SCT is given, i. e., the values of its resistances at temperatures T_1 and T_2 are known, then it may be used together with an additional resistance r_2 (Fig. 4). The unknown quantities in this case will be the resistance r_2 and current I_0. To determine r_2, we may make use of the condition of constant current in the common part of the circuit, which, for temperatures T_1 and T_2, will be

$$I_{h1} + \frac{I_{h1} r_1}{R_1 + r_2} = I_{h2} + \frac{I_{h2} r_1}{R_2 + r_2},$$

from which

$$r_2 = -\frac{R_1 + R_2 + r_1}{2} + \sqrt{\frac{(R_1 + R_2 + r_1)^2}{4} - \frac{I_{h1} R_2 (R_1 + r_1) - I_{h2} R_1 (R_2 + r_1)}{I_{h1} - I_{h2}}}.$$

The current in the common part of the circuit will be

$$I_0 = I_{h2} + \frac{I_{h2} r_1}{R_2 + r_2}.$$

The above method of calculation is based on the assumption that the SCT operates under linear conditions. However, in microthermostat circuits where the current through the SCT varies within quite wide limits, considerable heating may occur in the active part of the SCT. Therefore, after determining the circuit parameters, this same problem must then be solved by the graphical method [2].

LITERATURE CITED

1. G. K. Nechaev, Concerning certain properties of circuits containing thermistors. Avtomatika i Telemekhanika 18, 8 (1957).
2. N. P. Udalov, Temperature regulation of the active part of a heated thermistor, Avtomatika i Telemekhanika 19, 11 (1958).

All abbreviations of periodicals in the above bibliography are letter-by-letter transliterations of the abbreviations as given in the original Russian journal. *Some or all of this periodical literature may well be available in English translation.* A complete list of the cover-to-cover English translations appears at the back of this issue.

BIBLIOGRAPHY

LIST OF FOREIGN LITERATURE ON MAGNETIC ELEMENTS USED IN AUTOMATION, REMOTE CONTROL AND COMPUTER TECHNIQUE FOR THE YEAR 1959 (Conclusion)

G. V. Subbotina and I. S. Trefilova

6. Magnetic Voltage Amplifiers. Modulators. Probes (Magnetometers)

Balint, A. T., An improved magnetic modulator for static subharmonic generators.– Proc. C.M.A., 1959, Washington; AIEE, 1959, pp. 167-178, Fig. 6, Bibl. 36, Appendix 2.

Barr, J. D., Improvements in or relating to amplifier arrangements.– British Patent Class 38(4), 40(1), No.753; July 25, 1956.

Bullen, C. V., A triple-action positioning controller using a magnetic modulator.– Commun. and Electronics, 1959, January, No. 40, pp. 785-787, Fig. 5.

Elsner, R., Zur Theorie des magnetischen Ringmodulators.– Arch. Elektr. Übertragung, 1959, vol.13, No. 11, pp. 486-494.

Kletsky, E. J., Design criteria for low-level second-harmonic magnetic modulators.– Commun. and Electronics, 1959, January, No. 40, pp. 1013-1019, Fig. 11, Bibl. 9.

Lipkin, D. M., Radio frequency or carrier type transverse magnetic amplifier using square-wave power.– U.S. Patent Class 323-89, No. 2,888,637; May 26, 1959.

Manteuffel, E. W. and R. E. Cooper, Direct current charged magnetic pulse modulator.– Proc. C.M.A., 1959, Washington; AIEE, 1959, pp. 234-255, Fig. 15, Bibl. 4.

7. Computer Magnetic Elements

a) Books, Monographs and Dissertations

Humphrey, W. S., Switching circuits with computer applications.– McGraw-Hill Book Company, Inc., New York, 1958, p. 264, Fig. 179, Table 40, Bibl. 177.

Katz, H. W.(ed.), Solid state magnetic and dielectric devices.– John Wiley and Sons, Inc., New York, 1959, p. 542, Fig. 373, Table 5, Bibl. 466.

b) Surveys. Magnetic Elements in Logical Control Systems and Computers

Adachi, H. and J. Yamamoto, Ferrite Cores for Digital Computers.– Tetsudo gidzyutsu kenkyu cirē, J. Railway Engng. Res., 1958, vol. 15, No. 8, pp. 367-370 [in Japanese].

Digital amplifiers use saturable transformers.– Electronics, Engng. Edition, 1958, vol. 31, No. 27, pp. 74, 76.

Eichbaum, B. R., Evaluation of new high-speed magnetic ferrite system for use in computer components.– J. Appl. Phys., 1959, suppl. to vol. 30, No. 4, pp. 49S-52C, Figure, Bibl. 8.

Ferrite Cores– for computers (picture story).– Electronic Industries, 1949, vol. 18, No. 5, pp. 102-104.

Ferrites in the computer industry.– Factory Manager, 1958, vol. 27, No. 293, pp. 6-7, Fig. 5.

Hood, H. C. and S. Weber, New components head Wescon developments.– Electronics, 1959, vol. 32, No. 44, pp. 43-47.

Looney, D. H., Recent advances in magnetic devices for computers.– J. Appl. Phys., 1959, suppl. to vol. 30, No. 4, pp. 38S-42S, Fig. 7, Bibl. 15.

Magnetic amplifier computing control circuits.– El. Manufacturing, 1959, vol. 64, No. 6, pp. 102-110.

Der Magnetkern-Rechner, eine elektronische Neuentwicklung.– Industriekurier Wochenausg. Techn. und Forsch., 1958, vol. 11, No. 21, p. 324, Fig. 1.

Motooka, T., Magnetic Core Digital Circuits. Keisosu, Keisoku, J. Soc. Instrum. Technol., Japan, 1958, vol. 8, No.11, pp. 716-720 [in Japanese].

New magnetic amplifiers for digital computer uses.– Automat. Control, 1958, vol. 8, No. 5, pp. 52-53, Fig. 1.

Rajchman, J. A., Magnetics for computers–a survey of the state of the art.– RCA Rev., 1959, vol. 20, No. 1, pp. 92-135, Fig. 28, Bibl. 43.

Sakurai, I., Contemporary Applications of Cores with Rectangular Hysteresis Loops (Magnetic Amplifiers, Oscillators, Modulators, Frequency Converters, Magnetic Counters, etc.).– Erekutoronikusu, 1959, vol. 4, No. 5, pp. 499-504, Fig. 33, Bibl. 19 [in Japanese].

c) Memory Elements

Apertured ferrite plate memory.– Automat. Control, 1958, vol. 9, No. 6, p. 60, Fig. 3.

Baldwin, J. A. and J. L. Rogers, Inhibited flux–a new mode of operation of the three-hole memory core.– J. Appl. Phys., 1959, vol. 30, No. 4, pp. 58S-59S, Fig. 2, Bibl. 7.

Bittmann, E. E., Using thin films in high-speed memories.– Electronics, 1959, vol. 32, No. 23, pp. 55-57, Fig. 7.

Bobeck, A. H., The twistor: a new magnetic memory element.– Bell Labs Rec., 1959, vol. 37, No. 11, pp. 407-610, Fig. 4.

Boyajian, C. L., Transfluxor analog memory circuit.– Proc. C.M.A., 1959, Washington; AIEE, 1959, pp. 313-323, Fig. 10.

Boyer, G., Dispositif de commande pour matrice a tores magnétiques.– French Patent Class 12.3; No. 1137717; June 3, 1957.

Briggs, G. R. and K. C. Hu, Miniature frequency magnetic amplifiers for magnetic memory sensing.– Proc. C.M.A., 1959, Washington; AIEE, 1959, pp. 287-305, Fig. 20, Bibl. 12.

Broadbent, K. D., A vacuum evaporated random access memory.– Proc. C.M.A., 1959, Washington; AIEE, 1959, pp. 281-286, Fig. 6.

Chen, T. C. and O. B. Stram, Digital memory system keeps circuits simple.– Electronics, 1959, vol. 32, No. 11, pp. 130-133, Fig. 7.

Cole, W. A., Magnetic matrix stores.– Wireless World, 1959, vol. 65, No. 6, pp. 279-283.

Cook, M. H., E. H. Melan, and E. C. Schuenzel, High-speed ferrite core for a coincident current memory.– Proc., 1959, Electron. Compon. Conf. Philadelphia, Pa. S. I., 1959, pp. 128-131.

Digital buffer storage.– Automat. Control, 1958, vol. 9, No. 6, p. 51.

Ferromagnetic memories for computers.– Times Rev. Ind., 1958, vol. 12, No. 140, p. 25, Fig. 1.

Freedman, A. L., Magnetic core matrices for logical functions.– Electronic Engng 1959, vol. 31, No. 376, pp. 358-361, Fig. 5, Bibl. 3.

Goda, B. T., A line printer memory utilizing magnetic cores.– Computer and Automation, 1958, vol. 7, No. 8, pp. 12-13.

Guartly, C. I., A high-speed ferrite storage system.– Electron. Engng, 1959, vol. 31, No. 382, pp. 756-758, 775, 780.

Heijn, H. J. and N. C. Troye, Een snelle methode voor het lezen van magneetringgeheugens.– Philips Techn. Tijdschr., 1958, vol. 20, No. 6-7, pp. 180-195.

Heijn, H. J. and N. C. Troye, A fast method of reading magnetic core memories.– Philips Techn. Rev., 1959, vol. 20, No. 7, pp. 193-207.

Heijn, H. J. and N. C. Troye, Les memoires a tores.– Electronique Industr., 1959, No. 27, pp. 165-168, 170.

Infield, G. Metal "doughnuts" with memories.– Sci. Digest, 1958, vol. 43, No. 5, pp. 17-19.

Jaecklin, A., Umklappzeit von Ferriten als Speichermethode.– Techn. Mitt. PTT, 1959, vol. 4, No. 4, pp. 140-144, Bibl. 3.

Jaita, A., Magnetic Memory Device. Erekutoronikusu, 1959, vol. 4, No. 10, pp. 69-75, Fig. 9, Bibl. 9 [in Japanese].

Kraus, M., Transfluxor analog memory.– Control Engng., 1959, vol. 6, No. 12, p. 127, Fig. 1, Bibl. 1.

Lindsey, C. H., The square-loop ferrite core as a circuit-element.– Proc. IEE, 1959, vol. 106, part C, No. 10, pp.117-124; J. IEE, 1959, vol. 5, No. 50, p. 100.

Lukaszewicz, L., Permanent storage.– Bull. de L'Acad. Polonaise des Scienc., 1959, vol. 7, No. 7-8, pp. 497-502, Fig. 5, Bibl. 4.

Mémoires et procédés nouveaux pour l'avenir des calculatrices.– Automation, 1959, No. 35, pp. 203-206.

Oakland, L. J. and T. D. Rossing, Coincident-current nondestructive readout from thin magnetic films.– J. Appl. Phys., 1959, suppl. to vol. 30, No. 4, pp. 54S-55S.

Oterashi, M., Magnetic recording device for digital computers, Ohm. Electr. Mag., 1958, (45), vol. 9, pp. 1017-1018.

Raffel, J. I., Operating characteristics of a thin film memory.– J. Appl. Phys., 1959, suppl. to vol. 30, No. 4, pp.60S-61S.

Rokos, A., A Rotational Magnetic Memory Device Used in Telephone Registers.– Slaboproudý Obzor, 1959, vol. 20, No. 4, pp. 247-256, Fig. 20, Bibl. 8 [in Czech].

Rumble, W. G. and C. S. Warren, Coincident current applications of ferrite apertured plates. – IRE Wescon Convent Rec., 1958, vol. 2, part 4, pp. 62-65.

Small coincident current magnetic core storage systems.– Automat. Control, 1958, vol. 9, No. 6, p. 51.

Smith, D. O., Thin magnetic films for digital computer memories.– Electronics, 1959, vol. 32, No. 26, pp. 44-45, Fig. 1.

Stuart-Williams, R. and B. T. Goda, An extension of magnetic switching techniques in high-speed storage applications.– Proc. C.M.A., 1959, Washington; AIEE, 1959, pp. 268-280, Fig. 14, Bibl. 1.

Stucki, F., Der Twistor. Ein neues magnetisches Techn. Mitt. PTT, 1958, vol. 36, No. 1, pp. 33-35, Fig. 4, Bibl. 2.

Wells, F. N., Use of magnetic tapes and cores for nuclear data storage and computation.– Nucl. Instrum., 1958, vol. 2, No. 2, pp. 165-168.

West, R. H., High-speed readout for data processing.– Electronics, 1959, vol. 32, No. 22, pp. 83-85, Fig. 6, Bibl. 1.

Williams, F. C., Apparatus for the storage of digital information.– British Patent Class 40(4), 106(1), No. 797941; July 9, 1958.

Yamada, S., Magnetic Core Memories and Magnetic Core Switches.– Erekutoronikusu, 1959, vol. 4, No. 4, pp. 385-389, Fig. 11, Bibl. 9 [in Japanese].

Yamada, S. and T. Bessho, Method of AC Writing for Magnetic Core Matrices. Reports of the Electrical Communication Laboratory, Nippon Telegraph and Telephone Public Corporation, 1959, vol. 7, No. 2, pp. 44-47, Fig. 7.

d) Switches

Aleksić, T., Use of Nonlinear Chokes in Magnetic Switching Circuits.– Tehnika, 1958, vol. 13, No. 9; Electrotehnika, 1958, vol. 7, No. 9, pp. 129-133 [in Czech].

Bonn, T. H., Electric circuit with two stable states.– U.S. Patent Class 307-88, No. 2,813,207; November 12, 1957.

Bosch, L. L., Static control in automatic warehousing.– Applic. and Ind., 1959, vol. 1, No. 40, pp. 595-602.

Crane, H. D., A high-speed logic system using magnetic elements and connecting wire only.– Proc. IRE, 1959, vol. 47, No. 1, pp. 63-73.

"Surak"– Automation, 1959, November, No. 37, p. 271.

"Surak"– system logique statique au service de l'automatité industrielle. Industrial Catalog: "Le matérial électrique SW," 1959, p. 21.

Dennis, R. J., The use of static switching in sequential control systems.– Brit. Commun. and Electronics, 1959, vol. 6, No. 2, pp. 154-157.

Durkee, R. W., Core factors in static magnetic switch performance.– El. Manufacturing, 1959, vol. 64, No. 4, pp. 134-137, Fig. 5.

Freedman, A. L., Square-loop cores for logic circuits.– Electronics, 1959, vol. 32, No. 2, pp. 70-72.

Gianola, U. F. and T. H. Crowly, The laddic–a magnetic device for performing logic.– Bell System Techn. J., 1959, vol. 38, No. 1, pp. 45-72, Fig. 12.

Gutterman, A., Fast switching for industry control.– Electronics, 1959, vol. 32, No. 26, p. 51.

Hamaoka, F., Set of Contactless Relays.– Seisan chidzyutsu, Product. Techn., 1958, vol. 13, No. 7, pp. 10-20 [in Japanese].

Hamaoka, F. and E. Ono, Computer and Control Device Using Magnetic Logic Elements.– Mitsubisi denki, 1958, vol. 32, No. 5, pp. 490-499 [in Japanese].

Hiratsuka, M., Contactless relay "Logit."– Denki keisan, 1958, vol. 26, No. 8, pp. 1456-1461, 1469 [in Japanese].

Hiratsuka, M., Relay with Magnetic Amplifier.– Om Denki zassi, Ohm. Electr. Mag., 1958, vol. 45, No. 7, pp.869-872 [in Japanese].

Hruša, J., Bezkontaktni spínání u elektrických pohonů.– Electrotechn. Obz., 1959, vol. 48, No. 3, pp. 129-135, Fig. 18, Bibl. 16.

Johnson, D. W., Automatic control with static-switching circuits.– Electronics, 1959, vol. 32, No. 17, pp. 98-101, Fig. 7.

Kalbfell, D. C., Low-level magnetic commutators.– Electronics Design, 1958, vol. 6, No. 5, pp. 70-73, Fig. 5.

Kaplan, M., Magnetic device.– U.S. Patent Class 340-174, No. 2,813,260; November 12, 1957.

Kaposi, J. E., Rectangular hysteresis-loop magnetic cores as switching elements.– Electronic Engng, 1959, vol. 31, No. 375, pp. 278-283, Fig. 15, Bibl. 5.

Lhome, H., Les relais sans contacts. Leurs applications dans l'industrie.– Bull. Scientifique A. I. M., 1959, vol. 72, No. 8, pp. 473-486.

Lovell, B. W., Two-step switching of saturable reactors.– Proc. C.M.A., 1959; Washington, AIEE, 1959, pp. 103-115, Fig. 14, Bibl. 14.

Lucke, W. H., A magnetic amplifier commutating and pulse-width encoding circuit.– Commun. and Electronics, 1959, January, No. 40, pp. 884-892, Fig. 13, Bibl. 3.

Magnetic memory element exhibits 4-millimicrosecond switching speed.– El. Engng, 1959, vol. 78, No. 3, pp. 236-237.

Magnistor.– Instrum. and Automat., 1958, vol. 31, No. 2, p. 228.

"Magnistor" devices for digital and logic circuits.– El. Manufacturing, 1959, vol. 64, No. 2, pp. 74-77.

Meier, D. A., Millimicrosecond magnetic switching and storage element.– J. Appl. Phys., 1959, vol. 30, No. 1, pp. 122-123.

Meier, D. A., Millimicrosecond magnetic switching and storage element.– J. Appl. Phys., 1959, suppl. to vol. 30, No. 4, pp. 45S-46S.

Nakayama, K., Contactless Relays. Denki gakkai dzassi, 1959, vol. 79, No. 844, pp. 85-88, Fig. 9, Bibl. 6 [in Japanese].

Nakayama, K., Contactless Relays and Their Applications.– Erekutoronikusu, 1959, vol. 4, No. 1, pp. 29-32, Fig. 12 [in Japanese].

New encoder utilizes magnetic readout principles.– Automat. Control, 1958, vol. 9, No. 6, pp. 10-11, Fig. 2.

New uses for versatile magnistor.– Automat. Control, 1958, vol. 9, No. 5, p. 49.

Nolan, R. M., Magnetic unit uses extremely low power.– Missiles and Rockets, 1958, vol. 4, No. 23, p. 39.

Proebster, W. E., Circuits de commutation ferroresonants.– Automatisme, 1959, vol. IV, No. 10, pp. 383-384.

Ramey, R. A. and W. G. Hall, Flip-flop circuit elements for control circuits.– U.S. Patent Class 340-174, No. 2,792,564; May 14, 1957.

Rosa, J., A sensitive static relay circuit.– Proc. C.M.A., 1959, Washington, AIEE, 1959, pp. 154-166, Fig. 15, Table 1, Bibl. 2.

Rosenfeld, J. L., Magnetic core pulse switching circuits for standard packages.– IRE Trans. Electronic Comput., 1958, vol. EC-7, No. 3, pp. 223-228, Fig. 10.

Rossing, T. D. and S. M. Rubens, Effect of a transverse field on switching rates of magnetic memory cores.– J. Appl. Phys., 1958, vol. 29, No. 8, pp. 1245-1247, Fig. 4.

Rozner, F. and P. Pengelly, Transistor and cores in counting circuits.– Electronic Engng, 1959, vol. 31, No. 375, pp. 272-274, Fig. 5, Bibl. 2.

Sakamoto, N., Switches on magnetic amplifiers, Densi Kagaku, 1959, vol. 9, No. 8, pp. 37-39, Fig. 9.

Shevel, W. L., Millimicrosecond switching properties of ferrite computer elements.– J. Appl. Phys., 1959, suppl. to vol. 30, No. 4, pp. 47S-48S, Fig. 2, Bibl. 3.

Simmons, B. D., Saturable transformer switches (application to magnetic drum head selection).– Electronic and Radio Engineer, 1959, vol. 36, No. 3, pp. 82-90, Fig. 10, Bibl. 9.

Static magnetic switch.– Electronics, 1959, vol. 32, No. 46, p. 116. Communication of the firm "Magnetic Amplifiers, Inc."

Steagall, W. F., Monostable device.– U.S. Patent Class 307-88, No. 2,729,754; January 3, 1956.

Steagall, W. F., Phase-responsive bistable devices.– U.S. Patent Class 340-174, No. 2,783,456; February 26, 1957.

Stiebel, A., High-speed switching of low-level signals.– Electronics, 1959, vol. 32, No. 12, pp. 54-55, Fig. 5.

Tellefsen, H. and S. Alessio, Application of magnetic core logic to industrial controls.– IRE Nat. Convent. Rec., 1958, vol. 6, pt. 6, pp. 283-293, Fig. 12, Bibl. 2.

Tomlinson, T. B., Switching circuits using bidirectional nonlinear impedances.– J. Brit. IRE, 1959, vol. 19, No. 9, pp. 571-591.

A transistor magnetic core binary counter.— Proc. IRE, 1958, vol. 46, No. 42, pp. 1967-1968.

Warren, C. S., Magnetic switch.– U.S. Patent Class 340-166, No. 2,734,185; February 7, 1958.

Whilely, R. L., Magnetic switching device.– U.S. Patent Class 340-174, No. 2,816,278; December 10, 1957.

Yokosuka, M., F. Hamaoka, and E. Ono, On the contactless relay systems, Seigio kogio (Journal of the Japan Association of Automatic Control Engineers), 1957, vol. 1, No. 2, pp. 91-101, Fig. 16, Bibl. 18.

Yokosuka, M., F. Hamaoka, and E. Ono, Static Switches.– Mitsubishi Denki, 1957, vol. 31, No. 21, pp. 1028-1037 [in Japanese].

Zurbrick, J., Static switching passes a maintenance test.– Control Engng, 1959, vol. 6, No. 10, p. 95.

e) Registers

Bobeck, A. H. and R. F. Fischer, Reversible, diodeless, twistor shift register.– J. Appl. Phys., 1959, suppl. to vol. 30, No. 4, pp. 43S-44S, Fig. 1, Bibl. 2.

Lanning, W. C., Shifting register.– U.S. Patent Class 340-174, No. 2,828,477; March 23, 1958.

McMillan, W. M. and R. W. Lowrie, Magnetic core shift register.– U.S. Patent Class 340-174, No. 2,846,669; August 5, 1958.

New shift register uses "Twistor" principle.– Bell Labs Rec., 1959, vol. 37, No. 2, p. 69.

Prywes, N. S., Diodeless magnetic shift registers utilizing transfluxors.– IRE Trans. Electronic Comput., 1958, pt.EC-7, No. 4, pp. 316-324, Fig. 14, Bibl. 7.

Smith, B. K., Shifting register or array.– U.S. Patent Class 340-174, No. 2,834,007; May 6, 1958.

f) Decipherers

Bloch, E. and R. C. Paulsen, Magnetic core logic in a high-speed card-to-tape converter.– IRE Trans. on Electronic Computers, 1959, vol. EC-8, No. 2, pp. 169-181, Bibl. 2.

Emerson, M., Converter-printer for instrumentation data.– Automat. Control, 1958, vol. 9, No. 6, pp. 52-57, Fig. 3.

Lane, A. L. and A. Turczyn, A high speed N-pole, N-position magnetic core matrix switch.– IRE Nat. Convention Rec., 1958, vol. 6, No. 4, pp. 246-253, Fig. 10.

g) Timing Devices

Hardies, C. E., Long-time delays from a single magnetic storage core.– Commun. and Electronics, 1959, No. 45, pp. 457-461, Fig. 7, Bibl. 4.

Sicko, J. S., A timing circuit using a saturable reactor and a controlled rectifier.– Proc. C.M.A., 1959, Washington; AIEE, 1959, pp. 204-214, Fig. 10, Bibl. 3.

Van Allen, R. L., Time interval generation with transistor switches and magnetic cores.– Proc. NEC, 1958, vol. 14, pp. 884-897, Fig. 10, Table 2, Bibl. 8.

Vielehr, I. E., Static delay circuit.– Automation, 1959, May, p. 89.

h) Parametrons

Billing, H. E. and A. O. Rüdiger, The possibility of speeding up computers using parametrons.– UNESO/NS/ICIP/K, vol. 2, No. 11, 1959, pp. 1-14.

Donner desktop computers. – Automat. Control, 1959, vol. 11, No. 2, pp. 3-4.

Endo, Ishii, Watanabe, Yamamoto, Tomita, Hoguchi, Onodera, and Matsuo, Arithmetic unit of parametron computer SENAC–1 (NEAC 1102).–

Fukui, K., Further Developments in Parametron Properties.– Densi kagaku, 1959, vol. 9, No. 4, pp. 14-17, Fig. 11, Bibl. 4 [in Japanese].

Fushimi, K., On Parametron C.– Kagaku gidzyutsu tembo densi kagaku, 1959, vol. 9, No. 8, pp. 69-70, Fig. 3 [in Japanese].

Fukui, K., M. Shindo, T. Kurata, and K. Habara.– Binocular type parametron.– Report of El. Commun. Lab., 1959, vol. 7, No. 5, pp. 152-166, Fig. 28, Bibl. 4.

Goto, E., Electronic Parametron Computer.– Densi Kagaku, 1959, vol. 9, No. 4, p. 27, Fig. 1 [in Japanese].

Goto, E., The parametron, a digital computing element which utilizes parametric oscillation.– Proc. IRE, August, 1959, vol. 47, No. 8, pp. 1304-1306.

Hiruma, K., Development of Parametron Properties by Means of Ferrite Core Improvement.– Densi Kagaku, 1959, vol. 9, No. 4, pp. 23-25, Fig. 5 [in Japanese].

Hoguchi, Onodera, Matsuo, Endo, Ishii, Watanabe, Yamamoto, and Tomita, Control device of SENAC-1 (NEAC 1102).– Denki tsusin gakkai dzassi, 1959, vol. 42, No. 11, pp. 1008-1014, Fig. 9.

Hushimi, K. and K. Kataoka, Ferroelectric memory in the parametron circuits.– Report of Elect. Comm. Lab., 1959, vol. 7, No. 7, pp. 213-217, Fig. 5, Bibl. 2.

Ieiri, K., Theory of Parametron Amplifier Operation and New Devices.– Densi kogē, 1959, vol. 8, No. 6, pp. 7-15, Fig. 25, Bibl. 31 [in Japanese].

Kamada, K., The Use of Parametrons in Physical Investigations.– Densi kagaku, 1959, vol. 9, No. 4, pp. 36-39, Fig. 3 [in Japanese].

Katsura, Onodera, Hoguchi, Honda, Oizumi, Inawashira, Watanabe, Ishii, Endo, and Degawa, General descriptions of SENAC-1 (NEAC 1102) including the construction of instructing system.– Denki tsusin gakkai dzassi, 1959, vol. 42, No. 11, pp. 1000-1008, Fig. 2.

Kiyashi, Z. and S. Ikeno, Synthesis of Parametron Circuits (2). Kagaku gidzyutsu tembo densi kagaku, 1959, vol. 9, No. 8, pp. 101-107, Fig. 8 [in Japanese].

Kiyashi, Z. and S. Ikeno, Synthesis of Parametron Circuits (4).– Kagaku gidzyutsu tembo densi kagaku, 1959, vol. 9, No. 12, pp. 85-90, Fig. 7 [in Japanese].

Kiyashi, Z., S. Oshima, S. Yamato, and H. Yamada, On the Practical Application of the Parametron.– Densi kogē, 1959, vol. 8, No. 6, pp. 38-47 [in Japanese].

Kunuki, K., Parametron Memory Core and Its Measurements.– Densi kogē, 1959, vol. 8, No. 7, pp. 22-28, Fig. 10, Bibl. 5 [in Japanese].

Muroga, S., Elementary principle of parametron and its application to digital computers.– Res. and Engng, 1958, vol. 4, No. 5, pp. 31-34, Fig. 7.

Muroga, S., and K. Takashina, Parametron Computer M1.– Kagaku, 1958, vol. 28, No. 5, pp. 243-248 [in Japanese].

Nakai, Y., Parametron. Keisoku, 1958, vol. 8, No. 11, pp. 721-726, Fig. 19, Bibl. 8 [in Japanese].

Nawasaki, H., The Application of the Parametron to Electronic Commutators.– Densi kagaku, 1959, vol. 9, No. 4, pp. 28-29, Fig. 1 [in Japanese].

Oshima, S., H. Enomoto, and S. Watanabe, Analysis of Parametrons and Magnetic Amplifiers.– J. Inst. Electr. Commun. Engrs Japan, 1958, vol. 41, No. 10, pp. 971-978 [in Japanese].

Oshima, S., H. Enomoto, and S. Watanabe, Statistical analyzer mainly composed of parametron.– Denki tsusin gakkai dzassi, 1959, vol. 42, No. 8, pp. 744-749.

Otori, S., The Application of Parametrons to Telephone Apparatus.– Densi kagaku, 1959, vol. 9, No. 4, pp. 30-33, Fig. 6, Bibl. 5 [in Japanese].

Palounek, L., The Parametron, A New Doubler.– Slaboproudý Obzor, 1960, vol. 21, No. 4, pp. 236-239 [in Czech].

Pohm, A. V., A. A. Read, R. M. Stewart, and R. F. Schauer, High-frequency magnetic film parametrons for computer logic.– Proc. NEC, 1959, October 12-14, Chicago, vol. 15, pp. 202-214, Fig. 9, Bibl. 12.

Schmitt, E., Das Parametron und seine Verwendung in nachrichtenverarbeitenden Systemen.– Electronische Rundschau, 1960, vol. 14, No. 2, pp. 41-46.

Shaziki, S. and S. Ito, The Application of Parametrons to Digital Control Systems.– Densi kagaku, 1959, vol. 9, No. 4, pp. 33-36, Fig. 5 [in Japanese].

The APQ, A Stationary Device (Using Parametrons).– Densi kagaku, 1959, vol. 9, No. 4, p. 82, Fig. 2 [in Japanese].

Takahashi, H., The Requirements Which Led to the Creation of the Parametron.– Densi kagaku, 1959, vol. 9, No. 4, pp. 10-13, Fig. 2, Bibl. 4 [in Japanese].

The TDK Paramistor of the Type RM-40.– Densi kagaku, 1959, vol. 9, No. 4, p. 82, Fig. 3 [in Japanese].

Terada, H., The parametron–an amplifying logic element.– Control Engng, 1959, April, vol. 6, No. 4, pp. 110-115, Fig. 20.

Wang Chuan-shan and Lin Wen-tshen, Analysis and Calculation of the Parameters of Magnetic Contactless Distributors.– Tsyndunkhua, Automation, 1959, vol. 2, No. 8, pp. 273-282, Fig. 6, Bibl. 3 [in Japanese].

Yamada, S. and K. Kuri, Supersonic delay line device for parametron signal.– Report El. Commun. Lab., 1959, vol.7, No. 5, pp. 167-169, Fig. 6, Bibl. 1.

Zenichi, K., and K. Nishiguchi, Reading of recorded signals with a low frequency parametron.– Reports of the Elect. Comm. Lab., 1959, vol. 7, No. 2, pp. 48-52, Fig. 8.

8. Magnetic Amplifiers and Frequency Converters

Belamin, M., Periodic unidirectional pulses generated by a transductor (Siemens-Schuckertwerke Akt. Ges.).– U.S. Patent Class 317-123, No. 2,854,605; September 30, 1958.

Fūgli, R., Statische Frequenzumformung in festem Verhältnis 1:3 mittels Transformatoren.– Bull. Schweiz. Elektrotechn. Ver., 1958, vol. 49, No. 26, pp. 1224-1227, Fig. 2.

Harada, K., Double frequency type magnetic amplifiers and higher harmonic oscillations in magnetic frequency doubler.– Mem. Fac. Engng, Kyushu Univ., 1959, vol. 18, No. 2, pp. 23-61.

Harada, K., The Generation of Higher Harmonics in Magnetic Frequency Doublers.– Denki gakkai dzassi, J. Inst. Electr. Engrs Japan, 1958, vol. 78, No. 10, pp. 1308-1317 [in Japanese].

Jewett, W. E. and P. L. Schmidt, A more stable 3-phase transistor-core power inverter.– Commun. and Electronics, 1959, No. 45, pp. 686-691, Fig. 10, Bibl. 5.

Johnson, J. H., Theoretical and experimental analysis of the ferromagnetic explosively shocked current pulse generator.– J. Appl. Phys., 1959, suppl. to vol. 30, No. 4, pp. 241S-243S.

Jones, J. P., Magnetic core current driver.– U.S. Patent Class 340-174, No. 2,825,047, February 25, 1958.

Krinitz, A., Transistor-magnetic pulse generator.– Proc. NEC, 1958, vol. 14, pp. 37-55, Fig. 10, Table 4, Bibl. 4.

Lassiter, E. M., P. R. Johannessen, and R. H. Spencer, High-power pulse generation using semiconductors and magnetic cores.– Proc. C.M.A., 1959, Washington; AIEE, 1959, pp. 215-233, Fig. 15, Bibl. 11.

Miller, H. A. and H. Eisler, Magnetic amplifier pulse generators.– U.S. Patent Class 323-89, No. 2,873,422; February 10, 1959.

Mokrytzki, B. and R. A. Stuart, A magnetic amplifier-silicon transistor power supply for missile application.– Proc. C.M.A., 1959, Washington; AIEE, 1959, pp. 179-195, Fig. 8, Table 1, Bibl. 2.

Putkovich, R. P. and T. M. Corry, Applications of saturable cores in transistor power converters.– Proc. NEC, 1958, vol. 14, pp. 874-883, Fig. 10, Bibl. 7.

Sichling, G., Anordnung mit einem dielektrischen und einem magnetischen Verstärker zur Verstärkung bzw. Frequenzvervielfachung.– FRG Patent Class 21a^2, 18/08, No. 968862; April 3, 1958.

Stefanov, V. I., The Generation of Relaxation Oscillations with the Aid of a Magnetic Amplifier. Dokl. Bolgarskoi AN, 1959, vol. 12, No. 1, pp. 13-16.

Syrbe, M., Reset magnetic amplifier controlled rectifier and inverter apparatus.– U.S. Patent Class 321-25, No. 2,857,563; October 21, 1958.

9. Magnetic Measurements and Methods of Testing Magnetic Elements

Airth, H. B. and G. E. Lynn, A statistical determination of correlation between constant current flux reset core testers.– Proc. C.M.A., 1959, Washington; AIEE, 1959, pp. 340-346, Fig. 1, Table 1, Bibl. 1.

Automatic classifier speeds selection of magnetic memory cores.– Electronics Design, 1958, vol. 6, No. 5, pp. 74-75.

Automatic memory core tester.– El. Manufacturing, 1959, vol. 64, No. 1, p. 146.

Christensen, D. D., Method and apparatus for comparing relative conditions of magnetization in a magnetizable element.– U.S. Patent Class 340-174, No. 2,832,945, April 29, 1958.

Choudhury, J. K. and P. C. Sen, Magnetic measurements with bridged-T network.– Electronic and Radio Engr., 1959, vol. 36, No. 11, pp. 422-426, Fig. 7, Bibl. 10.

Drigo, A., Bulla possibilità di modificare le proprietà magnetiche dei corpi ferromagnetici mediante l'irradiazione con neutroni.– Energia Elettrica, 1959, vol. 36, No. 7, pp. 617-621.

Fully automatic tester analyzes bobbin and ferrite memory cores.– Automat. Control, 1959, vol. 11, No. 2, pp. 57-58.

Goral, A., The Measurement of Some Magnetic and Dielectric Properties of Soft-Magnetic Ferrites for the 10 Cycle to 1000 Megacycle Frequency Band.– Rozprawy Elektrotechniczne, 1959, vol. 5, No. 4, pp. 587-631, Fig. 27, Bibl. 14 [in Polish].

Greig, J., Problems Involved in the Measurement of the Characteristics of Soft Magnetic Materials.– Elettrotecnica, 1959, vol. 46, No. 2, pp. 58-65.

Haun, R. D. and T. A. Osial, Gain measurements on a pulsed ferromagnetic microwave amplifier.– Proc. IRE, 1959, vol. 47, No. 4, pp. 586-587, Bibl. 1.

Henniger, H., H. Rudloff, and G. Engelhardt, Elektrische Messungen an weichmagnetischen Ferriten.– Nachrichtentechnik, 1959, vol. 9, No. 9, pp. 392-395, Fig. 11, Bibl. 4.

Kaczkowski, Z., Pomiary wlasnosci materialow magnetycznych woltomierzem fazoczulym w zakresie czestotliwosci akustycznych.– Arch. Elektrotechn., 1959, vol. 8, No. 2, pp. 339-344, Fig. 4, Bibl. 3.

Kikuchi and Simizu, Direct Counting Device for the Direct Observation of Magnetic Hysteresis Curves by the Differential Method.– Electronician, 1957, vol. 6, No. 9, pp. 1-3 [in Japanese].

Koppelman, F. and G. Unger, Kalorimetrische Messung der Ummagnetisierungsverluste von Ringkernen.– Elektrotechn. Z., 1959, vol. A80, No. 22, pp. 773-777.

Krug, W., Messungen an Elektroblechen im Laboratorium und in der Fertigung.– ETZ, Ausg. A, 1959, No. 17, pp.593-599.

Lachowicz, H., J. Markowski, and W. Turewicz, Device for Measuring the Parameters of Pulsed Ferrite Switching Cores.– Przegl. telekommunikacyiny, 1959, vol. 32, No. 1, pp. 17-22.

Lombardini, P. P. and R. F. Schwartz, R–F measurements of ferrite cores.– El. Manufacturing, 1959, vol. 63, No. 4, pp. 148-155, Fig. 15.

Nalecz, M. and B. Osuchowska, The ferrometric method of testing the magnetic properties of ferromagnetic materials.– Rozprawy elektrotechniczne, 1959, vol. 5, No. 2, pp. 209-210.

Nitzan, D., Graphical evaluation of magnetic amplifier performance based on constant-voltage reset test.– Commun. and Electronics, 1959, No. 45, pp. 691-698, Fig. 15, Bibl. 4.

Oteri, Testing of magnetic materials, Ohm. El. Mag., 1958, vol. 45, No. 8, pp. 180-186.

Riethmuller, J., Appareillage de contrôle et classement en grande production des microtores à memoire.– Annales de radioélectricité, 1959, vol. 14, No. 56, pp. 156-168.

Segal, A., Device for Testing the Ferrite Elements of Memories Subject to Pulsed Operation.– Automat. si electron, 1959, vol. 3, No. 1, pp. 40-43.

Takata, M. and I. Itatta, A Device for Measuring Hysteresis Losses.– Japanese Patent Class 110-10, No. 6239; September 3, 1955 [in Japanese].

Van Allen, R. L., Covert, P. W., and T. G. Wilson, Some practical methods of obtaining time of response.– Proc. C.M.A., 1959, Washington; AIEE, 1959, pp. 358-368, Fig. 7, Table 1, Bibl. 5, Appendix 1.

Werner, E., Die zerstörungsfreie Messung von Verlusten und Feldstarken an Elektroblechen, Ganztafelmessung oder punktweise Messung.– E. und M., 1959, vol. 76, No. 3, pp. 57-60, Fig. 8, Bibl. 5.